PLACE IN RETURN BOX to remove this checkout from your record. TO AVOID FINES return on or before date due.

DATE DUE	DATE DUE	DATE DUE

MSU is An Affirmative Action/Equal Opportunity Institution choirclassedus.pm3-p.1

# COMPOSITE POLYMER ELECTROLYTES USING FUNCTIONALIZED FUMED SILICA AND LOW MOLECULAR WEIGHT PEO: SYNTHESIS AND CHARACTERIZATION

Ву

Jun Hou

### **A DISSERTATION**

Submitted to
Michigan State University
in partial fulfillment of the requirements
for the degree of

**DOCTOR OF PHILOSOPHY** 

Department of Chemistry

1997

#### ABSTRACT

# COMPOSITE POLYMER ELECTROLYTES USING FUNCTIONALIZED FUMED SILICA AND LOW MOLECULAR WEIGHT PEO: SYNTHESIS AND CHARACTERIZATION

By

#### Jun Hou

A new class of highly conductive and processable composite polymer electrolytes for use in rechargeable lithium batteries have been synthesized. The principal characteristic of these systems is the use of surface functionalized fumed silica fillers to control the mechanical properties of the composites. When a low molecular weight polyether solution is immobilized in fumed silica, an open three-dimensional network forms due to van der Waals attractions or hydrogen bond linkages between silica particles. The open network structure is conducive to high ionic mobility and responsible for the reinforcement of the composite.

The most promising electrolytes are cross-linkable composite polymer electrolytes that incorporate a silica that bears both hydrophobic and cross-linkable functional groups. Hydrophobic groups contribute to the formation of open networks, while cross-linking groups provides mechanical strength and dimensional stability through the formation of covalent bonds between silica particles.

Cross-linkable composite electrolytes were prepared from PEGDM-500, LiClO<sub>4</sub>, fumed silica, and 10 wt% of methyl, butyl, or octyl methacrylate. Before cross-linking, the electrolytes were thixotropic and had ionic conductivities >10<sup>-4</sup> S/cm. After UV-induced cross-linking, the electrolytes were rubbery and dimensionally stable. DSC results showed that the addition of silica and monomer to the polyether-Li salt matrix did not affect the glass transition of polyether. In addition, the conductivities were unchanged according to impedance spectroscopy. After solvent extraction of the cross-linked composites to remove the polyether, lithium salt, and homopolymer, the solid phase was analyzed. The FTIR spectrum showed qualitatively the grafting of the guest polymer, and TGA analyses demonstrated that nearly all the polymer had been chemically bound to the silica surface. These data all support a model where the added methacrylate monomer and initiator phase separate from polyether-Li salt matrix and form a thin layer surrounding the silica network. Upon photoinitiation, the added monomer copolymerizes with cross-linkable groups on silica surface to yield a silica/polymer phase and little or no polymer in the PEGDM-500 phase. Thus, the mechanical properties of the composite electrolyte and its ionic conductivity are de-coupled, and can be optimized independently.

To Hong and Annie.

#### **ACKNOWLEDGMENTS**

I wish to express my deep appreciation to Professor Gregory L. Baker for his guidance, patience and constant encouragement throughout the course of this research. I would also like to thank Professors Chris Chang, Robert Cukier, Mercouri Kanatzidis, and Robert Hollingsworth for serving in my committee. I would also like to thank all members in Baker group for making my life in the lab enjoyable.

Financial support from Department of Chemistry and the U. S. Department of Energy is also acknowledged.

Finally, I want to thank my wife Hong for her support and bringing to this world our daughter Annie with whom life had never been the same.

# **TABLE OF CONTENTS**

		Page
List of Abb	reviations	<b>x</b> i
List of Sche	emes	<b>xii</b>
List of Tabl	es	xiv
List of Figu	res	<b>xv</b>
INTRODUC	CTION	1
I.	Electrolyte Systems	1
	1. Primary and Secondary Batteries	
	2. High-Energy-Density Battery	2
	3. Electrolytes for Lithium Batteries	4
	4. New Polymer Electrolyte Systems	11
II.	Photoinitiation of Polymerization	29
	1. Theory	29
	2. Polymerization Initiators	32
	3. UV Induced Polymerization	38
	4. Inhibition and Retardation	40
RESULTS	·	44
I.	Silylation Conditions	46
	1. General	46
	2. Amounts of Amine Catalyst	47
	3. Reaction Time	47
•	4. Amount and Type of Silane	51
II.	Hydrophobic Silica	54
III	Hydrophilic Silica	67

	IV.	Polymerizable Silica	74
		1. Silylation Using Single Silanes	74
		2. Silylation Using Mixed Silanes	82
	V.	Composite Polymer Electrolytes	92
		1. Compatible Composite Polymer Electrolytes	92
		2. Cross-linked Composite Polymer Electrolytes	94
DIS	CUSSIC	ON	121
	I	Current System	121
		1. Composite Reinforcing mechanism: phase separation	121
		2. Cross-Linking and Emulsion Polymerization: A	
		Comparison	132
	II.	Future Work and Suggestions	138
		1. Optimization of Current System	138
		2. Core-active Initiators	138
		3. Two-Component Core-Shell Composites	139
		4. Highly Dispersible & Cross-Linkable Silicas for	
		Emulsion Polymerization	141
	III.	Summary	143
EXP.	ERIME	NTAL	145
	I.	Materials	145
	II.	Analytical Methods	146
	III.	Hydrophobic silicas	149
		FS-TEMS-1	149
		FS-TEMS-2	149
		FS-TEMS-3	149

	FS-TEMS-0	149
	FS-TEMS-2H	149
	FS-TEMS-13H	149
	FS-TMCS-1	150
	FS-TMCS-2	150
	TMCE-3	150
	TMES-1	150
	FS-C2	150
	FS-C8	151
	FS-C18	151
	FS-DM-C8-1	151
	FS-DM-C8-2	151
	FS-DM-C8-3	151
	FS-DM-H	152
	FS-H	152
	FS-OEt-H	153
	FS-OH-H	153
	FS-TMS-H	153
IV.	PEO-Modified Silicas	155
	Ethylene Glycol Allyl Methyl Ether (EGAME)	155
	Diethylene Glycol Allyl Methyl Ether (DEGAME)	155
	Tiethylene Glycol Allyl Methyl Ether (TEGAME)	156
	Poly(ethylene glycol-350) Allyl Methyl Ether (PEGAME-	
	350)	156
	Poly(ethylene glycol-550) Allyl Methyl Ether (PEGAME-	
•	550)	156

	Poly(ethylene glycol-750) Allyl Methyl Ether (PEGAME-	
	750)	156
	Chlorodimethyl(4,7-dioxaoctyl)silane	157
	Chlorodimethyl(4,7,10-trioxaundecyl)silane	157
	Chlorodimethyl(4,7,10,13-tetraoxatetradecyl)silane	157
	Poly(ethylene glycol-350) methyl 3-	
	(chlorodimethylsily)propyl ether (PEGMPE-350)	158
	Poly(ethylene glycol-550) methyl 3-	
	(chlorodimethylsily)propyl ethers	158
	Poly(ethylene glycol-750) methyl 3-	
	(chlorodimethylsily)propyl ethers	158
	FS-DM-EO!	158
	FS-DM-EO2	159
	FS-DM-EO3	159
	FS-DM-EO8	159
	FS-DM-EO12	159
	FS-DM-EO17	159
	FS-EO1	159
	FS-EO3	160
	FS-EO8	160
	FS-EO12	160
	FS-DM-S-EO1	160
	FS-DM-S-EO8	160
V.	Polymerizable Silicas	161
	5-(Tetrahydropyran-2-yloxy)pent-1-ene	161
	2-(8-Chlorooctyloxy)tetrahydropyran	161
	2-(7-Octenyloxy)tetrahydropyran	162

	FS-C8-P	162
	FS-C8-OH	162
	FS-C8-M-1	163
	7-Octen-1-ol	163
	Acrylic acid pent-4-enyl ester	163
	Methacrylic acid pent-4-enyl ester	164
	7-Octenyl methacrylate	164
	8-(Trichlorosilyl)octyl methacrylate	165
	FS-C8-M-2	165
	FS-C3-M	166
	FS-OTMS	166
	FS-TOM-1	166
	FS-TOM-2	167
	FS-TOM-3	167
	FS-TOM-4	167
	FS-TOM-5	167
VI.	Preparation of composites	168
	1. Compatible composites	168
	2. Cross-linkable composites	168
BIBLIOGRA	<b>APHY</b>	169

#### LIST OF ABBREVIATIONS

AIBN 2,2'-Azobisiso(butylronitrile)

BMA Butyl methacrylate BPO Benzoyl peroxide

CMC Critical micelle concentration

CP/MAS Cross -Polarization Magic Angle Spinning

DEA Diethyl amine

DEAP 2,2'-Diethoxyacetophenone

DEGAME Di(ethylene glycol) allyl methyl ether
DMAEMA Dimethylaminoethylmethacrylate

DMPA 2,2'-Dimethoxy-2-phenyl-acetophenone

dd Doublet of doublet

ddt Doublet of doublet of triplet

dt Doublet of triplet

DSC Differential scanning calorimetry

ETCS Ethyltrichlorosilane MMA Methyl methacrylate

m Multiplet

NVP *n*-Vinyl-pyrrolidone OMA Octyl methacrylate

ODMCS Octyldimethylchlorosilane
ODTCS Octadecyltrichlorosilane
OTCS Octyltrichlorosilane
OTMS Octyltrimethoxysilane

PEGAME Poly(ethylene glycol) allyl methyl ether PEGEMA Poly(ethylene glycol) ethyl methacrylate

PPO 1-Phenyl-1,2-propanedione-2-O-benzoyloxime

s Singlet

SDS Sodium dodecyl sulfate

TEGAME Tri(ethylene glycol) allyl methyl ether
TEM Transmission electron microscopy

TGA Thermogravimetric analyses

TMCS Trimethylchlorosilane.
TMES Trimethylethoxysilane

t Triplet

# LIST OF SCHEMES

Scheme		Page
Scheme 1.	Step-wise silylation mechanism	14
Scheme 2.	Chlorination/reduction of silica surface	15
Scheme 3.	Silanization/hydrosilation of silica surface	17
Scheme 4.	Basic functions of SCAs	22
Scheme 5.	TPM modified of silica	24
Scheme 6.	Composite of colloidal crystals of silica in PMMA	24
Scheme 7.	Functionalization of fumed silica	25
Scheme 8.	Preparation of coreactive initiators	27
Scheme 9.	Pathways to generate initiating radicals	33
Scheme 10.	Fragmentation of ketoxime	36
Scheme 11	Benzoquinone as an inhibitor	41
Scheme 12.	Nitrobenzene as an inhibitor: attack on ring	41
Scheme 13.	Nitrobenzene as an inhibitor: attack on nitro group	42
Scheme 14.	Tertiary amines as anti-oxidants	43
Scheme 15.	Silylations of A200 using modifiers of different lengths	54
Scheme 16.	Silylations of A200 with varying amounts of ODMCS	57
Scheme 17.	Silylations of A200 with dimethylchlorosilane	60
Scheme 18.	Silylations of A200 with triethoxysilane	61
Scheme 19.	Preparation of PEO tethered fumed silicas: first approach	68
Scheme 20.	Preparation of PEO tethered fumed silicas: Second approach	72
Scheme 21.	Preparation of cross-linkable fumed silicas: Method 1	75
Scheme 22.	Synthesis of 7-octen-1-ol	76

	polymer	109
Scheme 25.	Solvent extraction experiments to analyzed surface-grafted	
Scheme 24.	Preparation of cross-linked composite polymer electrolytes	95
Scheme 23.	Preparation of cross-linkable silicas: Method 2	78

# LIST OF TABLES

Table		Page
Table 1.	Useful IR absorptions for characterizing silica surfaces	13
Table 2.	Results of silylation of fumed silica with XSiMe <sub>3</sub>	52
Table 3.	Results of silylations of A200 with	
	octyldimethylchlorosilane (ODMCS).	57
Table 4.	Modified silica fillers and their properties	69
Table 5.	Mixed silylation of A200 with OTMS and TPM	84
Table 6.	Conductivity data of electrolytes with compatible fillers	93
Table 7.	IR data for UV initiated polymerization	100
Table 8.	Thermal properties of PEGDME-LiClO <sub>4</sub> system	103
Table 9.	Thermal transition data of composites before and after cross-linking	g 108
Table 10.	Conductivity data (×10 <sup>4</sup> ) for Figure 43	118
Table 11.	Conductivity data for Figures 47 and 48	126
Table 12.	Formulations of our and Bourgeat-Lami's systems	135
Table 13.	Reaction conditions for FS-TEMS series	173
Table 14.	TMS modified silicas	174
Table 15.	Reaction conditions for FS-Cn series	175
Table 16.	Reaction conditions for FS-DM-C8-n series	176
Table 17.	Preparation of PEO attached silicas: Method 1	177
Table 18.	Preparation of PEO attached silicas: Method 2	177
Table 19.	Products of mixed silylation reactions	177

# **LIST OF FIGURES**

Figure		Page
Figure 1.	Schematic of a battery cell showing its main components	
	and electron flow during discharge	2
Figure 2.	Hydrogen bonding between AEROSIL particles and with water	
	molecules	18
Figure 3.	Thixotropy: decrease in the viscosity during shearing	19
Figure 4.	Schematic representation of the interaction between AEROSIL	
	particles in liquids	20
Figure 5.	Characteristics of photo-induced electronic transitions in carbonyl	
	mompounds	31
Figure 6.	Schematic of UV induced photo-polymerization	39
Figure 7	IR spectra of amine-catalyzed silylation of A200 with excess methyl	
	triethoxysilane	49
Figure 8.	IR spectra showing the effects of reaction time on silylation of	
	A200 with excess MeSi(OEt) <sub>3</sub>	50
Figure 9.	IR spectra of the silylation products of A200 and Me₃SiCl	
	at three silane/Si-OH ratios	53
Figure 10.	IR spectra of silylation products of A200 with RSiCl <sub>3</sub>	55
Figure 11.	TGA curves of silylation products of A200 with RSiCl <sub>3</sub>	56
Figure 12.	IR spectra of silylation products of A200 and C <sub>8</sub> H <sub>17</sub> (Me) <sub>2</sub> SiCl	58
Figure 13.	TGA curves for silylation products of A200 and C <sub>8</sub> H <sub>17</sub> (Me) <sub>2</sub> SiCl	59
Figure 14.	IR spectra of hydride modified A200 as defined by Schemes 16 and	
	17	64
Figure 15.	TGA curves of samples FS-H and FS-DM-H	65

Figure 16.	DSC traces of samples FS-H and FS-DM-H	66
Figure 17.	TGA curves of samples FS-DM-EOn	<b>7</b> 0
Figure 18.	IR spectra of samples FS-DM-EOn	71
Figure 19.	IR spectra of (a) FS-DM-S-EO <sub>1</sub> ; (b) FS-DM-S-EO <sub>8</sub>	73
Figure 20.	IR spectra of samples FS-C5-M-1 and FS-C8-M-1	77
Figure 21.	IR spectra of polymerizable silicas: FS-C3-M and FS-C8-M-2	80
Figure 22.	Schematic representations of A200 (top left),	
	FS-C3-M (top right), and FS-C8-M-2 (bottom)	81
Figure 23.	A portion of the <sup>1</sup> H NMR spectrum of the residue from sample	
	TOM4	84
Figure 24.	Schematic representations of R805 (top) and FS-TOM-4	
	(bottom)	86
Figure 25.	TPM fractions on silica surface and in residue	87
Figure 26.	IR spectra of representative samples from Table 5	88
Figure 27.	<sup>29</sup> Si CP/MAS spectra of samples TOM4 (top spectrum) and	
	FS-C8-M (bottom spectrum)	90
Figure 28.	<sup>13</sup> C CP/MAS spectra of samples TOM4 (top) and FS-C8-M	
	(bottom)	91
Figure 29.	Schematic of PEO modified silicas	92
Figure 30.	Designed models for cross-linkable composite polymer electrolyte:	
	before (top) and after (bottom) cross-linking	96
Figure 31.	IR spectra of composites before (top) and after (bottom) cross-	
	linking	99
Figure 32.	IR-generated cross-linking kinetics. Spectra are a series, and	
	correspond to the original spectrum-the spectrum taken at time t	101
Figure 33.	Conversion of polymerization vs irradiation time	102
Figure 34.	DSC second heating scans for PEGDM-500/LiClO <sub>4</sub> electrolytes.	

	Conditions: run under He at a heating rate of 10 °C/min	105
Figure 35.	DSC second heating scans for PEGDM-500/fumed silica/LiClO <sub>4</sub>	
	electrolytes	106
Figure 36.	DSC second heating scans for cross-linked PEGDM-500/fumed	
	silica/LiClO <sub>4</sub> electrolytes	107
Figure 37.	IR spectra of surface modified silicas. Top scan: Aerosil A-200	
	fumed silica; middle scan: A-200 modified with surface-bound	
	methacrylates; bottom scan: cross-linked composite electrolyte	
	after exhaustive extraction with acetone	110
Figure 38.	TGA scans of surface-modified fumed silicas. Top scan: Aerosil	
	A-200 fumed silica; middle scan: A-200 modified with surface-	
	bound methacrylates; bottom scan: cross-linked composite	
	electrolyte after exhaustive extraction with acetone.	111
Figure 39.	TEM micrographs of A200	112
Figure 40.	TEM micrographs of cross-linkable silica.	113
Figure 41.	TEM micrograph of extraction residue of cross-linked composite	114
Figure 42.	Freeze-Fracture TEM images of composites before cross-linking	115
Figure 43.	Freeze-Fracture TEM images of composites after cross-linking	116
Figure 44.	Conductivity of composite electrolytes at selected	
	temperatures before and after cross-linking	119
Figure 45.	Arrhenius plots of the conductivity of cross-linked composite	
	electrolytes	120
Figure 46.	Scenario 1 (top) and 2 (bottom) as defined in the text	124
Figure 47.	Conductivity vs. solubility parameters difference between	
	PEO and PMA	127
Figure 48.	Conductivity vs. carbon to oxygen ratio in PMA	129
Figure 49.	TGA weight losses for samples as labeled	130

Figure 50.	Dynamic moduli (G' and G'') before and after cross-linking for	
	composites containing 10% cross-linkable silica and 10% butyl	
	methacrylate in a PEGDME-LiClO <sub>4</sub> matrix	
Figure 51.	Conductivity of cross-linkable composite polymer electrolytes	
	before and after cross-linking. Solution (Sol.) in legend is Li	
	imide + PEGDME. Proportions are given in weight percentage	
Figure 52.	A proposed route to a core-shell composite polymer electrolyte 140	
Figure 53.	Schematic of hydrophilic fumed silicas	

## **INTRODUCTION**

## I. Electrolyte Systems

## 1. Primary and Secondary Battery

A battery is defined as a power generating device which transforms chemical energy into electrical energy. Batteries can be classified into two different types: primary and secondary. A primary system is one where the stored energy is inherently present in the chemical substances used and whose useful life is ended once these substances have been consumed by the discharge processes. In contrast, a secondary battery, also known as a rechargeable battery, is capable of being charged or discharged when its chemical substances have been used up. The chemical reaction inside the cell can be reversed by passing current through the cell in the opposite direction to that of cell discharge. A secondary battery can therefore be considered as an electrochemical energy storage unit.

The major components of a simple battery cell consist of anode, cathode, electrode separator and electrolyte as illustrated schematically in Figure 1 where the two electrodes are connected electronically together and placed in an ionically conducting electrolyte. The electrolyte can be different materials with diverse characteristics and will be the center topic of the following discussion. Based on the physical state, an electrolyte can be defined as liquid, molten, solid, or gel electrolyte.

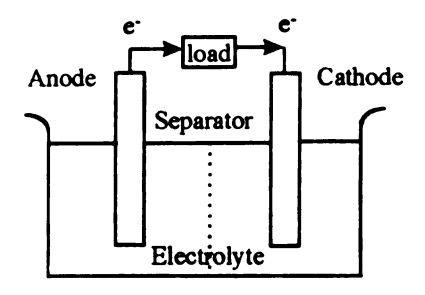


Figure 1. Schematic of a battery cell showing its main components and electron flow during discharge.

## 2. High-Energy-Density Battery

It is always desirable to develop new batteries incorporating high energy density and long operating life. In designing such a battery system, one has to consider factors associated with energy density. In the above example, if zinc is used as anode and copper as cathode, the half-cell reactions during charging are shown in equations 1 and 2:

At anode 
$$Zn = Zn^{2+} + 2e^{-}$$
 (1)

At cathode 
$$Cu^{2+} + 2e^- \rightleftharpoons Cu$$
 (2)

At equilibrium, the overall cell reaction is given by equation 3:

$$Cu^{2+} + Zn = Cu + Zn^{2+}$$
 (3)

The maximum electrical work available from this reaction can be expressed by the Gibbs free energy change of the reaction (equation 4):

$$\Delta G = -n F E \qquad (4)$$

where n is the number of mol of electrons passed, F is the Faraday constant (96487 C/mol), and E is the electromotive force (e.m.f.) and can be calculated from equation 5:

$$E = E_{cathode} - E_{anode}$$
 (5)

The energy density of a battery (E.D.) is directly related to the free energy variation ( $\Delta G$ ) of the cell reaction and to the weight of all chemical reactants ( $\Sigma wt_r$ ) (equation 6):

E.D. = 
$$(-\Delta G) / \Sigma wt_r = n F E / \Sigma wt_r$$
 (6)

Based on this equation, light electropositive metals such as alkaline and alkaline earth metals are therefore the elements of choice for a high energy-energy-density battery, since a more negative  $\Delta G$  (large E) and a small  $\Sigma wt_r$  will be possible. Among these elements, lithium is particularly attractive due to its high standard potential and low equivalent weight. The following sections will focus on Li-based electrolytes.

#### 3. Electrolytes for Lithium Batteries

### a. Liquid Electrolytes

As lithium reacts with water and other protic solvents, only aprotic organic solvents are feasible as the basic materials for lithium cell electrolytes. Polar organic compounds are often used. The most commonly used organic solvents include cyclic esters (ethylene carbonate, propylene carbonate, y-butylrolactone), linear esters, amides and sulfoxides. 1 A mixed solvent is sometimes preferred since the properties of the electrolyte solution (conductance, viscosity, etc.) and its reactivity towards lithium can often be "tailored" to give optimum performance. Choice of electrolyte salt is often limited mainly by solubility which must be high so that the resulting solution will have sufficient conductivity and hence the cell will have a relatively low internal resistance. In non-aqueous solutions of lithium salts, the lithium cation is solvated strongly by the solvent, while the anion is less subject to this influence. In choosing an organic solvent, it is important to consider the stability of the electrolyte in contact with lithium metal. It is generally accepted that no solvent is thermodynamically stable towards Li. The success of commercial Li battery systems is dependent on the kinetic stability of a passivating protective film,<sup>2</sup> consisting of insoluble reaction products of Li with the electrolyte. Its nature depends largely on the composition and purity of the electrolyte. The film acts as a solid phase between the metal and the solution. It has the property of a solid Li ion conductor with high electrical resistance and is referred as the SEI (solid electrolyte interphase).<sup>3</sup> The reaction of Li with propylene carbonate serves as a good example of

anode-electrolyte reactions and the formation of SEI phase (Li<sub>2</sub>CO<sub>3</sub> in this case, equation 7):

O + Li 
$$\longrightarrow$$
 CH<sub>2</sub>=CH—CH<sub>3</sub> + Li<sub>2</sub>CO<sub>3</sub> (7)

Film formation ensures long shelf-life for Li cells, but causes severe problems for good electrode cyclability. This, along with relative poor conductivity, led to research on cells with molten salts which offer true thermodynamic stability towards Li metal due to the absence of solvents. They also enable high power capacity to be achieved because of their excellent ionic conductivity. Unfortunately, there are many problems concerning reliability, safety, cycle life, corrosion and others connected with these advanced technology systems.

## b. Solid Polymer Electrolytes (SPEs)

An ideal battery cell should feature many characteristics, including the absence of the problems associated with liquid electrolytes. An ideal battery would have a long life time, a broad range of operating temperatures, no separator, and efficient construction and packaging. An all solid-state battery system would possess a number of these desirable characteristics. Unfortunately, high ionic conductivity in the solid state is still difficult to achieve. Moreover, good contact between solid state electrolytes and electrodes is difficult to maintain during successive discharge/charge cycles.

The discovery of a new class of solid state electrolytes, i.e., the solid polymer electrolytes (SPEs)<sup>4</sup> allowed many of the problems discussed above to be solved. Armand reported that certain heteroatom-containing high molecular weight polymers, poly(ethylene oxides) in particular, could conduct alkali metal ions to levels > 10<sup>-4</sup> S/cm. The physical properties of polymer electrolytes are such that they can easily be produced in thin high area sheets using standard thick film processing technologies. Although physically solid, polymer electrolytes behave as viscous liquids at the microscopic level and hence form an excellent interface with solid electrodes. Moreover, they can easily accommodate electrode volume changes during cycling by microscopic polymer flow. In other words, SPE makes it possible to manufacture all-solid-state cells and batteries without the difficulties generally associated with the use of rigid or liquid/molten electrolytes.

There has been much effort in developing devices using polymer electrolytes in the past twenty years.  $^{5-7}$  Although the potential benefits of SPE are well recognized, few such systems are used in applications. This is because the successful use of polymer electrolytes requires them to be highly conductive, mechanically strong, yet processable. NMR studies  $^{8}$  have shown conclusively that the amorphous phase is responsible for the ionic motion in polymer electrolytes. High molecular weight PEO is highly crystalline and its mixtures with salt tend to contain either crystalline PEO or high melting polymer-salt complexes. At ambient temperature, PEO-based electrolytes are generally poor conductors ( $\sigma < 10^{-8}$  S/cm) due to the high degree of crystallinity. Reasonable

conductivity can be achieved ( $\sigma > 10^{-5}$  S/cm) at temperatures of the order of 100 °C, but the mechanical properties of the polymer are significantly poorer due to the loss of crystallinity in the polymer hosts. Consequently, these electrolytes are themselves of limited applicability in the development of practical devices.

A number of approaches have been used to prepare amorphous forms of PEOs.

This includes copolymerization, <sup>9</sup> introducing defects into the polymer chain that disrupt the crystalline structure, <sup>10</sup> attaching PEO oligomers to polymers having low glass transition temperatures, <sup>11-15</sup> and the synthesis of branched and hyperbranched polymers. <sup>16-19</sup> A general review has appeared recently. <sup>20</sup> Typical conductivities at 30 °C for polymer-salt complexes derived from amorphous PEOs reached 5×10<sup>-5</sup> S/cm. Often, however, the mechanical properties of these materials were disappointing, those with the best conductivity often creeped and lacked mechanical stability.

Blends of a third component with polymer electrolytes can be used to increase the mechanical property, and ionic conductivity as well in some cases. One type of blend is a "gel electrolyte" which incorporates a plasticizer in addition to polymer and lithium salt. A number of polar polymers and low molecular weight substances have been used to make gel electrolytes and work in this area has been recently reviewed<sup>21</sup> and explored further by Abraham<sup>22</sup> and Wieczorek<sup>23</sup> and others.<sup>24</sup> To be brief, polymers used include poly(vinylidene fluoride) (PVdF), poly(ethylene oxide) (PEO), poly(vinyl chloride) (PVC), poly(vinyl alcohol) (PVA), poly(acrylonitrile) (PAN), and polystyrene (PS). In addition,

electrolytes made of low molecular weight polymers supported by a interpenetrating polymer networks (IPNs) have also been reported. 25,26 Plasticizers can be classified into two types: (1) low molecular weight organic solvents such as propylene carbonate (PC), ethylene carbonate (EC), THF, DMF, and y-butyrolactone (yBL); (2) low molecular weight polyethers including poly(ethylene glycol) (PEG) and derivatives and ethylene oxide (EO) and propylene oxide (PO) copolymers (EO-PO). Organic solvents offer higher conductivity whereas oligomers provide more reliability. PEGs were found superior to the methylated counterparts in terms of solvation of salt and conductivity. Unfortunately, OH groups on these substances are not stable towards lithium metal. These added plasticizers solvate the salt easily, reduces the viscosity, and increase the conductivity of the system due to their low molecular weight and high dielectric constant. The conductivity follows an Arrhenius-type temperature dependence and the activation energy is independent of polymer concentration, suggesting that ions migrate primarily through the solvent domain which surrounds the polymer matrix. Thus the role of the polymer in a gel electrolyte is no longer that of an ionic conductor, but rather as a binder or sponge that contains solvent and provides favorable mechanical properties. Gel electrolytes are attractive since they offer liquid-like conductivity with similar processability as solid state electrolytes. 27,28 Electrochemically, however, gel electrolytes contain organic solvents and retain many of the limitations of the corresponding liquid electrolytes such as diffusion and decomposition of the electrolyte at the electrode surface. Replacing organic solvents with low molecular weight polymers as plasticizers seems promising since these oligomers are much less volatile and more stable towards active metals.

Application of a polymer to PEO-salt complexes has been reported to improve mechanical stability. Tsuchida et al<sup>29</sup> studied systems of PEO-LiClO<sub>4</sub> (molecular weight = 400 - 20,000) supported by poly(methacrylic acid). Although the mechanical properties were increased, the conductivity was poor. Grav et al<sup>30</sup> reported a polystyrene supported PEO-LiCF<sub>3</sub>SO<sub>3</sub> electrolyte. Above the percolation limit, mechanical stability was significantly improved at high temperatures while conductivity was decreased only slightly. Similar studies were carried out with PEO-MX (MX = NaI, LiI, LiClO<sub>4</sub>, and LiBF<sub>4</sub>) blended with poly(methyl methacrylate). 31,32 A room temperature conductivity as high as 2.4×10<sup>4</sup> S/cm was realized for the polymer blend incorporating LiClO<sub>4</sub>. A copolymer of styrene and methoxypolyethylene glycol methacrylate was also used to improve mechanical stability and reduce crystallinity. 16 A new blend system was reported recently<sup>23</sup> involving free radical polymerization of methyl methacrylate in a solution of  $LiCF_3SO_3$  and ethylene oxide-propylene oxide copolymer (molecular weight = 2600). An ambient temperature conductivity of 3×10<sup>-5</sup> was obtained and the electrolyte-electrode interface was improved.

Blends of polymer electrolytes and fillers have been studied with the goal of improving the mechanical stability and conductivity of simple high molecular weight polymer electrolytes. This is significant since such polymers are often susceptible to creep, particularly at elevated temperatures. The earliest research in this area was done by Weston and Steele<sup>33</sup> who incorporated various proportions of an inert filler ( $\alpha$ -alumina) into PEO-LiClO<sub>4</sub>. Above 20 % by volume, the filler aggregated to form large insulating

regions. At 10 % filler, the conductivity was not significantly impaired but there was no evidence of creep up to 120 °C. A number of studies of PEO mixed with ceramic powders have been reported since then mainly by the Wieczorek<sup>34,35</sup> and Scrosati<sup>15,36,37</sup> research groups. One of the interesting findings was that hydrophilic fillers showed a stronger interaction with the polymer than the hydrophobic material, and composites formed with the hydrophilic material showed a reduction in polymer crystallinity and a higher conductivity. More recently, Scrosati and coworkers<sup>38</sup> reported a complex system involving filler material, high and low molecular weight PEO, lithium imide, and either propylene (PC) or ethylene carbonate (EC) in some cases. High conductivity was achieved and attributed to the plasticizing effect from both low molecular weight substances and the lithium salt, whereas good mechanical properties were thought to be due to the contribution from the filler material. It is now generally accepted that introducing an inert filler material is an effective means of increasing mechanical properties and stability of the lithium/electrode interface. Further more, if the particle size of the filler was small, (i.e., lower than 5 um. 36) the electrochemical properties of the electrolyte could be significantly enhanced. In most cases, the highest increase was found at the concentration range of filler up to 10-20 % by volume. NMR and X-ray diffraction studies<sup>35</sup> confirmed that the enhancement of conductivity was due to stabilized and increased PEO amorphous phase content in the composite polymer electrolyte. The explanation for this behavior was that the presence of highly dispersed particles in the polymer matrix affects the crystallization rate by preventing the agglomeration of polymer chains. A small particle size is important for assuring a highly dispersed distribution of the filler material throughout the polymer

matrix. An optimum concentration of the filler is necessary to suppress the crystallization rate of the polymer host and to prevent phase discontinuity and filler-catalyzed agglomeration of polymer chains.

There are problems associated with these composite polymer electrolyte systems.

The room temperature conductivity is still low (< 10<sup>-5</sup> S/cm) since high molecular weight

PEOs were used in most cases, and the long term stability of these composites are

questionable. Finally, the interpretation of conductivity data is rather complex.

## 4. New Polymer Electrolyte Systems

In 1992, Fritz and Stein reported a new system incorporating fumed silica as one of the components of a novel solid electrolyte.<sup>39</sup> This new type of electrolyte was obtained by immobilizing solutions of lithium salts in aprotic solvents in hydrophilic fumed silica. A room temperature conductivity as high as 10<sup>-2</sup> S/cm was realized which is comparable or even higher than the pure liquid electrolytes. Three years later, another publication appeared<sup>40</sup> on the rheology and conductivity of composite polymer electrolytes that incorporate hydrophobic fumed silica and low molecular weight PEO. In addition to a good conductivity, the composites were also mechanically stable and processable - characteristics attributed to the branched, three-dimensional fumed silica network. Research with an emphasis on the electrochemistry of the same system was also carried out.<sup>41</sup> High room temperature conductivity, a large potential window, and a relatively stable interface with lithium electrodes were demonstrated by these authors. To better understand these new systems, it is essential to know some of the fundamental

properties of fumed silica particles and their interactions among themselves and with organic molecules.

### a. Basic Characteristics of Fumed Silica

Representatives of fumed silica are those with the trade mark AEROSIL produced by Degussa. These fumed silicas are made through continuous flame hydrolysis of silicon tetrachloride. During this process, SiCl<sub>4</sub> is vaporized and then reacted with water vapor formed from an oxyhydrogen flame to produce the desired silicon dioxide. The only byproduct is gaseous HCl which is separated from the solid product. Fumed silicas thus produced are amorphous, nonporous, and thermally stable. Their primary particles are almost spherical and extremely small, ranging from 7 to 40 nm <sup>42</sup>.

In general, the most important characteristic of silica is its surface chemistry. Since the surface area is large in relation to the mass, the surface chemistry plays a significant role. There are two types of functional groups on the surface of silica: hydrophilic silanol groups and hydrophobic siloxane groups. The surface chemistry of pristine silicas is dominated by silanol groups which are necessary for certain applications. However, for other applications such as stationary phases for metal ion chromatography, <sup>43</sup> catalysts, <sup>44</sup> as well as immobilized enzymes, <sup>45</sup>, a hydrophobic surface is desirable. In this case, a chemical after treatment process can be used to modify the silica surface. Typically, an alkoxysilane or chlorosilane can be used to react with silica to replace silanol groups with organic groups - a process often termed silylation. It is sometimes important to know the density of silanol groups on the pristine and modified silicas. The most reliable method for

quantitative analysis so far is a lithium aluminum hydride method in which the amount of hydrogen gas released from reaction between silanol groups and hydrides is measured and the silanol group density is determined. IR spectroscopy, on the other hand, is a convenient method for qualitative analysis. <sup>46</sup> Table 1 lists some important IR absorption bands of furned silicas. There have been numerous reports on silica surface modification and characterization. <sup>46-52</sup>

Table 1 Useful IR absorptions for characterizing silica surfaces.

Functional Groups	IR Absorption (cm <sup>-1</sup> )
SiOH isolated	3747
SiOH bridged	3200-3800
SiOH bridged, proton acceptor	3720
SiOH bridged, proton donor	3520
SiOSi combination	1860
НОН	1620
	······

Two research groups, Blitz and co-workers and Tripp and co-workers, contributed most to the understanding of interactions between silanes and surface silanol groups. Blitz and co-workers<sup>53</sup> used diffuse reflectance FTIR spectroscopy to study the silylation of Cab-O-Sil, a commercial fumed silica, with alkoxysilanes by and concluded that silanes did not bond to the silica surface after high-temperature curing in the absence of water. When surface-adsorbed water was present, post-reaction curing increased hydrolysis and

condensation to form siloxane bonds. The same authors<sup>54</sup> also conducted silylation reactions in the presence of amines. They found that amines with exchangeable protons catalyzed the reaction greatly and proposed two possible mechanisms. Scheme 1 shows a step-wise reaction mechanism. The first step is adsorption of amine to the silanol site. Hydrogen bonding between amine nitrogen and silanol hydrogen makes the silanol oxygen more nucleophilic. The next step is nucleophilic attack of this oxygen to silane molecules and the subsequent formation of a penta-coordinated intermediate. The leaving group (OMe) abstracts a proton from the amine to form MeOH, and the amine takes away the silanol proton and starts another catalytic cycle. The second silylation mechanism involves concerted bond breaking and bond formation. This mechanism is expected to be energetically favorable due to a 6-membered ring transition state shown as I.

Scheme 1. Step-wise silvlation mechanism

More recently, Tripp and Hair<sup>55-57</sup> developed a method by which chlorosilanes can be effectively attached to the surface of AEROSIL silica through chemical bonding. This process also uses an amine adsorbed onto the silica surface to promote the reaction. Their proposed mechanism is similar to Blitz's step-wise mechanism in that a pentacoordinated intermediate was considered to be involved. The difference between when chlorosilanes are used instead of alkoxysilanes is that the by-product is a strong acid and needs to be neutralized by stoichiometric amounts of base. In other words, the base is no longer a catalyst.

Scheme 2. Chlorination/reduction of silica surface

Using a different silvlation reaction to modify silica surface, Sandoval et al<sup>58-60</sup> reported a novel synthetic approach to produce chemically bonded silica-based chromatography stationary phases. The procedure involves the preparation of a silica intermediate containing stable silicon hydride surface species, followed by the catalytic addition of this hydride modified silica to organic compounds bearing a terminal vinyl group - a reaction developed by Speier<sup>61</sup> thirty years ago and often referred to as hydrosilation. The preparation of the hydride intermediate was first carried out via chlorination of silica followed by reduction with lithium tetrahydridoaluminate (Scheme 2). 58,59 Since this chlorination / reduction sequence had limitations such as extreme sensitivity to moisture during both steps, they later developed a new approach, referred by these authors as "silanization" (Scheme 3), which involves the controlled deposition of the hydrolysis product of triethoxysilane or related silanes to preferentially form an Si-H monolayer on silica. 60 This new approach of making surface bonded materials was believed to have advantages over the traditional method since it results in stronger surface attachment. It has long been known that in the case of trifunctional silanes reacting with silica surface, the number of linkages range from 1 to 3. Such linkages result from covalent attachment of the silane to the silica surface and from cross-linking between adjacent silanes. Using silanes that contain a hydride instead of a bulky alkyl leads to greater condensation with silanols because of the minimal steric hindrance of the hydride. Products made from this method show greater hydrolytic stability, suggesting a larger number of siloxane linkages.

Scheme 3. Silanization/hydrosilation of silica surface

$$Si-OH + RO-Si-H \xrightarrow{H_2O, HCl} Si-O-Si-H + ROH$$

$$Pt Cat. CH_2=CHR'$$

## b. Thickening and Thixotropic Effects of Fumed Silica

The interactions between silica particles themselves and with the dispersion phase play a decisive role. Two important interactions are: (1) van der Waals attractive forces, and (2) hydrogen bond interactions. In comparison with precipitated silicas, fumed silicas have a lower silanol group density (2.5/nm²) and therefore little possibility exists for the formation of intra-particular hydrogen bridge linkages and only inter-particular hydrogen bonding needs to be considered. Figure 2 shows hydrogen bonding linkages between silica primary particles and with water. Hydrogen bonding becomes less important when silanol groups are replaced chemically by organic groups, and the extent of this effect depends on the degree of replacement and the length of organic groups. Long alkyl groups tend to shield the functional groups on the silica surface. The lower the silanol group density (or the higher the organic group coverage), or the longer the alkyl groups, the less hydrophilic

the silica surface. Silicas with significant amounts of alkyl groups show hydrophobic characteristics and van der Waals attractive forces may become dominant.

Figure 2. Hydrogen bonding between AEROSIL particles and with water molecules.

If AEROSIL is dispersed in a liquid, the surface groups interact with each other either directly or indirectly via the molecules in the liquid. The affinity can be attributed to hydrogen bonding in the case of hydrophilic silicas, and to both van der Waals attractions and hydrogen bonding between surface organic groups and residual silanol groups in the case of hydrophobic silicas. Such interactions result in a temporary, three-dimensional network structure and a thickening effect. Under a mechanical stress (intensive stirring or shaking), the structure is broken down and the viscosity drops. In the static state, the structure reforms. This process is termed thixotropy and is represented schematically in a viscosity-time plot shown in Figure 3. A more vivid picture showing the aggregation patterns of silica particles during shearing and standing is given in Figure 4 where only the

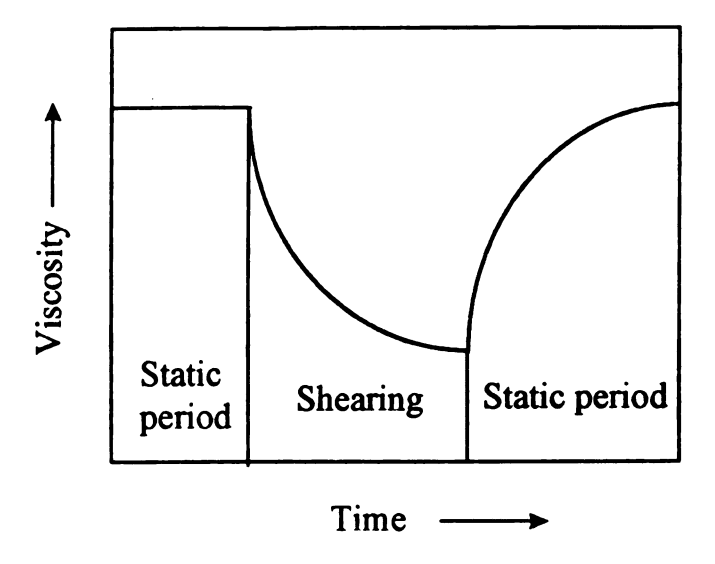
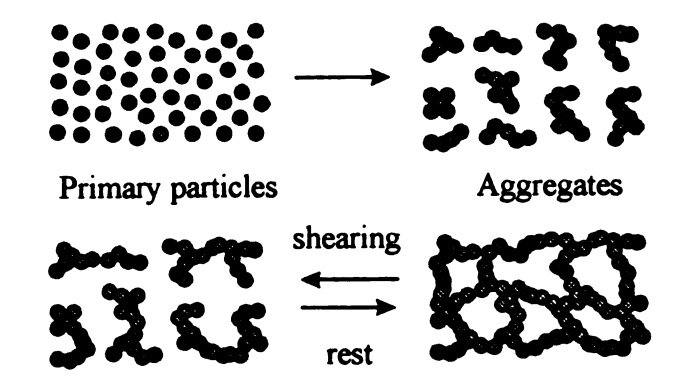


Figure 3. Thixotropy: decrease in the viscosity during shearing.

case of hydrophilic silica is shown. The thickening and thixotropic effect of AEROSIL silicas is the basis for many of their applications such as anti-setting agents and coatings. 62 Such effects depend on the relative polarity of silica surface and the liquid. In the case of hydrophilic silicas in polar solvents, the silica particles are solvated/wetted by the solvents and screened against external effects by hydrophobic alkyl groups from liquid molecules. Consequently, a destabilization of the thixotropic network occurs. For this reason, a gel is only possible with large amounts of hydrophilic silica. In contrast, gelation is possible in non-polar liquids by using small amounts of silica. To summarize, hydrogen bonding between AEROSIL particles is maximized in non-polar fluids.



Agglomerated aggregates Three-dimensional network

Figure 4. Schematic representation of the interaction between AEROSIL particles in liquids.

#### c. Current Work

With the fundamental knowledge of furned silicas, let us re-examine the new solid electrolyte systems mentioned earlier. In Fritz and Stein's system, <sup>39</sup> polar organic solvents and hydrophilic furned silica were employed. It is not surprising that they needed to use up to 20 wt% of furned silica to obtain a "paste-like" electrolyte. In the second system, <sup>40,41</sup> 10 % by weight of hydrophobic furned silica was enough to bring about a free-standing gel. As discussed above for polar solvents, which have to be used in order to dissolve reasonable amounts of lithium salt, a hydrophobic instead of a hydrophilic silica is a better choice. Another advantage of the second system was the use of low molecular weight poly(ethylene oxide), which has a much lower volatility. Finally, PEOs contain only the C-O functional group - one of the most stable groups in organic chemistry, and therefore should have favor electrochemical stability towards electrodes. We have known from previous discussions that complexes of high molecular weight PEO with salt are crystalline

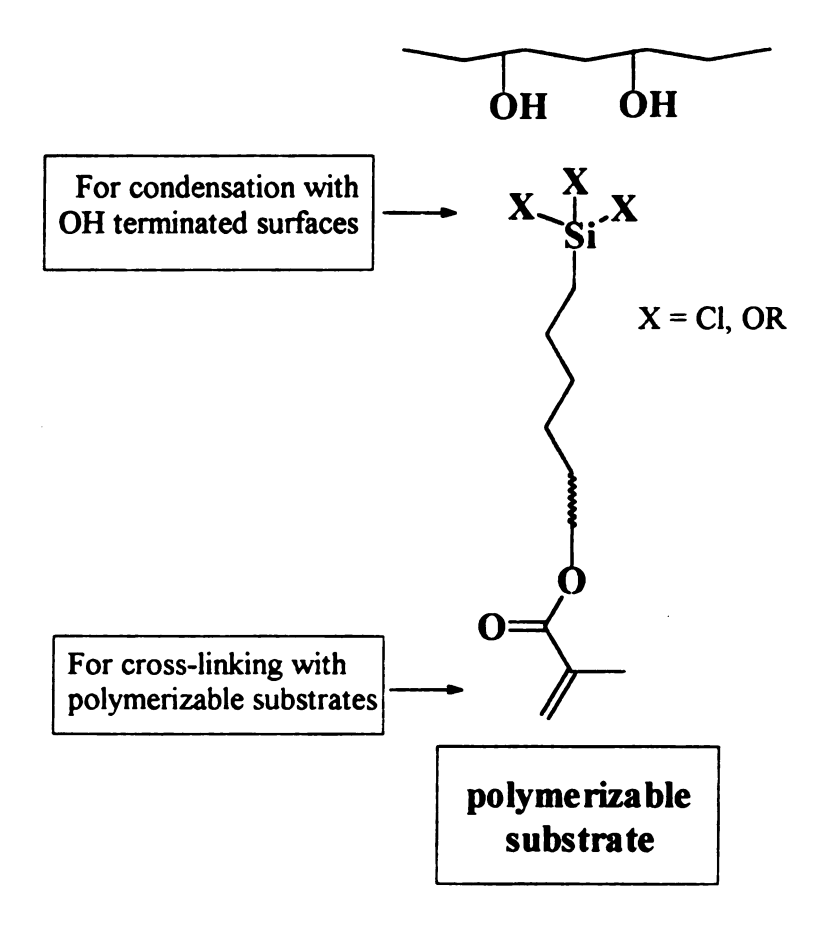
at room temperature and the conductivity is too low for practical usage unless a high temperature ( $> T_m = 60$  °C) is reached. Poly(ethylene glycol)s and derivatives with molecular weight lower than 500 are amorphous liquid at room temperature and therefore would offer high ionic conductivity once mixed with lithium salt. Although these oligomers are of little value by themselves as solid polymer electrolytes, they can be incorporated into a fumed silica network. In doing so, both high ionic conductivity and good mechanical properties will be ensured.

The major advantage of using fumed silica as a filler material is that it can be modified in many different ways. In addition to tuning the polarity and hydrophobicity, one can also attach a polymerizable group on fumed silica surface. This involves the use of a class of compounds called silane coupling agents (SCA) with the following general formula (equation 8):

$$R_{(4-n)}SiX_n \qquad (8)$$

where X is a hydrolyzable group such as a chloro or alkoxy group; R is a non-hydrolyzable functional group such as ethylene oxide, (meth)acrylate, hydroxyl or thiol. A schematic representation of a silane coupling agent and its functions is shown in Scheme 4. These compounds are effective linkers between two inorganic substrates or between an inorganic substrate and an organic moiety. They play an important role in many areas in industry. 63

Scheme 4. Basic functions of SCAs.



Silicas containing pendant polymerizable groups are useful in making composite polymeric materials. They serve as a "monomer" and will co-polymerize with another monomer. In a recent example, Ford and coworkers<sup>64,65</sup> published papers on a composite of colloidal crystals of silica in poly(methyl methacrylate) (PMMA).

Monodisperse silica particles were prepared using a sol-gel process by hydrolyzing tetraethoxysilane in the presence of water and ammonia. 3-(Trimethoxysilyl)-propyl methacrylate (TPM) was introduced on silica surface by basic hydrolysis and condensation to form TPM oligomers which were then adsorbed and condensed on silica surface. (Scheme 5). These TPM modified particles form colloidal crystals spontaneously once dispersed in a proper solvent. Such dispersions are useful materials as optical rejection filters and optical limiters. Addition of methyl methacrylate and copolymerization with polymerizable silica (Scheme 6) formed robust films while the crystal structure was retained. These novel materials are more stable and may find wider applications in selective filters and other optical devices.

Another recent example involving SCA modified silica was reported by Guyot and coworkers. 66-69 They carried out emulsion polymerization of poly(ethyl acrylate) in the presence of functionalized and non-functionalized fumed silica particles. SCA modification of the silica surface was done in two steps using two different kinds of coupling agents, 3-(trimethoxysilyl)-propyl methacrylate (TPM) and 3-(trimethoxysilyl)-propane thiol (TESPT). The SCA was first hydrolyzed in water, the partly condensed silane was added to a silica suspension in toluene (Scheme 7). The pre-hydrolysis step helps increase the

Scheme 5. TPM modified of silica.

$$RSi(OEt)_{3} \xrightarrow{hydrolysis} RSi(OH)_{3} \xrightarrow{condensation} \xrightarrow{R} OH$$

$$TPM oligomer$$

$$Si(OEt)_{4} \xrightarrow{EtOH} SiO_{2} -OH \xrightarrow{R} RSi(OH)_{3} \xrightarrow{SiO_{2}} OH$$

$$R = CH_{2}CH_{2}CH_{2}OCC = CH_{2}$$

$$CH_{3}$$

# Scheme 6. Composite of colloidal crystals of silica in PMMA

Scheme 7. Functionalization of fumed silica

$$(CH_3O)_3$$
—Si— $(CH_2)_3$ —R

1.  $H_2O$ 

2.  $SiO_2$ —OH in toluene

 $SiO_2$ —O—Si— $(CH_2)_3$ —R

R = SH TESPT-grafted silica

degree of attachment of the coupling agent. The TPM modified silica serves as a commonomer whereas TESPT modified silica is not polymerizable and acts only as a chain transfer agent. In the first case, large amounts of polymer was grafted onto silica surface through small sized "loops". In the second case, although chemical bonding between surface and polymer is also present, no such loops formed. Their studies showed that, while both functionalized and non-functionalized silicas can result in significant reinforcement effects as evidenced by an increase in Young's modulus, the mechanical properties at large strains are greatly improved only when silicas with polymerizable groups were used.

An alternative way of making covalently surface-bound polymer is to carry out polymerization using photo-initiators chemically attached to the surface - the so-called core-active initiators. Koehler and Ohngemach<sup>70</sup> were the first to introduce a photo-initiator group to a surface. For example, triethoxylsilyl substituted (2-hydroxy-2-propyl) phenone was prepared by hydrosilation followed by silylation with silica gel (Scheme 8). Such core-active photo initiators were used under unstirred conditions to polymerize dimethylaminoethylmethacrylate (DMAEMA) and *n*-vinyl-pyrrolidone (NVP). By changing the monomer concentration and the initiator content on the silica surface, they were able to regulate the amount of polymer bonded to surface. The intermolecular distance of monomers was believed to determine the radical transfer which in turn affected the photo-polymerization process.

We are interested in making composite polymer electrolytes with desirable conductivities, permanent mechanical properties and dimensional stability, and processability. This can be done by extending the work done by Khan <sup>40</sup> and Fan <sup>41</sup> by using SCA or core-active initiator modified silicas. It is not difficult to imagine that if a combination of an appropriate polymerizable silica, PEO oligomer, lithium salt, free radical initiator, and small amount of co-monomer (e.g., alkyl methacrylate) would result in a gel-like material due to the thickening effect discussed above. Upon irradiation with UV light, co-polymerization between this silica and the added monomer would take place, yielding a cross-linked composite polymer electrolyte. In the case of core-active initiator modified silica, a free radical initiator will no longer be necessary yet a similar material

# Scheme 8. Preparation of coreactive initiators

$$(CH_{3}CH_{2}O)_{3}SiH + CH_{2}=CHCH_{2}OCH_{2}CH_{2}O - C - C - OH CH_{3}$$

$$(CH_{3}CH_{2}O)_{3}Si - CH_{2}CH_{2}CH_{2}OCH_{2}CH_{2}O - C - C - OH CH_{3}$$

$$(CH_{3}CH_{2}O)_{3}Si - CH_{2}CH_{2}CH_{2}OCH_{2}CH_{2}O - C - C - OH CH_{3}$$

$$SiO_{2} - O - Si - CH_{2}CH_{2}CH_{2}OCH_{2}CH_{2}O - C - C - OH CH_{3}$$

$$SiO_{2} - O - Si - CH_{2}CH_{2}CH_{2}OCH_{2}CH_{2}O - C - C - OH CH_{3}$$

$$SiO_{2} - O - Si - CH_{2}CH_{2}CH_{2}OCH_{2}CH_{2}O - C - C - OH CH_{3}$$

$$O - CH_{3} - CH_{3}CH$$

would be expected to be realized. The significance of cross-linking process lies in the fact that, instead of a temporary three-dimensional network resulted from thixotropic effect, a permanent robust network structure would be created which features long-term mechanical and dimensional stability.

There are multiple issues involved in the successful preparation of such a cross-linkable composite. (1) surface properties (polarity/hydrophobicity) of polymerizable silica. We have pointed out that hydrophobic silica would be the material of choice since low molecular weight PEOs are polar solvents. On the other hand, most polymerizable functional groups, e.g., methacrylate, are polar and methodology has to be developed to compensate accordingly. (2) selection of co-monomer. This is crucial since the property of formed polymer will directly influence the conductivity of electrolyte. (3) conditions necessary to bring about a photo-polymerization. The next section will discuss certain aspects regarding photo-initiation of polymerization.

## II. Photoinitiation of Polymerization

Many chemical reactions are induced by external energy such as heat and light.

Light-initiated reactions, or photochemical reactions are attractive since light intensity can be controlled conveniently and the light sources can be turned on or off very easily. Other benefits of photochemical reactions include rapid reaction, low energy requirements, low temperature operation, and non-polluting in cases of solvent-free systems. Since light can only penetrate a thin layer, photo-polymerization is mainly used for thin-film applications. In this section, we will first give a brief summary regarding interactions of light with absorbing species, including photo-induced electronic transitions, and then move on to photoinitiation of polymerization.

## 1. Theory

The relationship between absorbance, the sample thickness, and the concentration of the absorbing species can be expressed by Lambert-Beer law:

$$A = Log_{10} (I_0/I) = \epsilon c b$$
 (9)

A: absorbance,

I<sub>0</sub>: incident light intensity,

I: Intensity of light exiting the sample,

c: concentration of solute in moles/liter,

b: optical path length in cm,

ε: molar absorptivity in mol<sup>-1</sup>cm<sup>-1</sup>.

If we define I<sub>abs</sub> as the fraction of light absorbed by a solution, then

$$I_{abs} = I_0 (1-10^{-ecb})$$
 (10)

A UV spectrum is usually a plot of wavelength vs. molar absorptivity. The former represents the energy necessary to bring about an electronic transition between ground state and excited state; and the latter is an indication of probability of such transitions. Figure 7 gives electronic transitions and their characteristics in the case of carbonyl compounds (only one nonbonding orbital is shown). The  $n \to \pi^*$  transitions of single chromophoric groups are symmetry forbidden (non bonding orbital on oxygen is orthogonal to  $\pi$  anti-bonding orbital), and as a result, the molar absorptivity is low ( $\varepsilon$  < 100).  $\pi \to \pi^*$  transitions, on the other hand, are allowed and therefore often show strong absorptions ( $\varepsilon$  > 10,000). In Figure 7, S<sub>0</sub>, S<sub>1</sub>, and S<sub>2</sub> are ground, first and second excited singlet states, respectively, T<sub>1</sub> and T<sub>2</sub> are first and second triplet excited states. Internal conversion (IC) is a term often used to describe transitions between S<sub>2</sub> and S<sub>1</sub>, and intersystem crossing (ISC) represents transitions between singlet and triplet states.

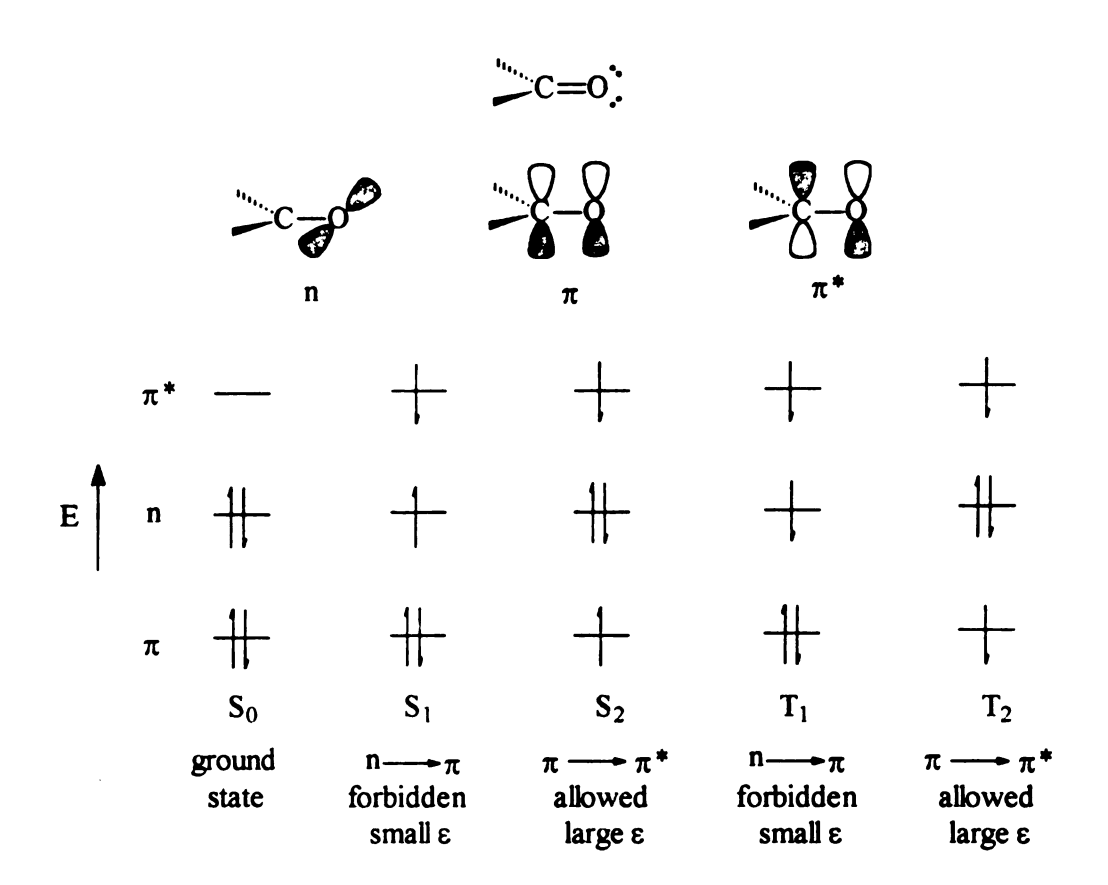


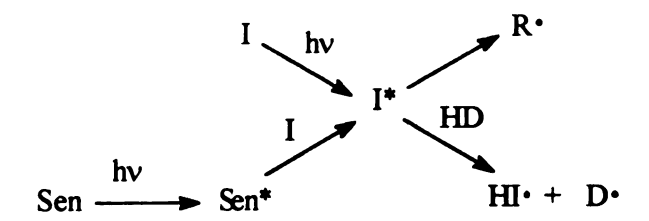
Figure 5. Characteristics of photo-induced electronic transitions in carbonyl compounds.

### 2. Polymerization Initiators

As in other chain reactions, polymerization involves three basic steps: initiation. propagation, and termination. In principle, any monomer will undergo photolysis upon absorption of light with enough energy. But only conjugated monomers absorb above the vacuum UV region (>200 nm). Often times, even these monomers themselves do not form reactive enough radical species upon light absorption to initiate a chain reaction. In other words, the initiation efficiency is too low. For this reason, other molecules are often used that combine sensitivity to UV radiation and ability to provide a reasonable initiating efficiency. In choosing an initiation system, one has to consider the availability of light sources and reaction vessels. Quartz transmits light above 200 nm whereas glass does so only above 325 nm. As far as the light source is concerned, low pressure mercury lamps only generate significant numbers of photons at 254 nm and therefore medium (or high) pressure mercury lamps are often used that give light with a broader energy distribution (254, 280, 297, 303, 313, 334, 366 nm). 71 Light filters can be used if a light with a certain wavelength is desirable. Since Pyrex reaction vessels are always more handy than quartz ones, people tend to choose an initiator system which absorbs above 325 nm and matches well one of the lines in the spectrum of medium (or high) pressure mercury lamps.

Scheme 9 show three pathways to generate reactive species. The simplest case is when only one kind of molecule, the initiator (I), is involved. This initiator absorbs light (hv), is excited (I\*), and finally yields radicals (R•) to initiate polymerization. When a hydrogen donor (HD) (often termed a co-initiator) is present, initiators in excited states,

Scheme 9. Pathways to generate initiating radicals



typically those built on benzoyl chromophore, abstract a hydrogen from the co-initiator to generate a pair of radicals (HI• and D•). These radicals initiate polymerization directly or do so after a few fragmentations. A photo-sensitizer (Sen), defined as a molecule capable of absorbing light and transferring excitation to the initiator, is sometimes used. The idea behind a photo-sensitizer is that when I\* cannot be produced directly by irradiation of I with a certain wavelength, the excitation is accomplished by first photo-exciting the photosensitizer, and then the excited sensitizer Sen\* transfers the energy to I.

Many compounds are useful as photo-initiators for polymerization, including peroxides, azo compounds, and especially carbonyl compounds. These substances undergo homolysis by either or both of the two processes: fragmentation and hydrogen abstraction. Benzoyl peroxide (BPO) is representative of peroxide initiators. This molecule fragments into two benzol radicals (II) upon absorption of UV light: 72

The O-O bond energy is only 30 kcal/mol and radicals form easily. Disadvantages include poor thermal stability, absorption below 300 nm, and low reactivity towards monomers.

Azo compounds are another family of useful initiators. An important member of this family is 2,2'-azobisiso(butylronitrile) (AIBN) which generates radicals III upon UV absorption (equation 12):

The generated radicals are very effective in initiating polymerization since one molecule of nitrogen gas is released from each AIBN molecule, leaving a small distance between the two just-formed radicals and reducing the chance for them to recombine.

Carbonyl compounds, especially aromatic ketones, have found wide spread application in industry. The main mode of fragmentation is through  $\alpha$ -cleavage (Norrish I photo-scission). 2,2'-Dimethoxy-2-phenyl-acetophenone (DMPA),<sup>73</sup> a commercial

product (Irqacure 651), has a very high initiation efficiency due to the reactive methyl radical (IV) produced through a two step process:

A similar compound, 2,2'-diethoxyacetophenone (DEAP) gives a reactive ethyl radical (V) in the same way: 74

$$CH_{2}CH_{3}$$

$$CH_{3}CH_{2}CH_{3}$$

$$CH_{3}CH_{2}CH_{2}CH_{3}$$

$$CH_{3}CH_{2}CH_{2}CH_{3}$$

$$(15)$$

$$CH_{3}CH_{2}CH_{2}CH_{3}$$

$$(16)$$

1-Phenyl-1,2-propanedione-2-O-benzoyloxime (PPO), a ketoxime ester of benzoin, generates a very aggressive initiating species, phenyl radical VI.75 Small molecules, CO<sub>2</sub>

# Scheme 10. Fragmentation of ketoxime

and CH<sub>3</sub>CN, are released during fragmentation (Scheme 10). As in the case of AIBN, recombination of formed radicals is suppressed.

Irradiation of ketones in the presence of a hydrogen donor solvent results in coinitiation processes. Amines, alcohols, thiols, and ethers are common co-initiators. Below is an example of benzophenone as initiator and isopropanol as co-initiator:<sup>76</sup>

$$Ph - C - Ph \longrightarrow \begin{pmatrix} O \\ Ph - C - Ph \end{pmatrix}^* \longrightarrow \begin{pmatrix} O \\ Ph - C - Ph \end{pmatrix}^*$$

$$(17)$$

$$\begin{pmatrix}
Ph-C-Ph
\end{pmatrix}^{*} + H-C-OH$$

$$\begin{pmatrix}
CH_{3} \\
CH_{3}
\end{pmatrix}$$

An initiation system containing anthraquinone and THF was reported by Taylor et al. (equation 19)<sup>77</sup> Here, THF provides hydrogen and also acts as the principal initiating species (VII). Other initiation mechanisms include  $\beta$ -cleavage, <sup>78</sup> Norrish II photoscission, <sup>79</sup> and charge transfer. <sup>80</sup>

### 3. UV Induced Polymerization

Figure 6 is a simple view of UV initiated radical polymerization. UV light absorption by the initiator causes electronic transition from the ground state to excited singlet state. After intersystem crossing, a triplet excited state is realized which then fragments (or abstract a hydrogen if present) to generate initiating radicals. These radicals add to monomer to form the first monomeric radicals which propagate to result in polymer chains. Propagating radicals terminate by coupling or by disproportionation. Chain transfer processes are involved in many cases.

As mentioned earlier, most polymerization reactions are induced by initiators in triplet states. The quantum yield for initiation,  $\phi_i$ , is defined as the number of polymer chains initiated per absorbed photon. The rate of initiation  $R_i$  can be described as:

$$R_i = 2 \phi_i I_{abs} \tag{20}$$

where  $I_{aba}$  is the fraction of light absorbed by initiator. For any chain polymerization reaction, the rate of polymerization  $R_p$  is written as:

$$R_{p} = k_{p}[M] (R_{i}/2 k_{t})^{1/2}$$
 (21)

Substitution of equations 10 and 20 into 21, we end up with

$$R_{p} = k_{p} [M] [\phi_{i} I_{0} (1-10^{-ccb}) / k_{t}]^{1/2}$$
 (22)

Using steady-state treatment, the kinetic chain length is obtained as:

$$v = R_p / R_t = R_p / R_i = [k_p / 2k_t^{1/2}] [M] [\phi_i I_0 (1-10^{-ecb}) / k_t]^{-1/2}$$
(23)

the ratio of  $k_p/2$   $k_t^{1/2}$  is termed characteristic ratio of the monomer system which measures the ability of monomer to support a radical chain reaction.

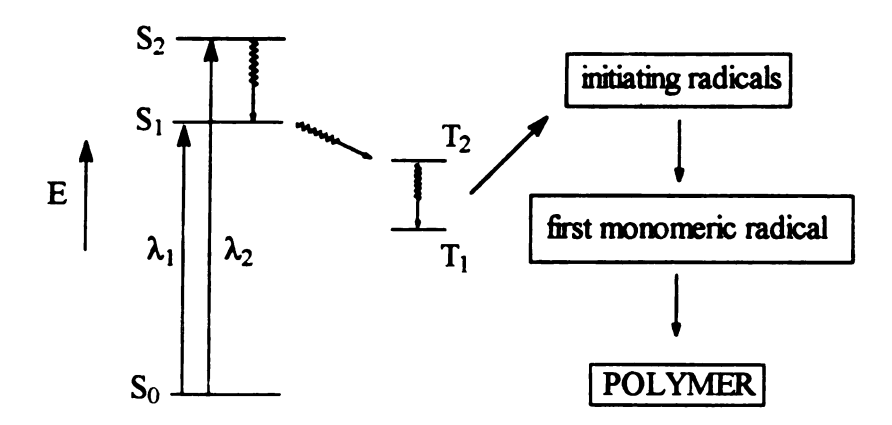


Figure 6. Schematic of UV induced photo-polymerization.

#### 4. Inhibition and Retardation

Apart from reacting with monomer molecules to initiate and propagate the chain polymerization, radicals also react with other substances present in reaction system. As a result, polymerization is suppressed. 81 Depending on the degree of suppression, these substances are classified as inhibitors which stop the reaction until consumed, or retarders which only slow down the reaction to some extent. Inhibitors or retarders are added intentionally to stabilize commercial monomer products, for example, a tiny amount (< 100 ppm) of hydroquinone monomethyl ether is often added to methacrylate monomers, and 4-t-butyl-catechol is often added to styrene. In such cases, the inhibitor is often removed before use by distillation, chromatography, or extraction. If the monomer is synthesized in the lab, impurities due to incomplete purification may act as an inhibitor or retarder. Many kinds of compounds can act as inhibitor or retarder, quinones are most common inhibitors. As shown in Scheme 11, propagating radicals can attack either at oxygen or at the ring to generate two different radicals: VIII and IX. VIII can terminate or add monomers; IX may couple with another radical to form X or rearrange to XI.

Aromatic nitro compounds are another family of substances that are used as inhibitors or retarders. The more nitro groups on the ring, the more polymerization is suppressed. Radicals can attack either the aromatic ring or the nitro group on these compounds.

# Scheme 11. Benzoquinone as an inhibitor.

$$O = \underbrace{\begin{array}{c} \text{coupling disproportionation add monomer} \\ O = \underbrace{\begin{array}{c} \text{O} \\ \text{VIII} \\ \text{O} \\ \text{O} \\ \text{IX} \end{array}}_{\text{No}} O + M_{n}H$$

Scheme 12. Nitrobenzene as an inhibitor: attack on ring.

In the first case (Scheme 12), radical XII is formed which either couples with another radical or re-aromatizes by transferring a hydrogen radical to a monomer molecule. In the second case (Scheme 13), radical XIII is generated which couples directly or indirectly with another radical, or fragments through  $\alpha$ -cleavage.

Scheme 13. Nitrobenzene as an inhibitor: attack on nitro group.

The oxygen molecule reacts with most radicals and is a powerful inhibitor:

This is one reason why an induction period is often observed in polymerization processes. From the industrial applications standpoint, a long induction period is not tolerable and both physical and chemical means have been reported to tackle this problem. Physical means include inert gas protection and vacuum application. Chemical means involve adding a chemical substance to trap oxygen through a chain process 82 or transform triplet oxygen into singlet oxygen. 83 In systems where tertiary amines are added as hydrogen donors, oxygen can be removed according to the following cycle (Scheme 14):

Scheme 14. Tertiary amines as anti-oxidants

$$R + H_3CN(CH_3)_2$$

$$CH_2N(CH_3)_2 + HOOCH_2N(CH_3)_2$$

$$O_2 + H_3CN(CH_3)_2$$

$$OOCH_2N(CH_3)_2$$

This cycle is able to consume up to 12 molecules of oxygen by same number of amine molecules with the loss of only one radical. This explains why tertiary amines are effective antioxidants.

## **RESULTS**

We were interested in making composite polymer electrolytes incorporating low molecular weight PEO (PEGDME-500), lithium salt, and functionalized fumed silica. Although a few fumed silicas are commercially available, they are limited in terms of the organic chain length and kind, and organic group coverage. We know that both pristine hydrophilic and hydrophobic silicas can be effective thickening agents, and while the thickening mechanism seems quite clear for the former, it is still ambiguous for the latter. In order to optimize mechanical properties of the composite polymer electrolyte system and investigate the interaction between filler materials and conducting polymers in general, we prepared a series of functionalized fumed silicas, including hydrophobic silicas with different alkyl groups, PEO oligomer modified silicas, and most importantly, hydrophobic and cross-linkable silicas. As we will see later, fumed silicas carrying both hydrophobic and cross-linkable groups, combined with PEGDME-Li salts, monomer and initiator, are extremely useful materials for realizing a permanent three-dimensional networks. In particular, good mechanical properties are achieved without impairing the conductivity of the composite electrolyte. All of these silica materials have been or are being used by our collaborative partners at North Carolina State University to investigate rheology and electrochemistry of fumed silica composites. Information from these studies will help us to optimize the physical and chemical properties of composite polymer electrolyte systems that incorporate fumed silicas as filler materials.

This section describes experimental conditions leading to good silylation products, the preparation of various functionalized fumed silicas, and finally the formation and basic characteristics of composite polymer electrolytes.

The terminology used to describe the modified silica samples in this report is as follows: For all the samples, FS is used to represent Fumed Silica. For most samples, the abbreviation for the silane used to modified the silica follows FS. For example, FS-TMCS-1 is a trimethylchlorosilane modified fumed silica. The number following the abbreviation is simply the run number. Exceptions are: 2H and 13H which represent the time of reaction in hours; C2, C8, and C18 denote the number of carbons in the hydrocarbon chain. TOM denotes a mixture of Trimethoxysilypropyl and Octyltrimethoxy Methacrylate. DM stands for DiMethyl, H for Hydride, EO, for number of Ethylene Oxide units, and M for Methacrylate. A few other samples not covered above can be found in the related reaction schemes.

## I. Silylation Conditions

### 1. General

In order to obtain the desired silica products, a series of control experiments were carried out to optimize the reaction conditions for silylation. We were primarily concerned with the amounts of the amine catalyst, the reaction time, and the relative amount of the silane compound. Based on Blitz's finding<sup>54</sup> that amines with exchangeable hydrogen(s) show catalytic activity when alkoxysilanes are used in silylation reactions, diethyl amine (DEA), a liquid at room temperature, was chosen for all experiments in this report. Ethyl amine and ammonia have more exchangeable hydrogen atoms and should catalyze silylation more efficiently, however, both are gases and are less convenient for lab use. For silylation reactions involving chlorosilanes, the type of amine is less important since it serves as a base instead of a catalyst.

FTIR spectroscopy was used to monitor changes during silylation reactions between fumed silicas and silane compounds. Usually, the attenuation or disappearance of the isolated silanol peak (3744 cm<sup>-1</sup>) and the appearance of new C-H absorption bands were observed. Since silica is not transparent to infrared below 1300 cm<sup>-1</sup>, only the 4000 - 1300 cm<sup>-1</sup> portion of the spectra will be shown. Thermogravimetric analysis (TGA) and lithium aluminum hydride titration techniques were used to supplement FTIR in some cases.

### 2. Amounts of Amine Catalyst

Infrared spectra of Aerosil modified with excess methyl triethoxysilane (relative to silanol groups on silica surface) in the presence and absence of DEA are shown in Figure 7. When the reaction is carried out in the absence of DEA, the silane C-H stretch modes are barely seen and the peak characteristic of isolated silanol groups remains strong. This spectrum (curve a) is similar to that of the starting AEROSIL silica where the band at 3744 cm<sup>-1</sup> is assigned to isolated silanol groups, the broad peak ranging from 3000 to 3800 cm<sup>-1</sup> is attributed to the hydrogen bonded OH groups, the Si-O-Si combination band appears at 1869 cm<sup>-1</sup>, and the peak at 1628 cm<sup>-1</sup> arises from the deformation mode of the adsorbed water. Addition of 1 mol % of DEA results in significant attachment of the silane (curve b), suggesting that the DEA does catalyze the silylation reaction, as previously reported. 54 Bands in the 2800-3000 cm<sup>-1</sup> region come from the C-H stretch modes of the tethered silane. Qualitatively, addition of more amine does not seem to change the amount silane attached to the silica, but condensation between the adjacent silane molecules might be enhanced as implied by the relative increase of C-H asymmetric stretch of Si-CH<sub>3</sub> at 2980 cm<sup>-1</sup>.

#### 3. Reaction Time

Reaction time also plays an important role in silylation reactions, especially when using multifunctional silanes, since hydrolysis of the second and third functional groups and the cross-linking reaction need longer time. In a study of silylation of Cab-O-Sil with trimethoxysilane, Blitz<sup>54</sup> reported that a reaction time of two hours was enough for complete reaction. Using triethoxysilane and fumed silica, we carried out silylation for 2 h

and longer times (Figure 8). We found that the silane loading became constant after 13 h - a condition employed throughout our experiments. Although we found that silane attachment could be increased by increasing the silylation temperature from ambient temperature to 70 °C, we never applied this condition to our actual preparations since satisfactory results could often be achieved at room temperature.

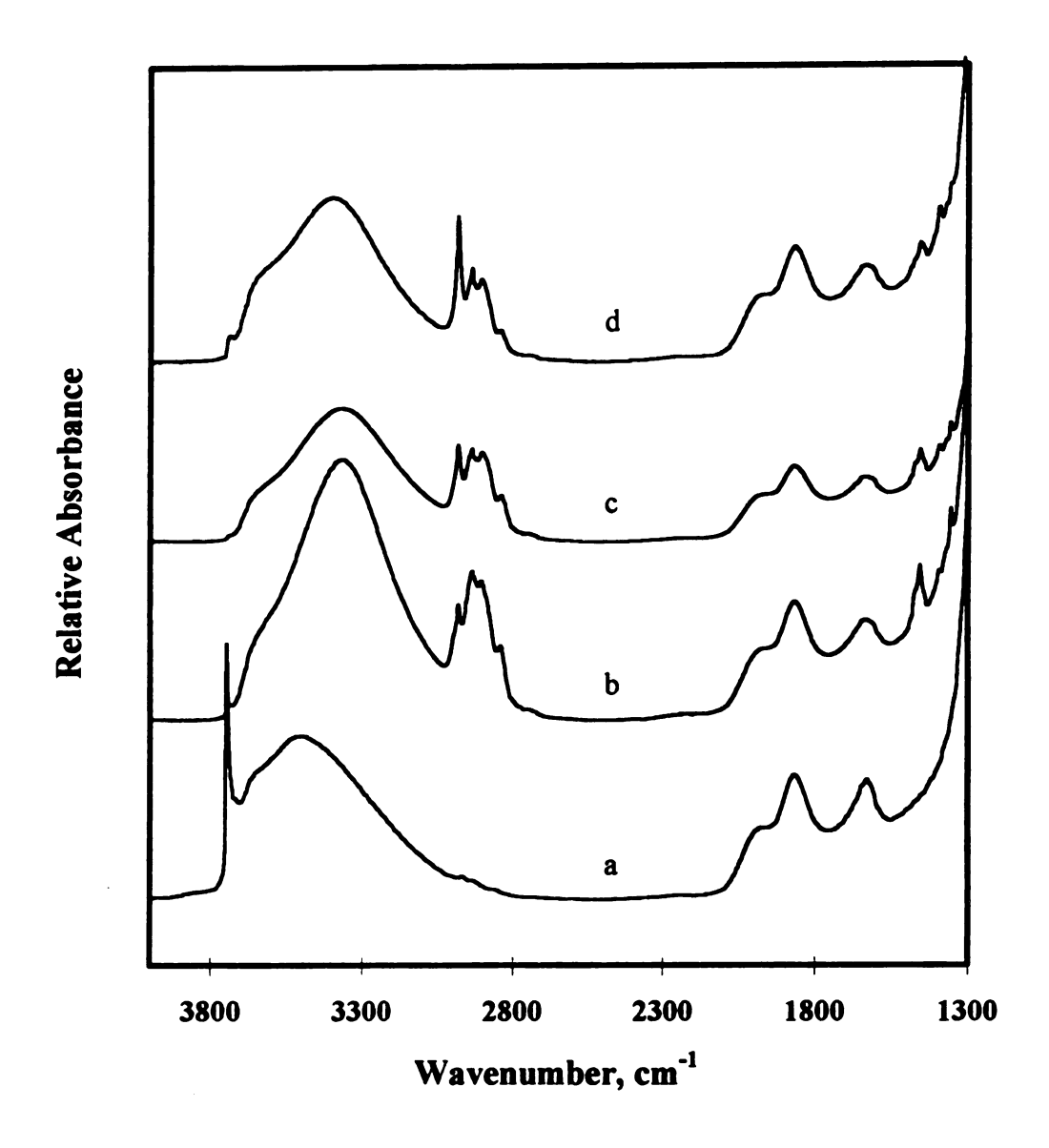


Figure 7. IR spectra of amine-catalyzed silvlation of A200 with excess methyl triethoxysilane: (a) FS-MTES-0, without amine; (b) FS-MTES-1, 1 mol % of amine based on surface silanol content; (c) FS-MTES-2, 25 mol %; (d) FS-MTES-3, 100 mol %.

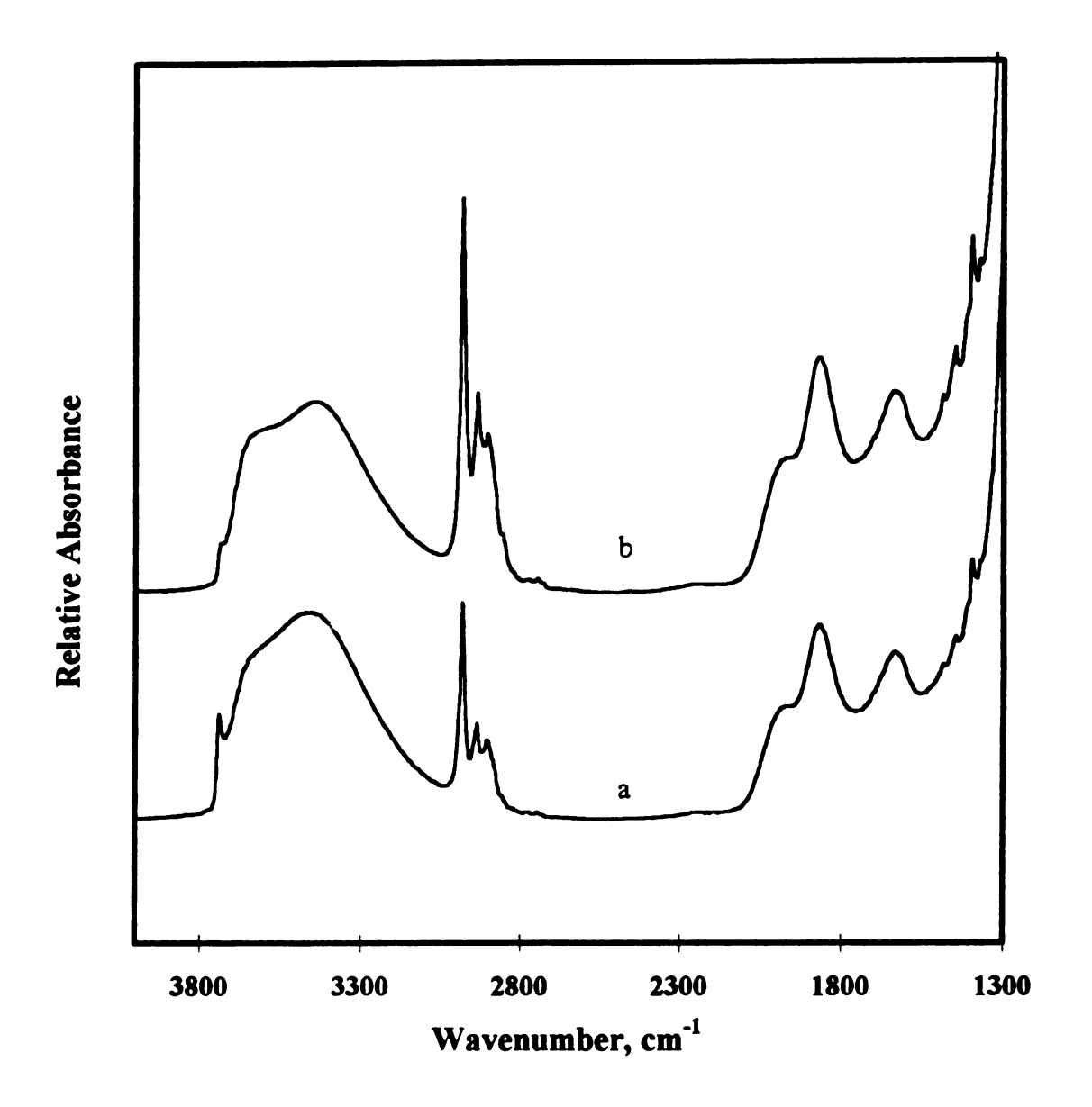


Figure 8. IR spectra showing the effects of reaction time on silylation of A200 with excess MeSi(OEt)<sub>3</sub>: (a) FS-MTES-2H, 2h; (b) FS-MTES-13H, 13h.

### 4. Amount and Type of Silane

Aerosil surfaces can be modified by either multifunctional or monofunctional silanes. Multifunctional silanes are more effective in generating high density organic surfaces due to reactions of their functional groups with multiple surface silanol groups and condensation reactions between silanes. Often however, the modified surface is not well-defined since there always exist some unreacted functional groups which makes the characterization and interpretation of data more complex. An end-capping procedure is sometimes used to solve this problem. In contrast, monofunctional silanes yield better defined surfaces which can be characterized more easily. A disadvantage is that a stable surface with high organic group coverage is often difficult to achieve.

Silylation reactions between monofunctional silanes (XSiMe<sub>3</sub>) and fumed silica were carried out to prepare well-defined surfaces with known silanol coverage. The TGA and titration results are shown in Table 2. When X = Cl, replacement of silanol groups by TMS groups is quantitative until a maximum coverage of 73 % is reached. Further increases in the silane/Si-OH ratio do not enhance the attachment as evidenced by titration and also IR spectra (Figure 9). When X = OEt and one equivalent of the silane is used, only 35% of the surface silanol groups reacted.

Table 2. Results of silvlation of fumed silica with XSiMe<sub>3</sub>.

Entry Number	Sample Name	Silane/Si-OH Ratio <sup>a</sup>	TGA loss, wt %	Coverage of TMS, % <sup>b</sup>
1	A200	-	0.59	0
2	FS-TMCS 1°	0.25	1.8	24
3	FS-TMCS 2	0.70	2.3	73
4	FS-TMCS 3	1.0	2.4	73
5	FS-TMES 1 <sup>d</sup>	1.0	0.74	35.0

- a) Molar ratio of silane to A200silanol groups.
- b) Calculated from titration experiments.
- c) TMCS = trimethylchlorosilane.
- d) TMES = trimethylethoxysilane.

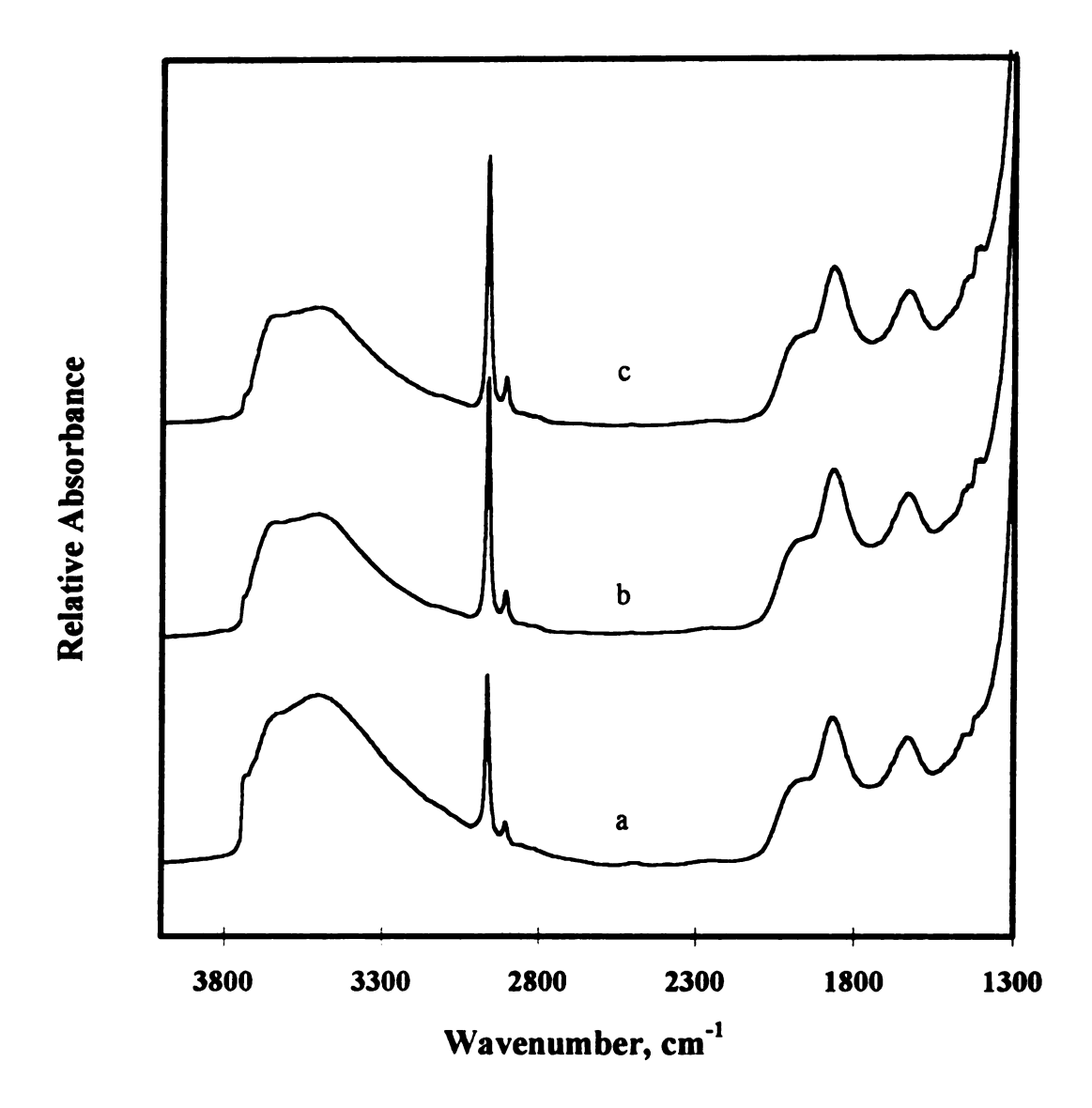


Figure 9. IR spectra of the silylation products of A200 and Me<sub>3</sub>SiCl at three silane/Si-OH ratios: (a) FS-TMCS-1, 0.25; (b) FS-TMCS-2, 0.70; (c) FS-TMCS-3, 1.0.

## II. Hydrophobic Silica

Based on the above silylation conditions, we first prepared hydrophobic silicas with different alkyl groups (Scheme 14). Figure 10 shows IR spectra of these silica products. The corresponding TGA curves are given in Figure 11. We did not try to quantify the organic group coverage through titration, since it is not possible to differentiate between residual surface silanols and those from the hydrolysis of silane molecules. IR spectra demonstrate a steady increase in the intensity of C-H absorption bands in going from short (C<sub>2</sub>) to long (C<sub>18</sub>) chains, and TGA curves show a constant increase in weight losses. The increase, however, is not linear - a consequence of the steric effects of long alkyl groups.

Scheme 15. Silvlations of A200 using modifiers of different lengths.

$$(SiO_2)$$
—OH + RSiCl<sub>3</sub>  $\xrightarrow{\text{HNEt}_2/\text{toluene}}$   $(SiO_2)$ —O-R

FS-C2, 
$$R = C_2H_5$$
; FS-C8,  $R = C_8H_{17}$ ; FS-C18,  $R = C_{18}H_{37}$ 

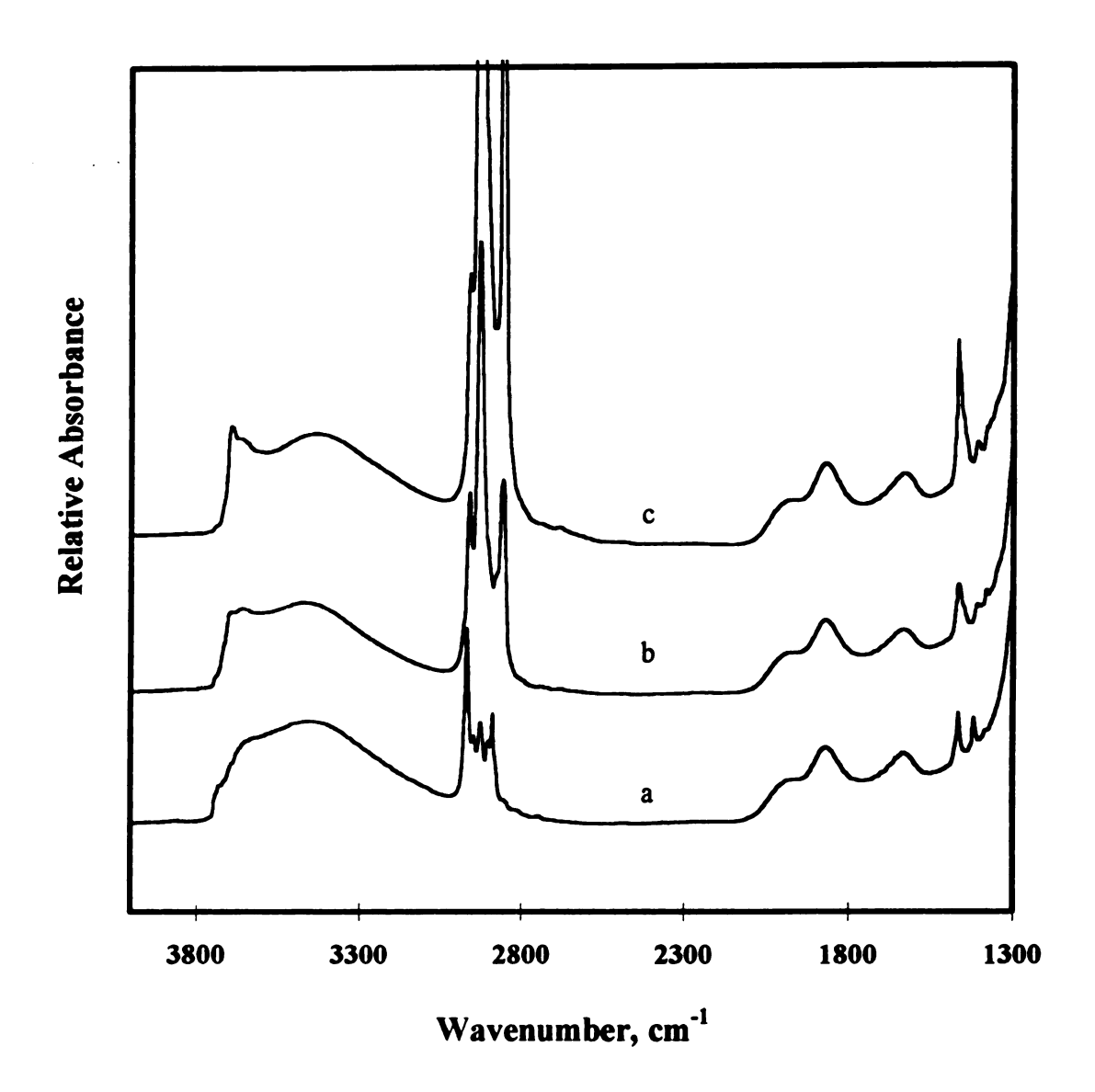


Figure 10. IR spectra of silylation products of A200 with RSiCl<sub>3</sub>:

(a) FS-C2, 
$$R = C_2H_5$$
; (b) FS-C8,  $R = C_8H_{17}$ ; (c) FS-C18,  $R = C_{18}H_{37}$ .

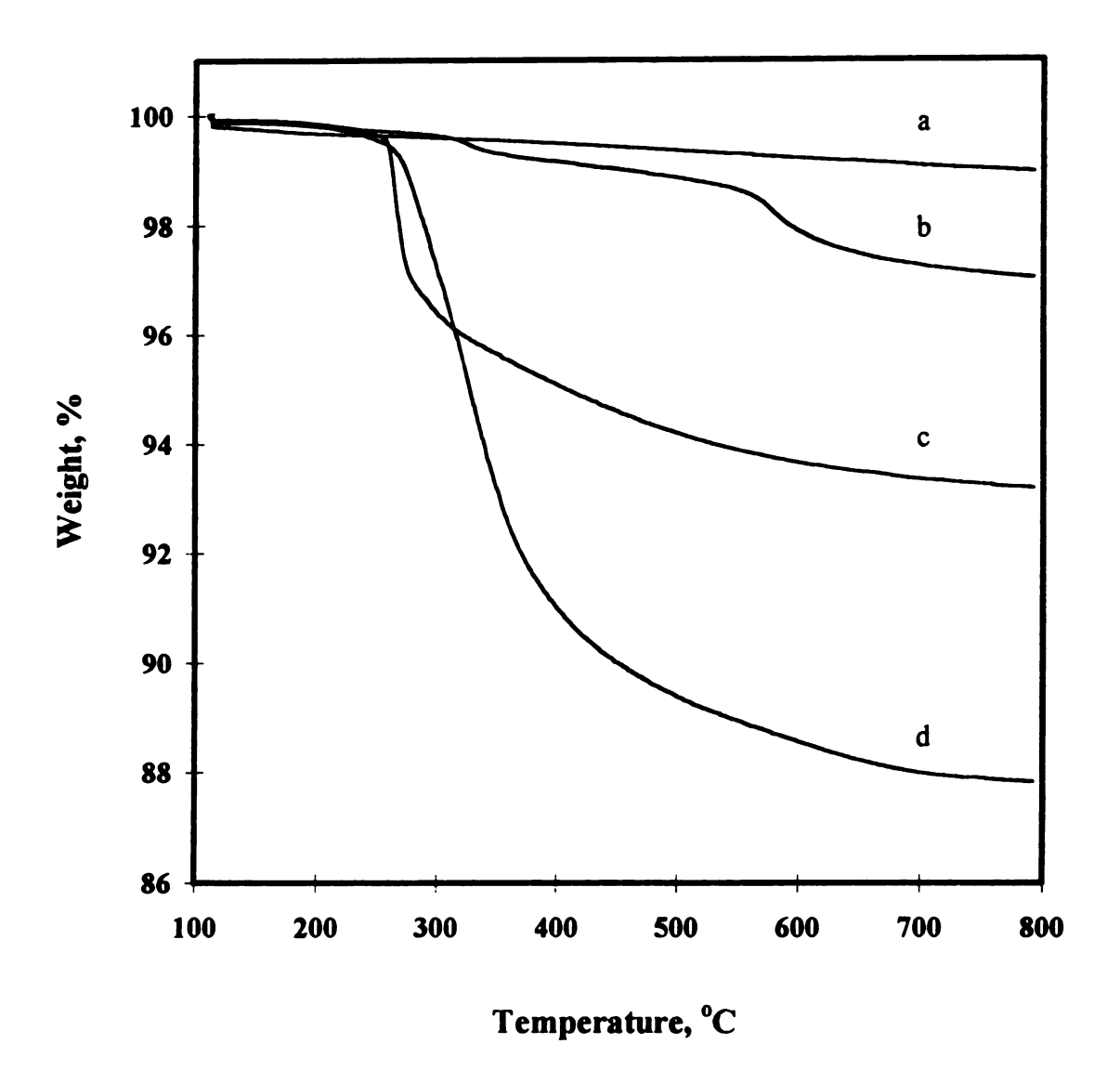


Figure 11. TGA curves of silylation products of A200 with RSiCl<sub>3</sub>:

(a) A200; (b) FS-C2, 
$$R = C_2H_5$$
; (c) FS-C8,  $R = C_8H_{17}$ ; (d) FS-C18,  $R = C_{18}H_{37}$ .

A series of A200 derivatives featuring different alkyl coverages were prepared using octyldimethylchlorosilane (ODMCS), C<sub>8</sub>H<sub>17</sub>(Me)<sub>2</sub>SiCl, a monofunctional silane (see Scheme 15). IR spectra and TGA data for the samples are given in Figures 12 and 13, respectively, and the results of silanol titrations and TGA weight losses are listed in Table 3. Increasing the silane/SiOH ratio (i.e., increasing the silane amount) leads to an increase in silanol group replacement as high as 42%, attenuation of the isolated silanol peak, and the increase in C-H relative absorption on IR spectra and in sample weight losses on TGA curves.

Scheme 16. Silylations of A200 with varying amounts of ODMCS.

SiO<sub>2</sub>—OH + 
$$C_8H_{17}Si(Me)_2Cl$$
 HNEt<sub>2</sub>/toluene  
SiO<sub>2</sub>—O—Si— $C_8H_{17}$   
Me

FS-DM-C8-n (n = 1, 2, 3)

Table 3. Results of silvlations of A200 with octyldimethylchlorosilane (ODMCS).

Sample Name	Silane/OH Molar Ratio	TGA loss wt %	OH Replaced mol %
FS-DM-C8-1	0.034	1.6	1
FS-DM-C8-2	0.24	2.4	31
FS-DM-C8-3	1.0	3.9	42

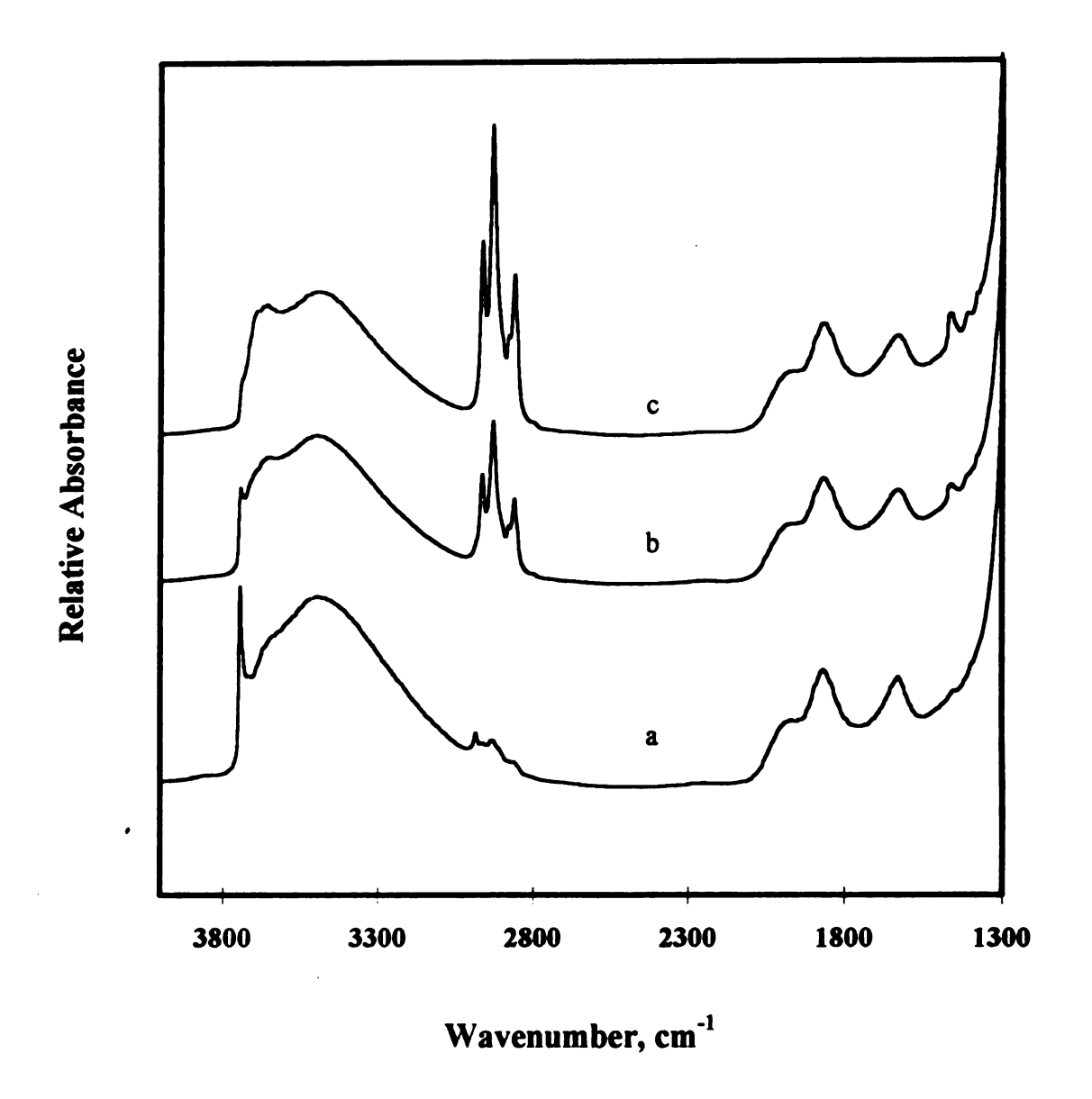


Figure 12. IR spectra of silylation products of A200 and C<sub>8</sub>H<sub>17</sub>(Me)<sub>2</sub>SiCl obtained at different silane/Si-OH molar ratios: (a) FS-DM-C8-1, 0.03; (b) FS-DM-C8-2, 0.3; (c) FS-DM-C8-3, 1.0.

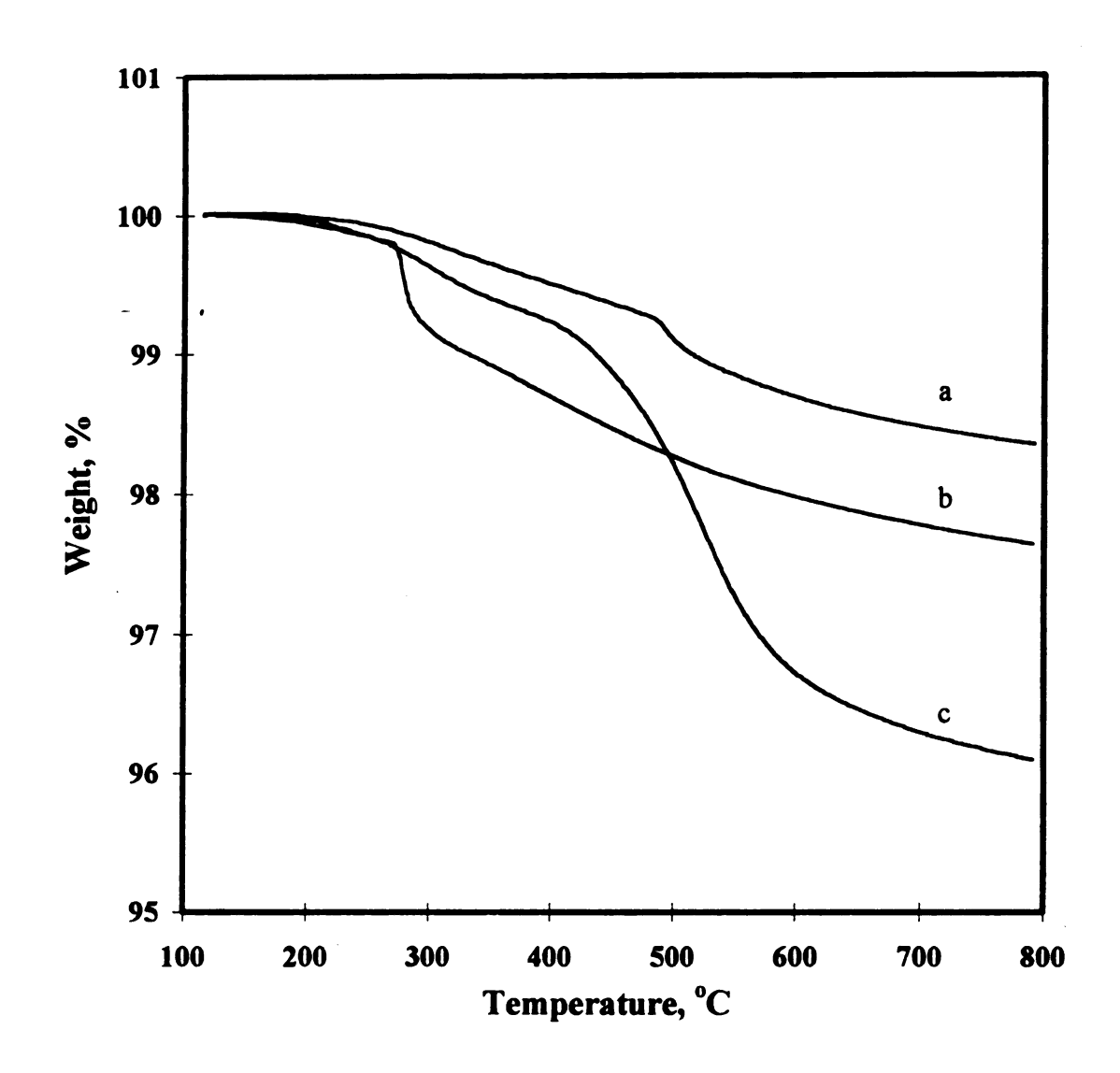


Figure 13. TGA curves for silylation products of A200 and C<sub>8</sub>H<sub>17</sub>(Me)<sub>2</sub>SiCl obtained at different silane/OH molar ratios: (a) FS-DM-C8-1, 0.03; (b) FS-DM-C8-2, 0.3; (c) FS-DM-C8-3, 1.0.

Scheme 17. Silylations of A200 with dimethylchlorosilane.

FS-DM-H

Hydride modified silicas, as envisioned by Sandoval et al., <sup>58,59</sup> are useful intermediates in the synthesis of many surface bonded materials. Hydride modified silica surfaces are hydrophobic in nature due to siloxane and Si-H linkages, and for some cases, alkyl groups. There are several ways of introducing the Si-H functionality onto silica surface. Both mono- and multi-functional silanes can be used, and in most cases, a catalyst/promoter (either an acid or a base) is added. We first tried silanization using dimethylchlorosilane (Scheme 16) using a base promoted process. The product could be filtered easily and by-products and excess silane could be removed by a combination of solvent rinsing and vacuum drying at elevated temperatures. The yields were usually quantitative. An IR spectrum of sample FS-DM-H is shown in Figure 14, curve d, where the band at 2250 cm<sup>-1</sup> is due to the Si-H absorption.

Scheme 18. Silylations of A200 with triethoxysilane.

(i) HCl/H<sub>2</sub>O/dioxane, (ii) HNEt<sub>2</sub>/toluene, (iii) HCl/H<sub>2</sub>O/dioxane, (iv) HNEt<sub>2</sub>/toluene/TMSCl.

We also used trialkoxysilane as a modifier. In this case, we tried two different approaches. The first was an acid-catalyzed process (Scheme 17) in which ethoxy silane molecules hydrolyze and condense with surface silanol groups. The advantage of this method is that it gives a more stable surface due to cross-linking of adjacent silanes and the absence of non-hydrolyzed alkoxy groups. Two conclusions could be made based on the IR spectrum of the product (Figure 14, curve e). Acid hydrolysis of alkoxy groups was complete since the C-H absorption due to ethoxy groups nearly disappeared, but the condensation between silanol groups was incomplete as evidenced by a strong absorption at 3744 cm<sup>-1</sup> due to isolated silanol groups.

The second method we employed was a base-catalyzed silanization process. In contrast to the first method, these products show incomplete hydrolysis of ethoxy groups, a lower Si-H density, and a lower Si-OH density (Figure 14, curve a). The residual ethoxy groups were hydrolyzed in an acidic medium, and except for a lower density of hydrides, the product generated resembles the one made using an acid catalyst (curves b and e). The silanol groups generated from the hydrolysis reaction were end capped using a small silane compound, TMSCl, in the presence of a base catalyst. As can be seen from curve c, the silanol groups are replaced by TMS groups to a significant extent and the product is similar to that obtained by direct silylation using dimethychlorosilane (curve d). In both cases, the C-H asymmetric and symmetric stretch modes of the methyl groups are clearly seen (curves c and d).

Due to the oxidation of Si-H linkages with oxygen, hydride modified silica products show thermal transitions at elevated temperatures which which can be used to verify the presence of hydrides. The TGA curves for samples FS-DM-H and FS-H are given in Figure 15. Three distinct stages are seen in TGA curves that can be rationalized in the following way: (1) an initial weight loss due to the condensation of residual silanol groups; (2) a weight gain due to the oxidative transformation of Si-H into Si-OH moieties; (3) further weight loss from further condensation of new silanol groups. The presence of hydrides on modified silica surfaces is also evident in their DSC traces, Figure 16. We were unable to quantify the hydride coverage from DSC results due to the lack of standards, but qualitatively, sample FS-DM-H shows a lower hydride coverage and lower thermal stability compared to FS-H. The endothermic transition is weaker in DSC traces and less weight was gained in TGA experiments at lower temperatures during the oxidation period. The same conclusion can be drawn from IR spectra of the two samples where FS-H shows a stronger Si-H absorption at ca. 2260 cm<sup>-1</sup>.

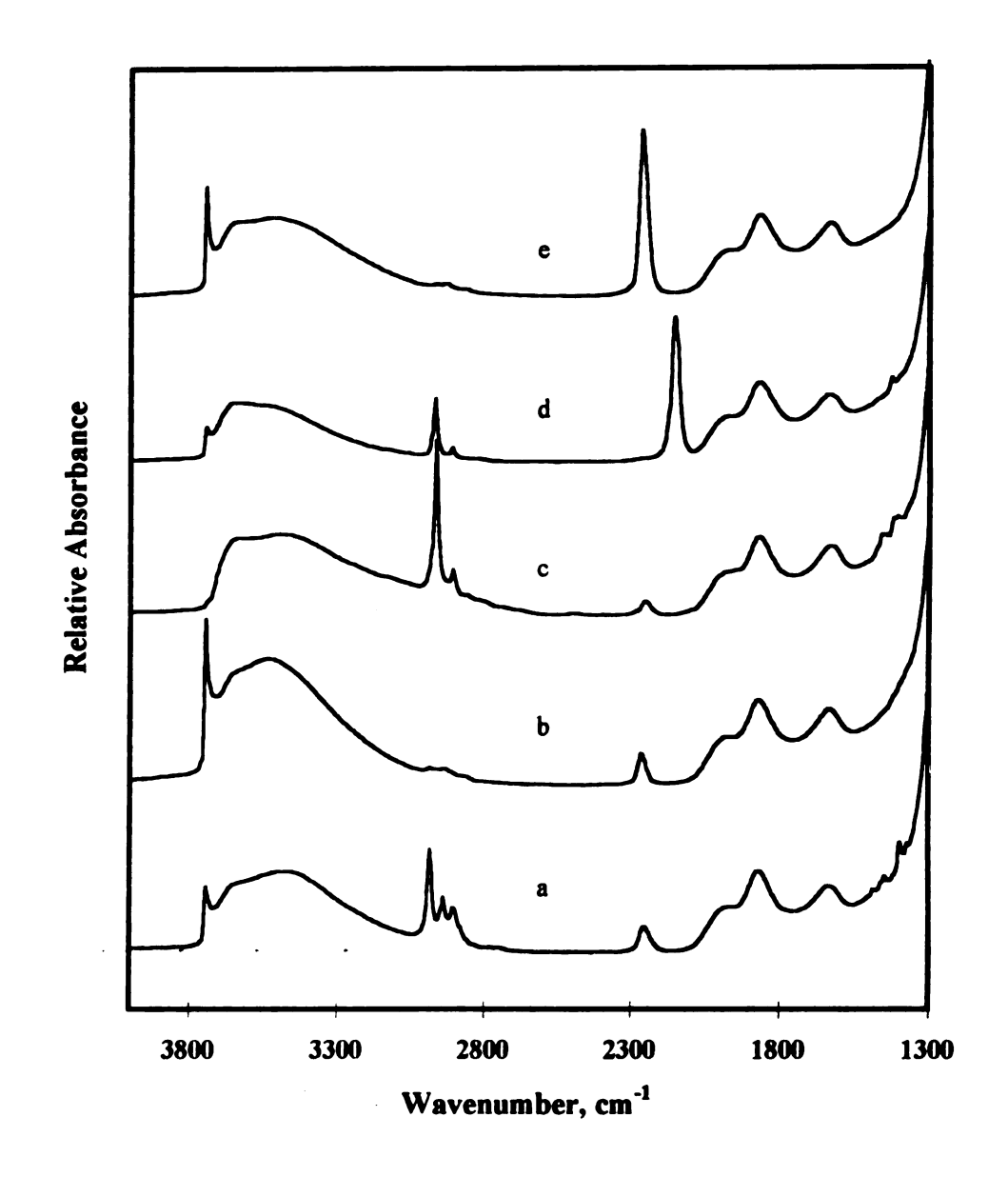


Figure 14. IR spectra of hydride modified A200 as defined by Schemes 16 and 17:

(a) FS-OEt-H; (b) FS-OH-H; (c) FS-TMS-H; (d) FS-DM-H; (e) FS-H.

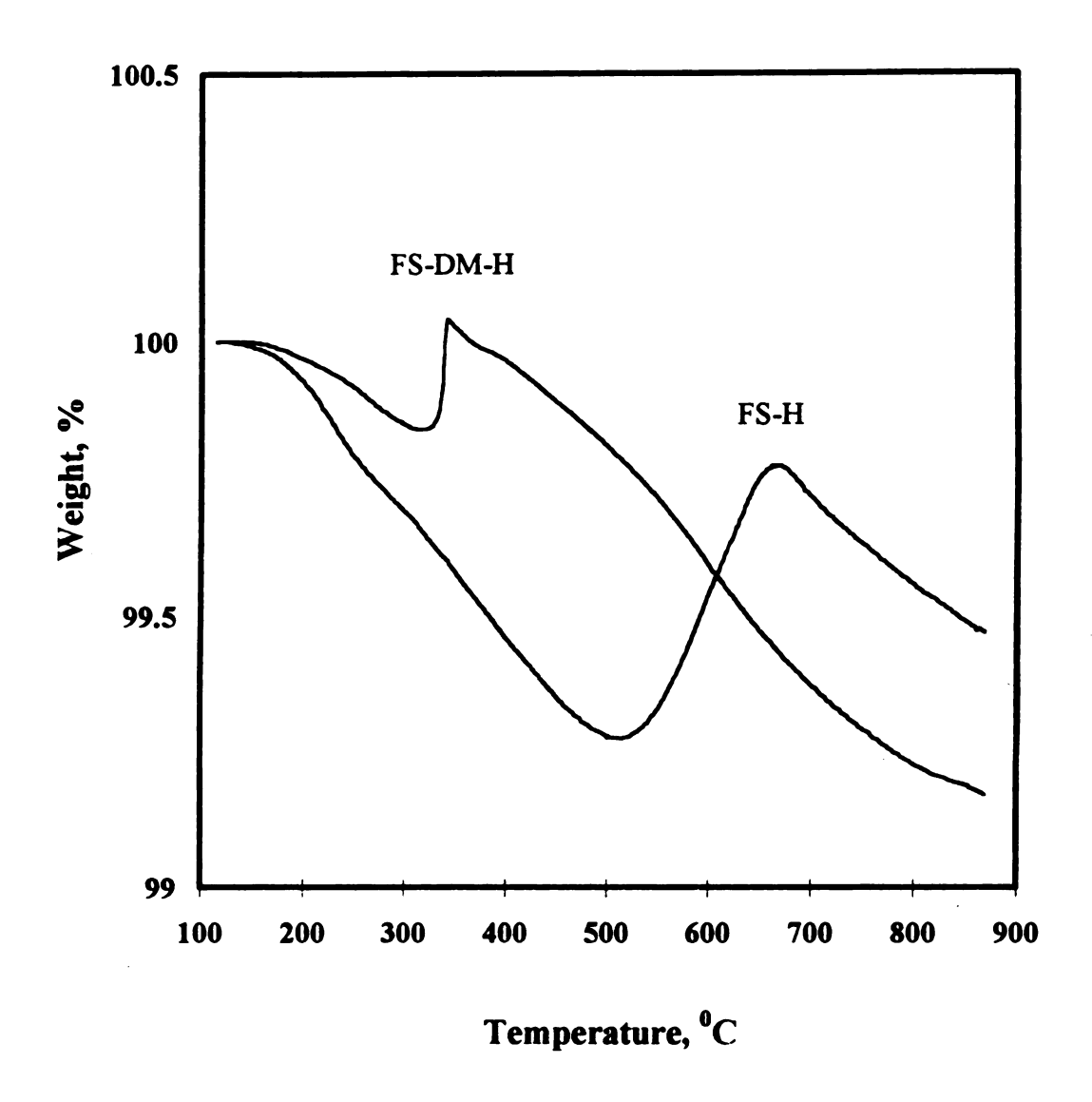


Figure 15. TGA curves of samples FS-H and FS-DM-H.

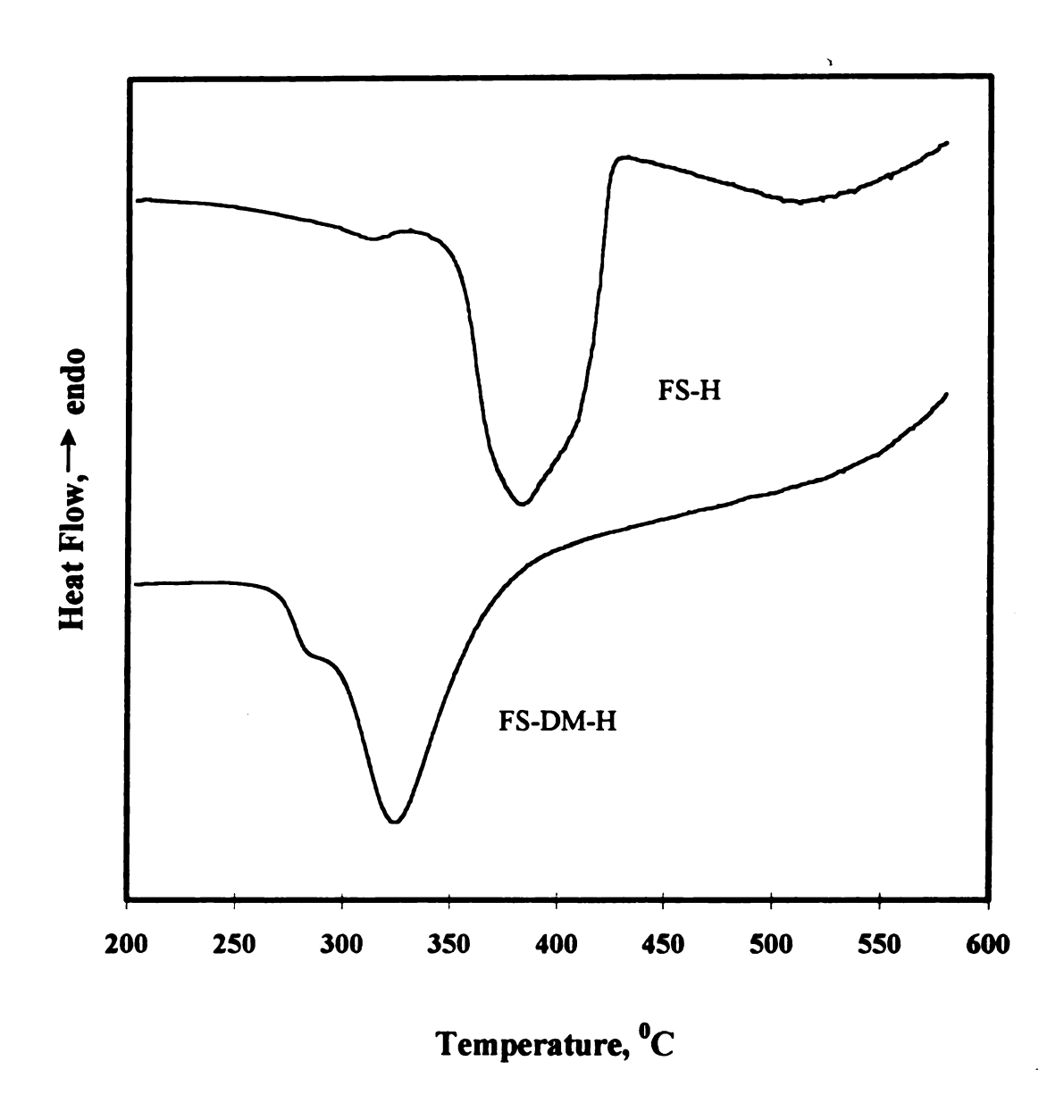


Figure 16. DSC traces of samples FS-H and FS-DM-H.

# III. Hydrophilic Silica

In the Introduction, we discussed electrolyte systems that incorporate silica as filler materials. We mentioned that hydrophobic silica is superior to hydrophilic silica in terms of its thickening effects in polar liquids. However, the silanol groups on pristine fumed silica are acidic and electrochemically unstable, and thus are not suitable for making electrolytes for rechargeable lithium batteries. If however, a fraction of the silanol groups are replaced with stable organic groups, the remaining silanols would be shielded and this problem could be suppressed. We first decided to make silica fillers compatible with PEO derivatives by tethering PEO oligomers onto the silica surface. By doing so, the electrochemical stability of silica toward lithium metal would be enhanced, and the compatibility of the PEO oligomer and the filler would be improved.

Scheme 18 shows reactions leading to chlorosilanes containing ethylene oxide units and their attachment to fumed silica surfaces. The properties PEO modified silica samples are listed in Table 4. As seen in the Table, 40 mol % of the silanol groups could be replaced by short PEG chains. As the chain length increases, replacement of silanol groups becomes more and more difficult and only 20% replacement was possible for the chains with 17 ethylene oxide repeat units. This is mainly due to the steric effects. TGA curves for these samples are given in Figure 17 which show that the percentage weight losses increase with the chain length as expected. The same conclusion was made from their IR spectra (Figure 18) which show a progressive increase in the intensity of the C-H absorption of ethylene oxide units. The peak at 1752 cm<sup>-1</sup> was not expected and has not

Scheme 19. Preparation of PEO tethered fumed silicas: First approach.

 $FS-DM-EO_n$  ( n = 1, 2, 3, 8, 12, 17 )

(i) NaH/THF; (ii) CH<sub>2</sub>=CH-CH<sub>2</sub>Br; (iii) HSi(Me)<sub>2</sub>Cl; Pt cat., toluene; (iv) A200, HNEt<sub>2</sub>/toluene.

Table 4. Modified silica fillers and their properties.

Sample Name	TGA loss, wt %	Coverage of Si-OH, mol %
A200	0.6	100
FS-DM-EO <sub>1</sub>	2.1	62
FS-DM-EO <sub>2</sub>	4.9	60
FS-DM-EO <sub>3</sub>	6.4	65
FS-DM-EO <sub>8</sub>	8.8	76
FS-DM-EO <sub>17</sub> ª	16.4	80

<sup>&</sup>lt;sup>a</sup> Average number of ethylene oxide units.

yet been assigned. Although it is now difficult to explain why the weight loss occurs at a lower temperature for sample FS-DM-EO<sub>17</sub>, our TGA experiments have shown that, compared with pure PEO, the physical blend of PEO and pristine fumed silica starts to lose weight at much lower temperature (ca. 100 °C lower), an indication of involvement of silanol groups in decomposing the PEO chains, probably as a result of acid catalysis.

We also tried another approach to making PEO modified silicas (Scheme 19). Poly(ethylene glycol) allyl methyl ethers were prepared as before and were allowed to react with hydride modified silica intermediates FS-DM-H and FS-H. IR spectra of the products are shown in Figure 19. When FS-H was used, the residual Si-H peak is still

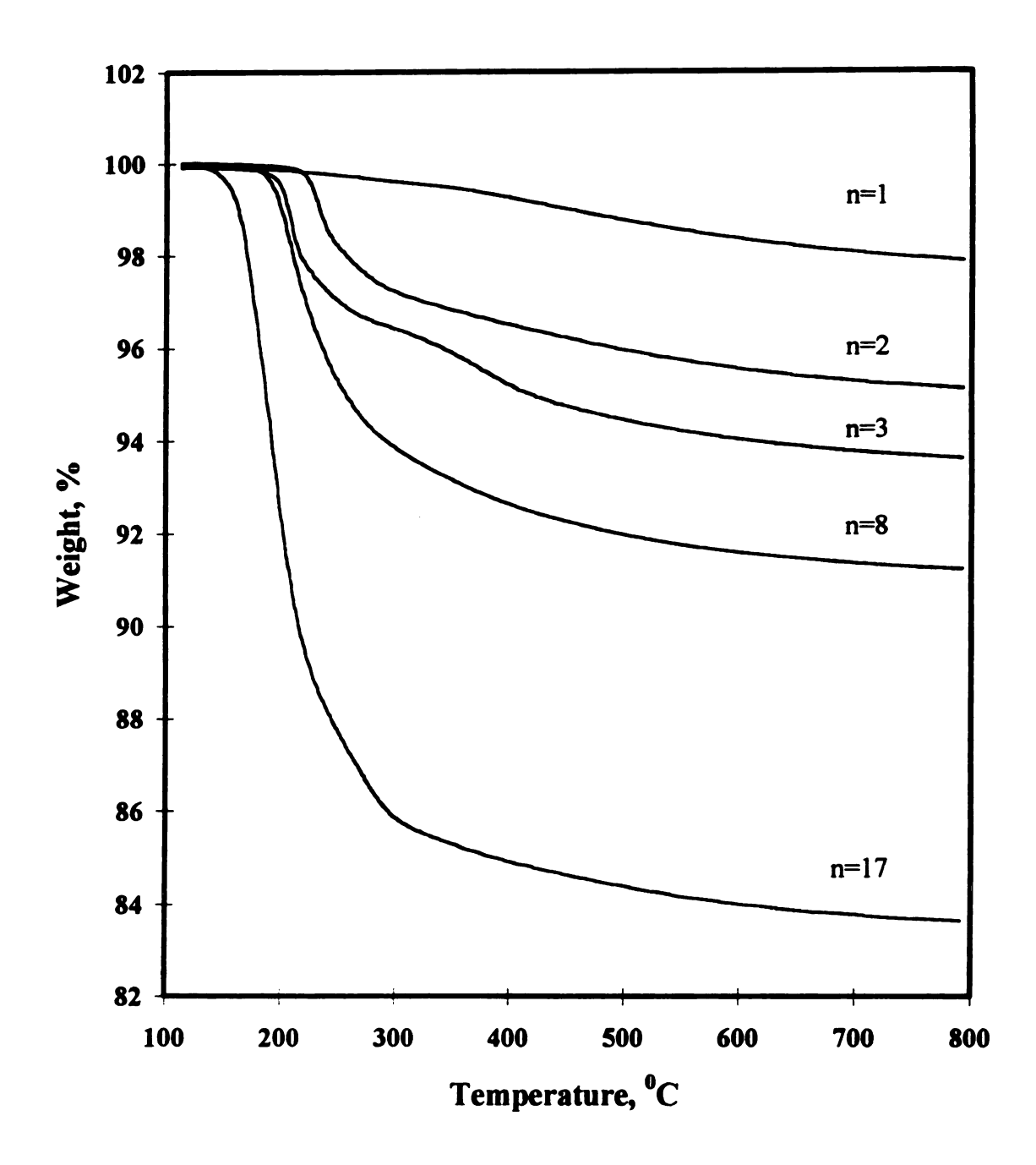


Figure 17. TGA curves of samples FS-DM-EOn.

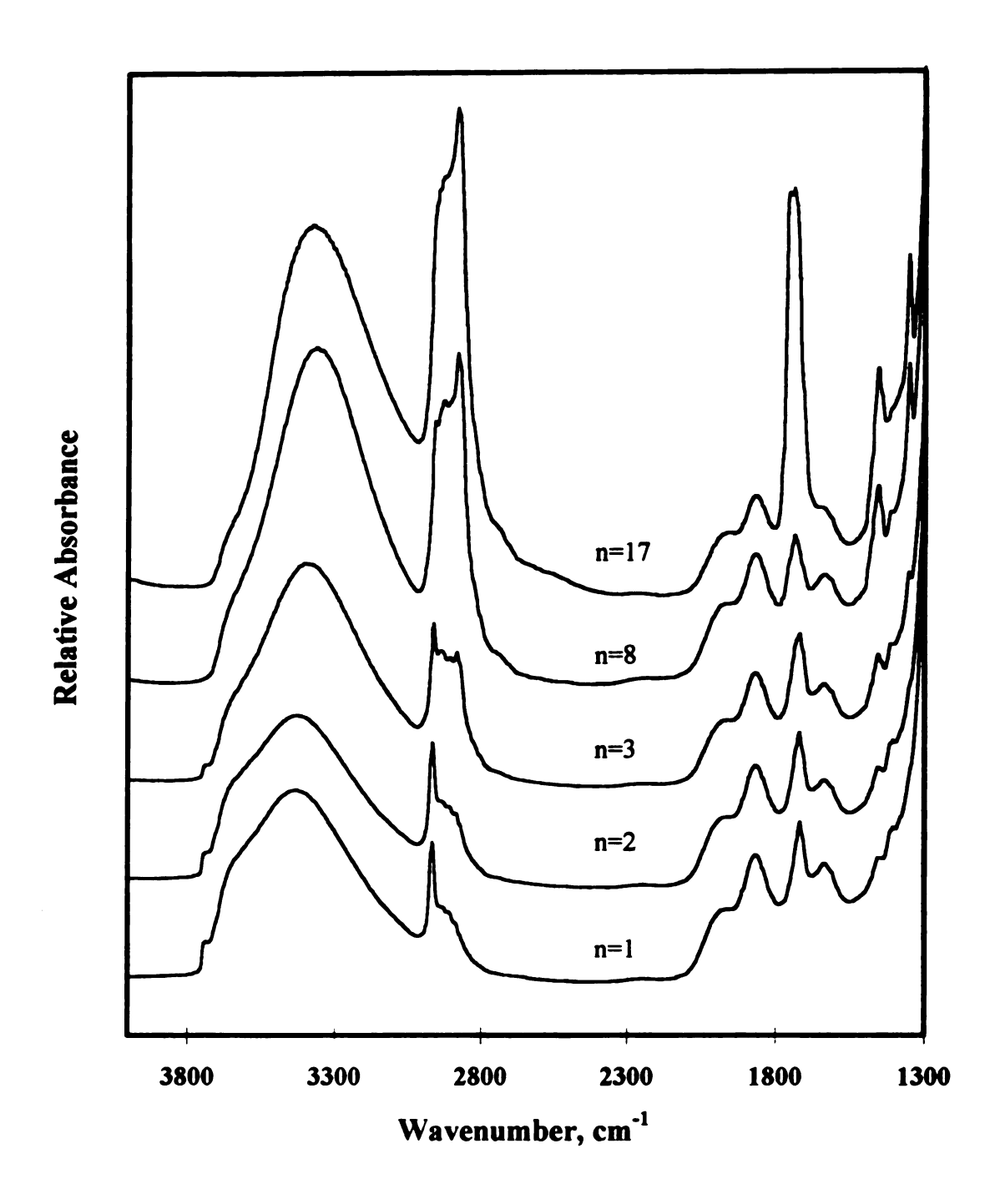


Figure 18. IR spectra of samples FS-DM-EOn.

discernible after the hydrosilation reaction, not surprising since increased amounts of attached ethylene oxide chains lead to increased steric shielding of the Si-H bond. However, when FS-DM-H was used, the Si-H bond is no longer seen after the reaction. A reasonable explanation for this result is that a portion of the silyl groups bearing Si-H linkages left the surface during hydrosilation. This did not happen in the case of FS-H due to its higher stability compared to FS-DM-H.

Scheme 20. Preparation of PEO tethered fumed silicas: Second approach.

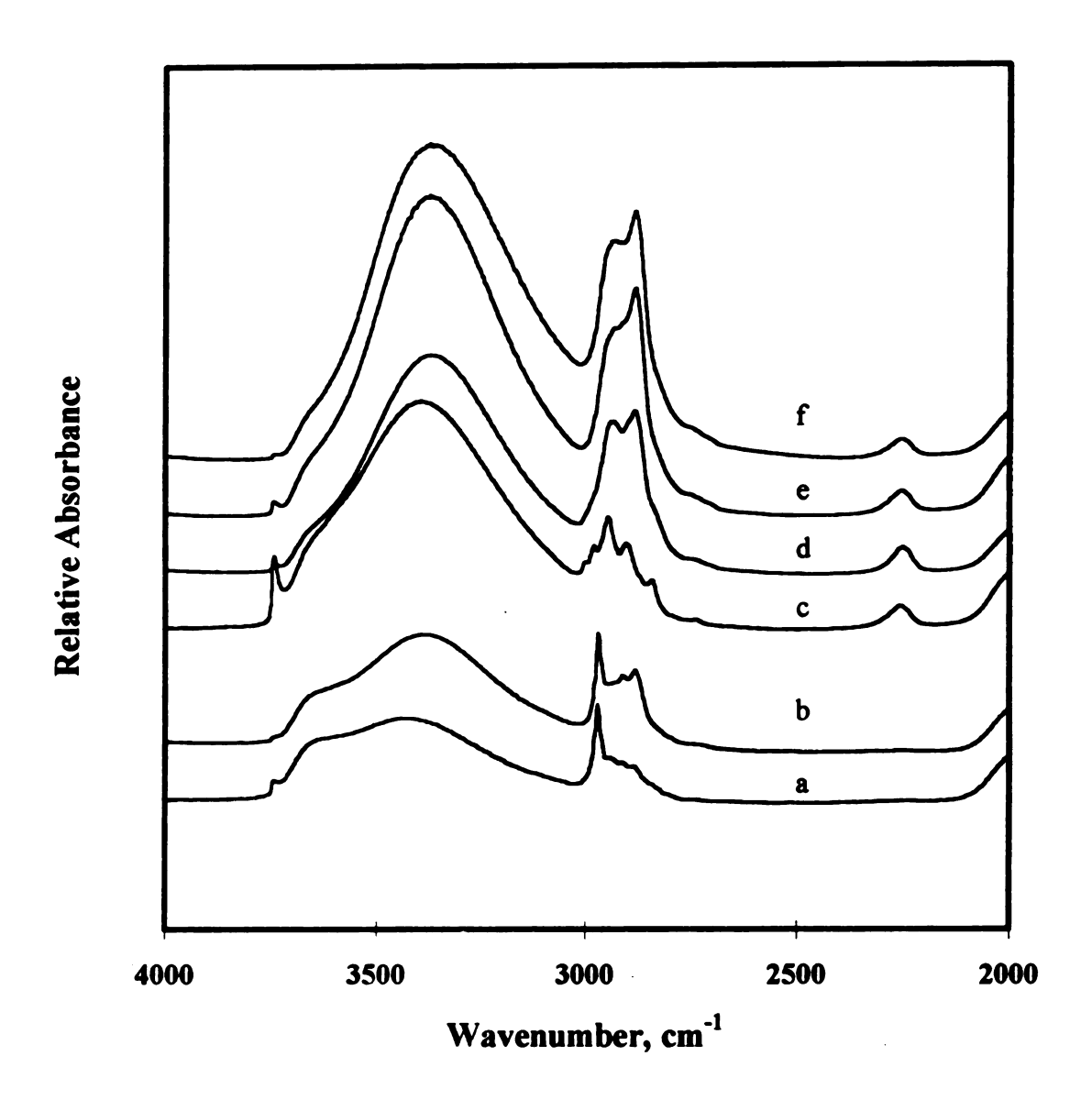


Figure 19. IR spectra of (a) FS-DM-S-EO<sub>1</sub>; (b) FS-DM-S-EO<sub>8</sub>; (c) FS-EO<sub>1</sub>; (d) FS-EO<sub>3</sub>; (e) FS-EO<sub>8</sub>; (f) FS-EO<sub>12</sub>.

### IV. Polymerizable Silica

### 1. Silylation Using Single Silanes

As mentioned earlier, silica particles can form three-dimensional networks, but this structure is only temporary and is easily broken down on shearing. For long term reliability, permanent dimensional stability desirable. In composite polymer electrolytes using fumed silicas as fillers, dimensional stability can be introduced as a cross-linking step that binds adjacent fumed silica particles into a stronger network structure. Early work on the preparation of polymerizable fumed silicas focused on using the coupling agent 3-(trimethoxysilyl)propyl methacrylate (TPM), an economical commercial product with a short hydrocarbon spacer (C<sub>3</sub>). As seen later, silylation of A200 with TPM can generate products with very high coverage of functional groups. Unfortunately, this product gave us a liquid-like gel upon mixing with oligomeric PEO due to hydrophilic character of the ester functional group on the surface modified silica product. In order to impart both polymerizability and hydrophobicity to fumed silica, we prepared two coupling agents with longer hydrocarbon spacers (C<sub>5</sub> and C<sub>8</sub>), hoping that longer spacers would confer hydrophobic characteristics to the surface.

Polymerizable silicas were initially prepared through several steps according to Scheme 20, method 1. The needed 4-penten-1-ol (20) is commercially available while 7-octen-1-ol (21) was prepared via its THP ether (25) as outlined in Scheme 21. The THP ethers of  $\alpha$ , $\omega$ -alkenols (22 and 23) were allowed to undergo hydrosilation reaction with

Scheme 21. Preparation of cross-linkable fumed silicas: Method 1.

(i) TsOH, dioxane; (ii) FS-DM-H or FS-H, Pt cat., toluene; HCl/H<sub>2</sub>O/ EtOH; (iv) methacryloyl chloride, pyridine, toluene.

Scheme 22. Synthesis of 7-octen-1-ol.

HO 
$$\stackrel{i}{\longleftrightarrow}_{6}$$
  $\stackrel{i}{\longleftrightarrow}_{C}$   $\stackrel{i}{\longleftrightarrow}_{0}$   $\stackrel{iii}{\longleftrightarrow}_{0}$   $\stackrel{iii}{\longleftrightarrow}_{0}$   $\stackrel{iii}{\longleftrightarrow}_{0}$   $\stackrel{25}{\longleftrightarrow}_{6}$   $\stackrel{25}{\longleftrightarrow}_{6}$   $\stackrel{21}{\longleftrightarrow}_{23}$ 

(i) TsOH, DHP, dioxane; (ii) KO t-Bu, DMSO; (iii) HCl/H<sub>2</sub>O/ EtOH.

either FS-DM-H or FS-H. Deprotection of these intermediates afforded silica surfaces containing alkyl chains terminated with hydroxyl groups. Polymerizable silicas, FS-C5-M-1 and FS-C8-M-1, were obtained through the base promoted acylation of surface hydroxyl groups with methacryloyl chloride. Two representative IR spectra of the products thus generated are shown in Figure 20. As seen, high surface attachment was not achieved, probably due to both incomplete hydrosilation and acylation.

In Method 2, shown in Scheme 22, hydrosilation would take place in a homogeneous phase and a higher yield would be expected. Initially, we chose acryloyl chloride (26a, R= H) over methacryloyl chloride (26b, R = Me) for the acylation (reaction i) because the former has higher reactivity towards radical polymerization. Much work was devoted to optimizing the hydrosilation reaction, but satisfactory results were not obtained. According to the literature, 84 hydrosilation of terminal alkenes takes place

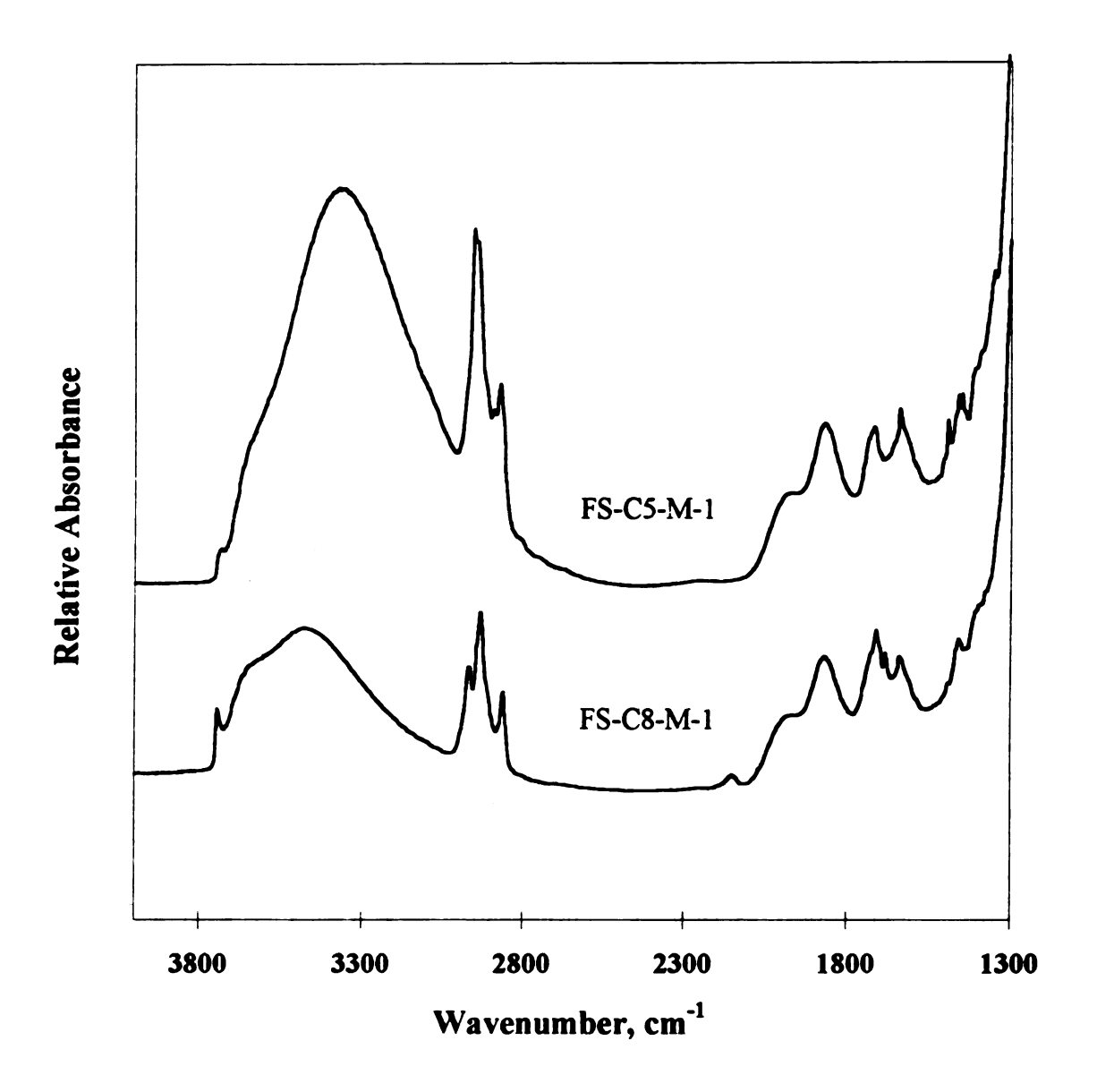


Figure 20. IR spectra of samples FS-C5-M-1 and FS-C8-M-1 as defined in Scheme 20.

Scheme 23. Preparation of cross-linkable silicas: Method 2.

- (i) CCl<sub>4</sub>, 3A mol. sieves, 80 °C; (ii) HSiX<sub>3</sub>, Pt cat., toluene, 60 °C overnight;
  - (iii) FS-H or FS-DM-H, Pt cat., toluene; (iv) A200, HNEt2, toluene.

at temperatures just above room temperature, but the conjugated double bond of the acrylate group is less reactive and hydrosilation occurs in only moderate yields at temperatures of 100 °C or higher. Based on this precedent, hydrosilation of our alkenyl acrylate (27a and 28a, reaction ii) should occur selectively at the alkenyl group. Unfortunately, hydrosilation at the acrylate double bond occurred under a range of reaction conditions. The same results were obtained for hydrosilation of the same alkenyl acrylate using hydride modified silica in heterogeneous phase (reaction iii). When methacrylol chloride (26b) was used for the acylation reaction, hydrosilation reactions occurred specifically at the alkenyl double bond. Clearly, the steric bulkof the methyl group on the alkenyl methacrylate plays an important role in inhibiting hydrosilation.

Separation problems were common when triethoxysilane was used. Crystallization was not successful, and chromatography and vacuum distillation gave either little or none of the desired monomer product. Removal of the excess of triethoxysilane under vacuum was not successful due to its high boiling point (bp 134 °C). By switching to the lower boiling trichlorosilane (bp 32 °C), excess silane could be removed by vacuum.

The IR spectrum of a polymerizable silica made from 8-(trichlorosilyl)octyl methacrylate (31), sample FS-C8-M-2, is shown in Figure 21 along with FS-C3-M, a sample made using commercial TPM. Their schematic structures are shown in Figure 22.

The absorption bands characteristic of carbonyl and C=C double bonds are comparable in

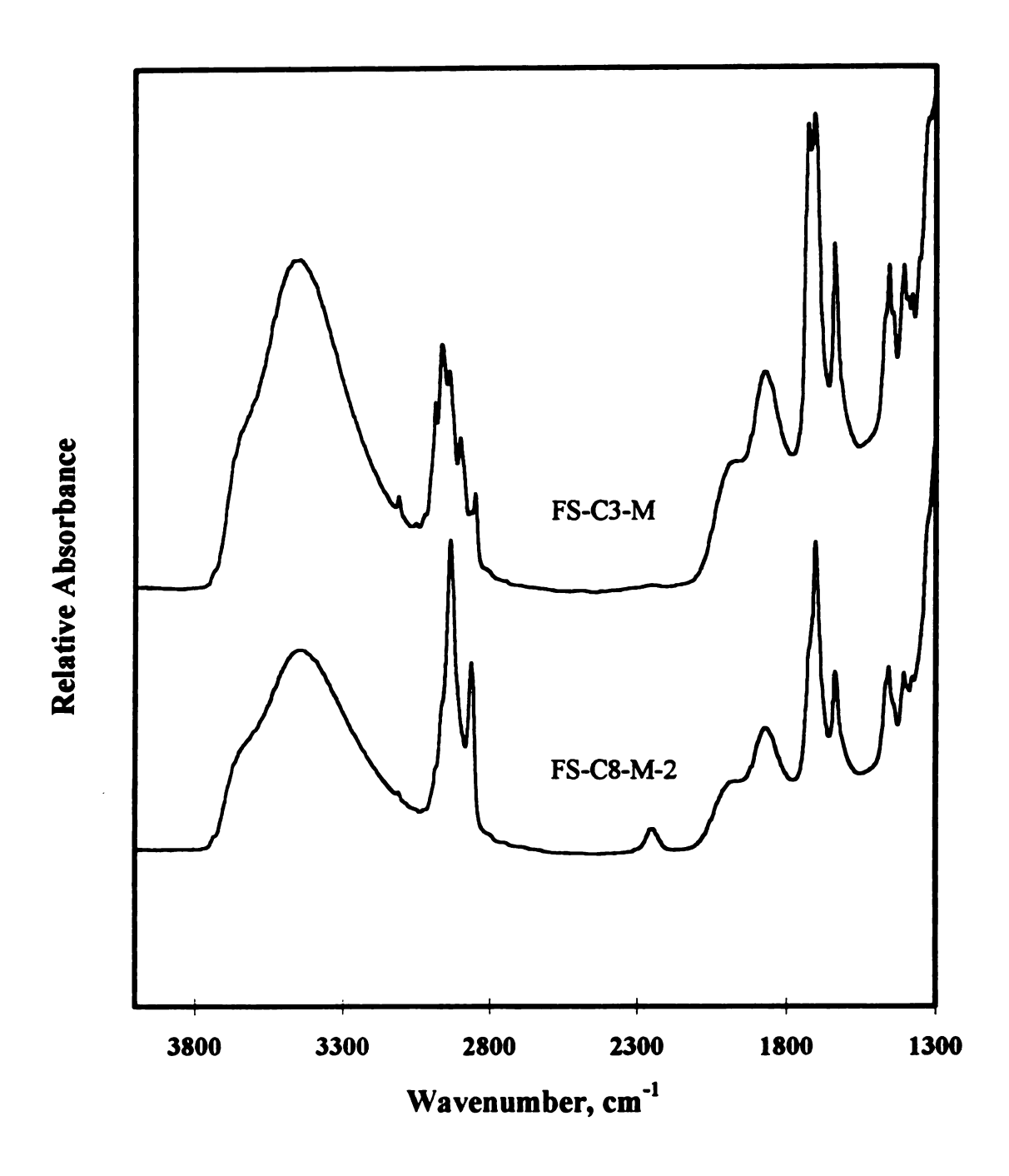


Figure 21. IR spectra of polymerizable silicas: FS-C3-M and FS-C8-M-2.

Figure 22. Schematic representations of A200 (top left),

FS-C3-M (top right), and FS-C8-M-2 (bottom).

intensity for both samples, and are stronger than for the silicas shown in Figure 20, suggesting a higher coverage of methacrylates. The small peak at ca. 2260 cm<sup>-1</sup> in the spectrum of sample FS-C8-M-2 is due to the small amount of Si-H impurity.

The significance of the above experiments is that the thickening effect of the silicas was enhanced as the hydrocarbon spacer was increased. The best results were obtained when a C<sub>8</sub> spacer was present between silica surface and methacryloyl group. We were targeting a silica filler which, upon mixing with PEG oligomer and lithium salt, would generate a physically stable gel thin enough to allow trapped air bubbles to be pumped out by applying a moderate vacuum. FS-C8-M-2 meets the above requirements very nicely.

#### 2. Silylation Using Mixed Silanes

The major difference between samples FS-C3-M and FS-C8-M-2 is the length of carbon spacer that tethers the methacrylate group to the silica surface. The methacrylate group by itself is polar in nature, whereas the hydrocarbon spacers are non-polar. The direct result of increasing the the spacer length is to increase the hydrophobicity of the silica, and in turn its thickening effect in polar solvents. Based on this rationale, we developed a second route to polymerizable hydrophobic fumed silicas - silylation using mixtures of silanes. One silane would carry a hydrolyzable group for attachment to silica and a polymerizable group; while the other silane would only need to have a hydrolyzable group. The advantage of mixed silylations is that a variety of commercial silane products become useful to us. Although only a few TPM-like coupling agents are available commercially, there are many silanes such as octyltrimethoxysilane (OTMS) that bear

hydrolyzable groups. Ranging from short chains (methyl group) to longer chains (decyl and octadecyl groups), each of these silanes can be either monofunctional or multifunctional. Many combinations of silanes are possible, and the relative amounts of the two silanes within each combination are also tunable. In summary, by using the mixed silylation scheme, the polymerizable silica surface can be "tailored" in a delicate and sophisticated way.

We selected TPM and OTMS for our mixed silylation reactions. The former offers polymerizability through its methacryloyl group and the latter provides hydrophobicity due to its long octyl chain. Table 5 lists the experimental conditions and results of such studies (TOMn will be used in the following discussion to represent such products). Known amounts of the two silanes were weighed to give the desired TPM mole fraction. The relative and total degree of attachment of the silanes were determined from the mass and <sup>1</sup>H NMR spectrum of the reaction residue collected through filtration and solvent rinsing of the silica. A portion of the <sup>1</sup>H NMR spectrum for the residue of sample TOM4 is shown in Figure 22. As can be seen, the peak for the methyl group adjacent to the double bond on TPM (1.95 ppm) and the terminal methyl group on OTMS (0.89 ppm) are well-separated from other peaks and were used for integration. The calculated weight losses for TGA experiments were derived using the following assumptions:

- Each silane molecule reacts with one silanol group.
- All of the methoxy groups convert to siloxane during silvlation.
- Upon heating, the silicon-carbon bonds first break to form silanol groups, and two such silanol groups then condense to give siloxane linkage.

Table 5. Mixed silylation of A200 with OTMS and TPM.

Sample Name	TPM Feed	mol % Residue	,,	Total Silane mmol/g SiO <sub>2</sub>	Weight Loss TGA (expt.)	Weight Loss, TGA (calc.)
FS-OTMS	0.0	0.0	0.0	400	4.0	4.6
FS-TOM-1	9.0	0.0	7.2	330	3.9	4.0
FS-TOM-2	20	1.3	31	510	5.3	5.8
FS-TOM-3	24	5.6	35	520	4.8	6.3
FS-TOM-4	31	13	37	490	6.0	6.2
FS-TOM-5	50	21	82	380	5.0	4.9
FS-C3-M	100	100	100	550	6.5	6.7

CH<sub>3</sub> in TOM

2.0

1.5

1.0

0.5

Figure 23. A portion of the <sup>1</sup>H NMR spectrum of the residue from sample TOM4.

Although the actual situation deviates somewhat from this model (some unreacted methoxy groups present after the silylation), the calculated weight losses are very close to those measured by TGA analyses.

When the two pure silanes were used separately for silvlation, the TPM modified product showed a slightly higher coverage than OTMS-modified silica (Table 5). The situation changed dramatically when the silvlation reaction was carried out using a mixed silane solution. Compared to OTMS, TPM attaches to the silica surface preferentially. Results on mass balance studies listed in Table 5 were plotted in Figure 23. Although the TPM fractions on silica surface and in residue are all approximately proportional to the TPM fraction in feed, the fraction on surface is always larger than that in the residue. In addition, the rate of increase of TPM fraction on the surface is always higher (larger slope) than that in the residue. Considering the structure differences in the two silane molecules, the above observation can best be explained in terms of selective adsorption of TPM over OTMS, since the former has ester functional groups. The schematic representations of sample FS-TOM4 as well as a commercial hydrophobic silica R805 are given in Figure 24. Compared with R805, the modified silica FS-TOM4 has not only hydrophobic groups (octyl), but also cross-linkable groups. Thus, the TPM fraction on silica surface can be controlled by adjusting the feed composition. IR spectra of the selected samples from Table 5 are shown in Figure 25 which clearly show the expected increases in the relative absorbances of the carbonyl and double bond as the proportion of TPM is increased.

Figure 24. Schematic representations of R805 (top) and FS-TOM-4 (bottom).

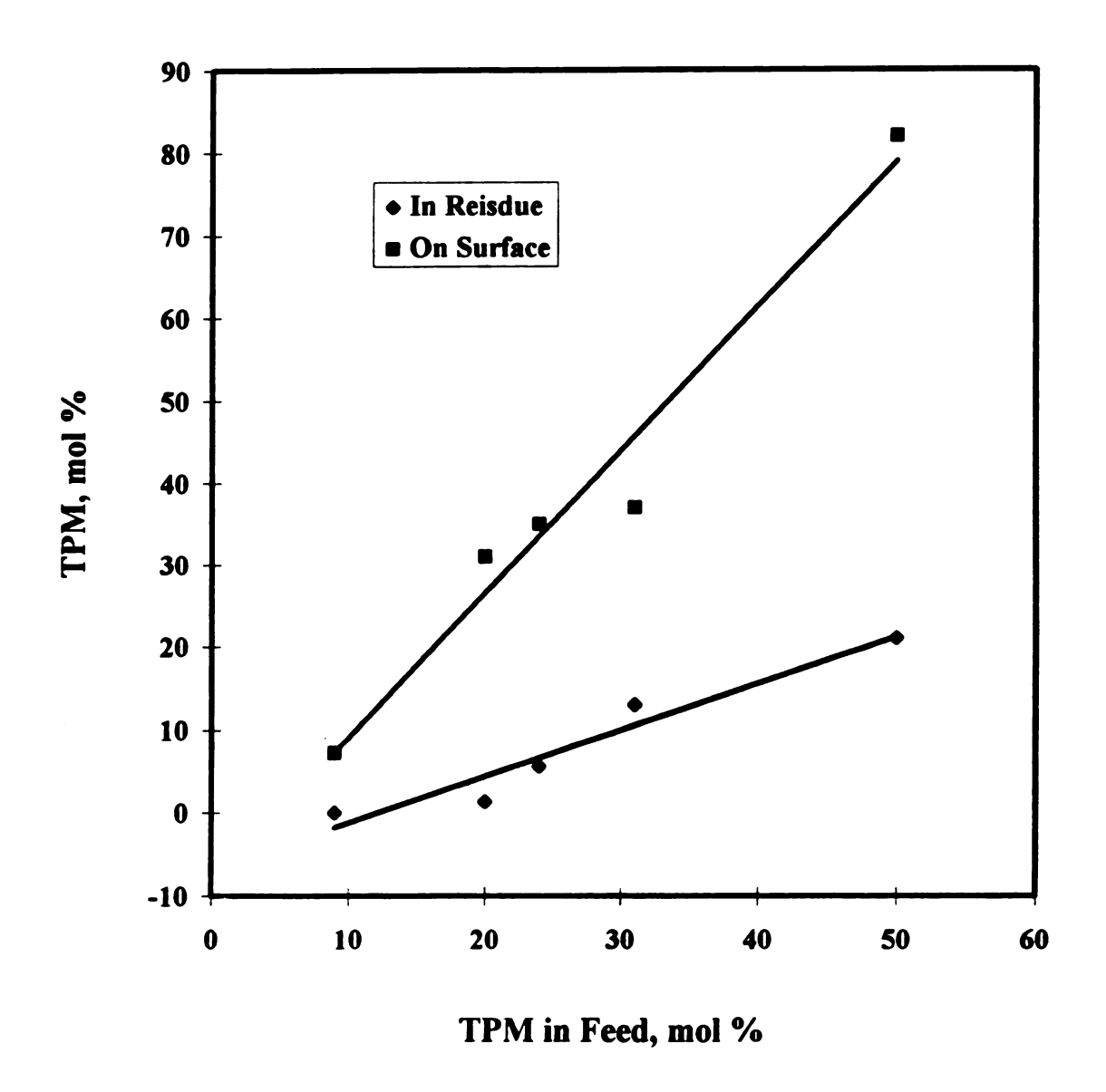


Figure 25. TPM fractions on silica surface and in residue.

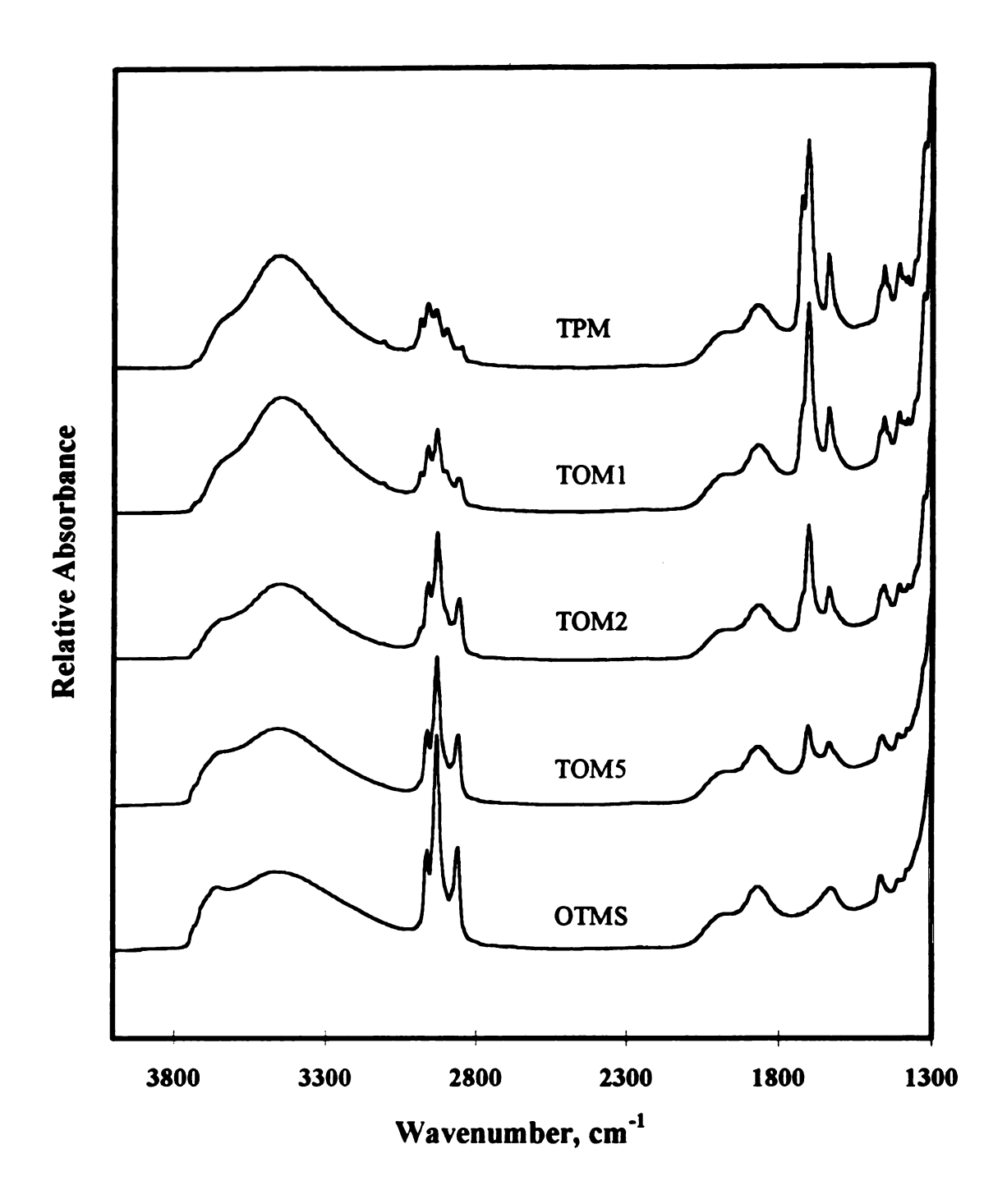
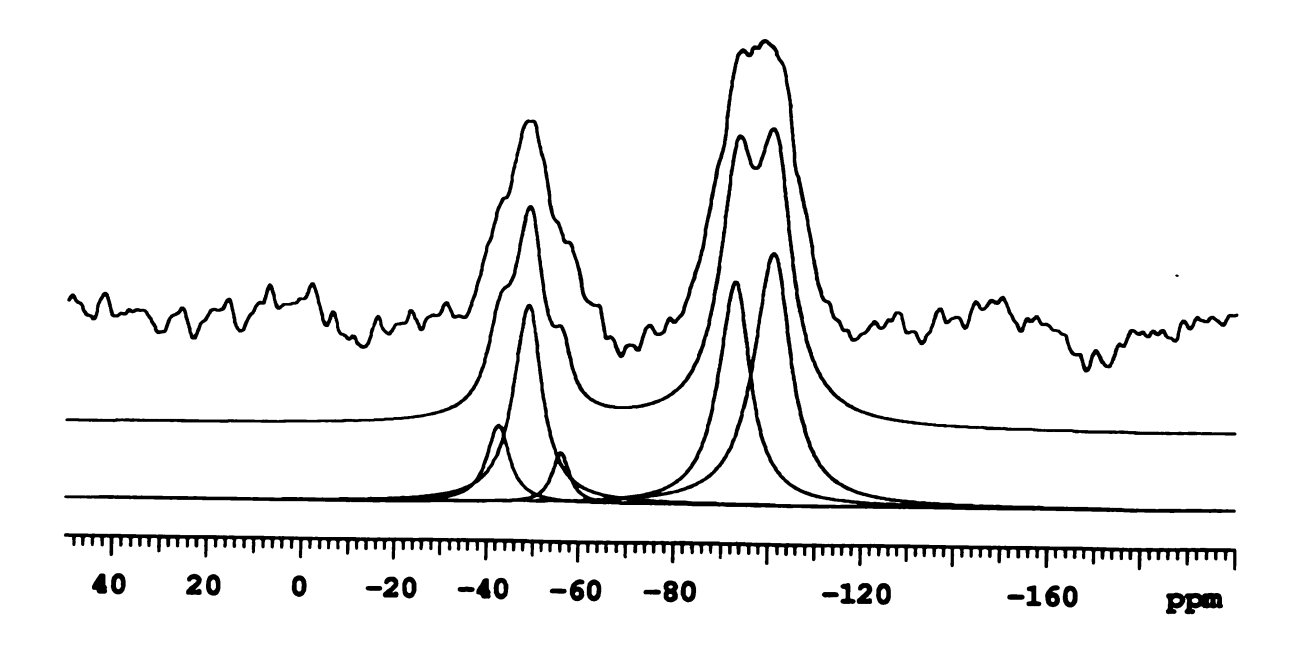


Figure 26. IR spectra of representative samples from Table 5.

The chemical attachment of silane coupling agents to silica surfaces was also verified by Cross-Polarization Magic Angle Spinning (CP/MAS) NMR spectroscopy. The <sup>29</sup>Si CP/MAS spectra of samples TOM4 and FS-C8-M are given in Figure 25. The broad peak from -80 to -110 ppm contains more than one component and is characteristic of fumed silicas without Si-C linkages. The resonances can be assigned to silicon atoms surrounded by four oxygen atoms. The other broad peak, ranging from -30 to -60 ppm, is also multi- component and is related to silicon atoms that have three oxygen atoms and one carbon in their nearest neighborhood. The <sup>13</sup>C CP/MAS NMR spectra of the same samples are shown in Figure 26 where the carbonyl carbon is seen at 170 ppm. The two peaks corresponding to the methacrylate double bond overlap due to the poor spectral resolution and the peak at 50 ppm can be assigned to unreacted methoxy groups which are not present in the spectrum of FS-C8-M due to the complete hydrolysis of chlorosilyl groups.



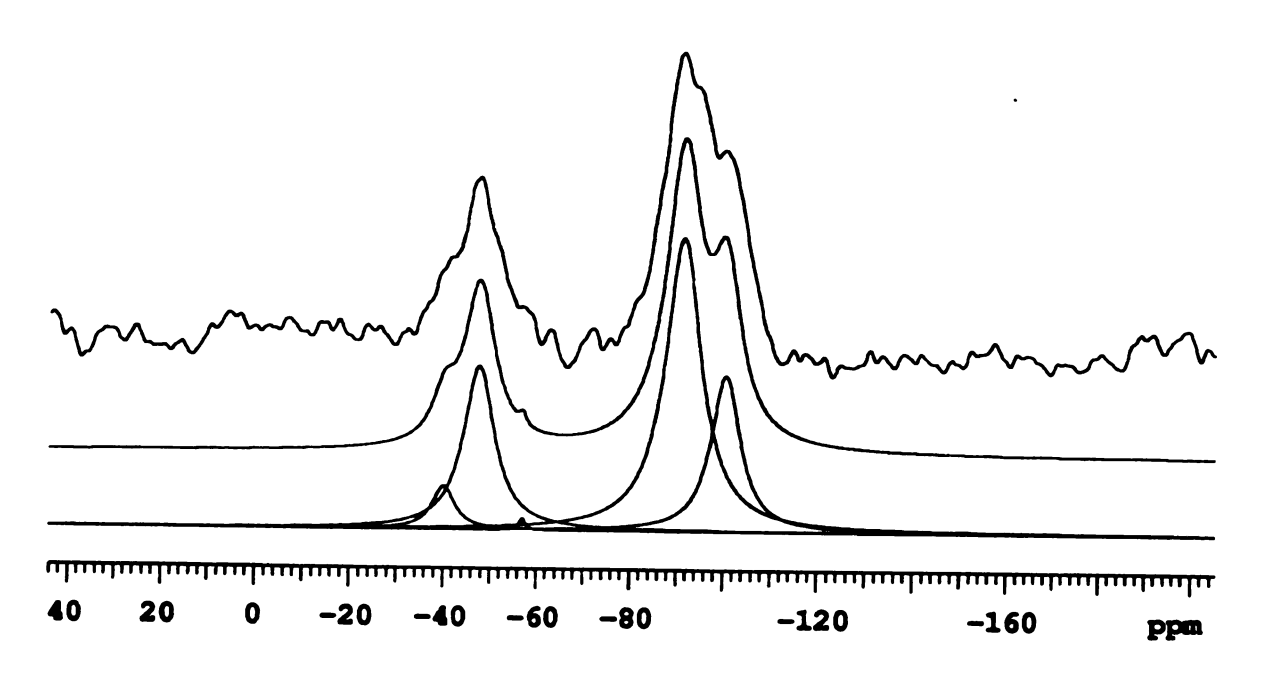


Figure 27. <sup>29</sup>Si CP/MAS spectra of samples TOM4 (top spectrum) and FS-C8-M (bottom spectrum). For each sample from top to bottom: actual spectrum, full fit and individual component plots.

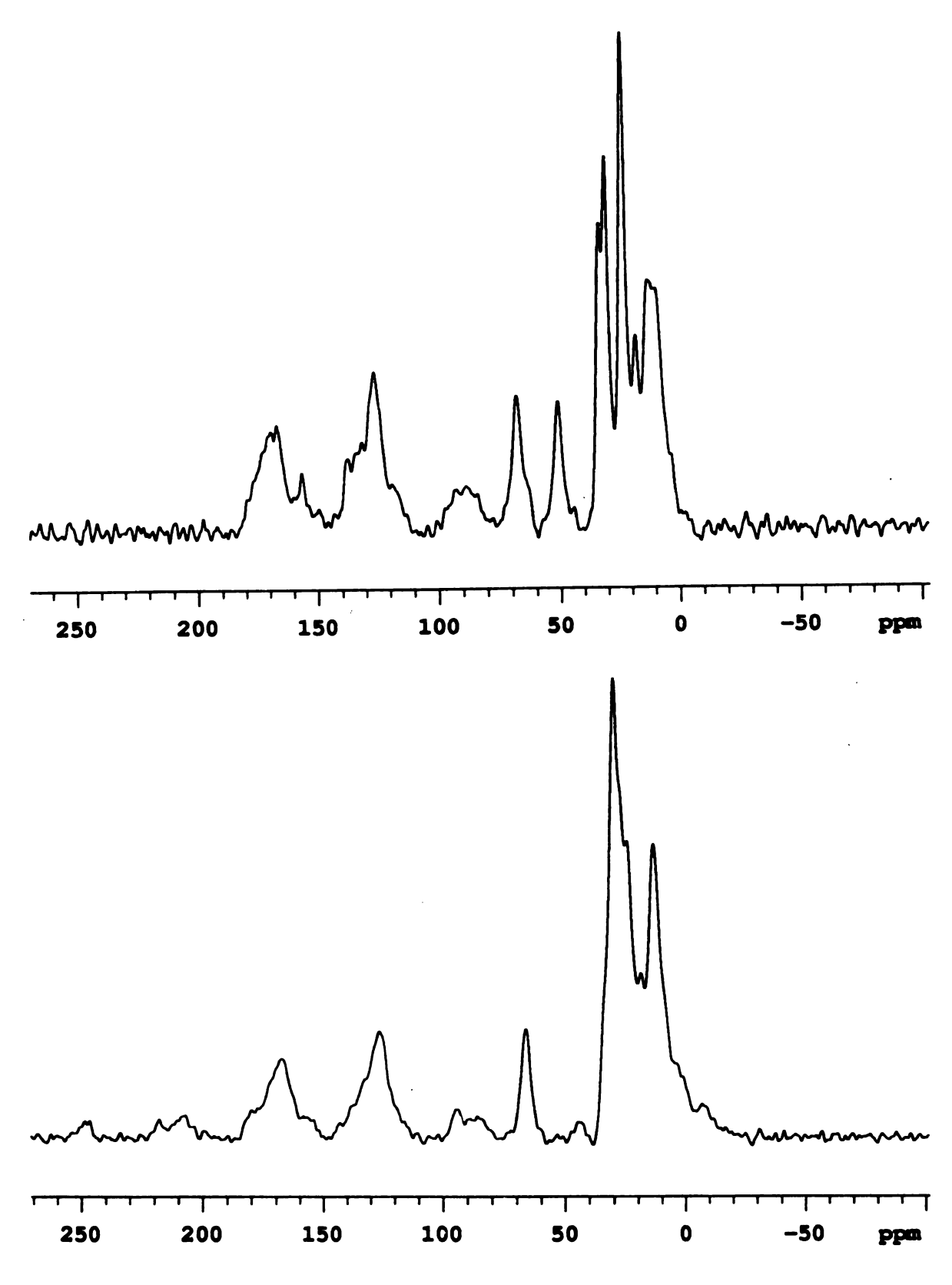


Figure 28. <sup>13</sup>C CP/MAS spectra of samples TOM4 (top) and FS-C8-M (bottom).

# V. Composite Polymer Electrolytes

We prepared composite polymer electrolytes using all the silica products prepared.

While both oligomeric PEO-bearing silicas and hydrophobic and cross-linkable silicas were used, emphasis was given to the latter since the mechanical properties of the composite were enhanced with the addition of a monomer and subsequent cross-linking.

## 1. Compatible Composite Polymer Electrolytes

Most composite polymer electrolyte samples were made using 15 wt % of silica, but others required more filler to prevent the electrolyte from flowing. When the filler is a pure silica or one modified with long PEO chains, more than 25 wt % of silica is needed for gelation (samples A200 and FS-DM-EO<sub>17</sub>, Table 6). Conductivities for all electrolytes

Figure 29. Schematic of PEO modified silicas.

Table 6. Conductivity data of electrolytes with compatible fillers.

Sample Name	Silica, wt %	σ*10 <sup>4</sup> , S/cm		
A200	25	1.01		
FS-DM-EO <sub>1</sub>	15	1.18		
FS-DM-EO <sub>2</sub>	15	1.89		
FS-DM-EO <sub>3</sub>	15	1.49		
FS-DM-EO <sub>8</sub> ª	15	1.66		
FS-DM-EO <sub>17</sub> ª	28	1.05		

<sup>&</sup>lt;sup>a</sup> Average number of ethylene oxide units.

fall in a narrow range. Electrolytes containing pure silica and FS-DM-EO<sub>17</sub> show similar but lower conductivities than the others, probably due to a "diluting effect" from the filler materials (25 and 28 wt %, respectively). All of these electrolytes are processable gels with good mechanical stability. For example, no sign of phase separation or of filler settling out has been seen over a period two years. It is interesting to note that the filler with the longest PEG chain requires less PEGDME to form a gel. Therefore, it might be possible to prepare a two-component composite polymer electrolyte incorporating only lithium salt and a "core-shell" material, featuring both good mechanical properties due to the silica "core" and high ionic conductivity because of a "shell" of PEG chains. There are many ways to realize such materials. For example, copolymerization of a polymerizable silica with a monomer such as poly(ethylene glycol) ethyl methacrylate, or similar monomers, would generate a core-shell structure.

### 2. Cross-linked Composite Polymer Electrolytes

The cross-linking experiments were carried out by adding a small portion of organic monomer (10 wt %) initiator to the recipe used for making composite electrolytes from fumed silica and polyethers. Cross-linking was achieved by exposure to UV light.

Scheme 23 shows how a cross-linked fumed silica composite was made starting from commercial fumed silica. The four steps involved were:

- Hydration of Aerosil 200 to increase the silane attachment;
- Silylation at room temperature in an organic solvent;
- blending of the electrolyte components;
- UV light initiated cross-linking.

The models of the target composite before and after cross-linking are shown in Figure 29. In short, our goal was to prepared first a temporary three-dimensional network, and then lock this network in place through a cross-linking step. In order to achieve this goal, the following issues were crucial to us. (1) The modified fumed silica would have to bear both hydrophobic and cross-linkable groups. The former would provide a physical gel through van der Waals attractions, and the latter would copolymerize with the added monomer to turn the gel structure into a dimensionally stable material. (2) The monomer would have to be able to access to the cross-linkable groups on the silica surface in order for the cross-linking to occur. The most extreme and favorable case is where the monomer phase separates from the PEGDME-500 and forms a thin layer around the silica network. Upon cross-linking, the monomer copolymerizes with silica functional groups

Scheme 24. Preparation of cross-linked composite polymer electrolytes.

**Cross-linked Fumed Silica Composite** 

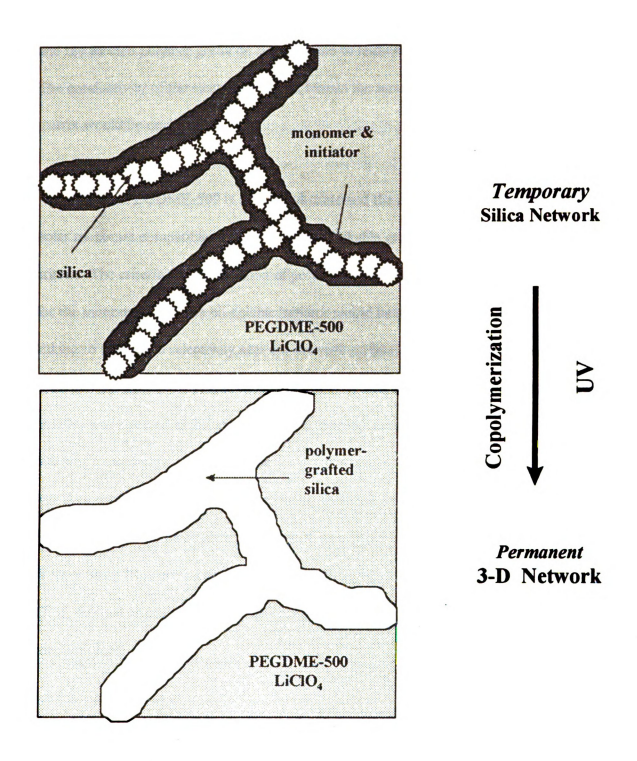


Figure 30. Designed models for cross-linkable composite polymer electrolyte: before (top) and after (bottom) cross-linking.

and the formed polymer grafts on silica surface to reinforce the strength of the network.

The conductivity of the electrolyte would remain the same because the polyether-Li salt matrix would be unchanged.

Since PEGDME-500 is a polar substrate and the network is hydrophobic, a non-polar monomer compatible with surface cross-linkable groups would meet the above criteria. The criteria for the selection of polymerization initiator would be similar to that for the monomer where an oil-soluble initiator would be desirable in order for the cross-linking to take place selectively near the network surface. A few monomer were tested and butyl methacrylate (BMA) was chosen as the monomer, and 2,2'-azobisisobutyronitrile (AIBN) was selected as initiator. BMA was distilled under vacuum before use. PEGDME-500 was treated with calcium hydride for three days at room temperature and the liquid was then distilled under vacuum. A series of studies were carried out, including the physical state of the electrolyte in relation to its composition, monitoring the cross-linking process using IR spectroscopy, morphology studies of composites using Freeze-Fracture TEM, thermal characterization of composites, and the temperature and salt-dependent conductivities.

The physical state of the composite depends on the type of fumed silica used, as well as the amount of fumed silica and LiClO<sub>4</sub> in the composite. In general, the viscosity increases with the increase of silica and lithium salt contents. This trend follows the well known increase in T<sub>8</sub> seen for PEG electrolytes with increasing salt concentrations. The silica content in the composite was 10 wt% in all preparations, since lesser amounts tend

not to provide an adequate thickening effect, and larger amounts usually results in a dilution effect that leads to lower conductivities. The air bubbles trapped in the composites prepared from methacrylates other than MMA during blending were removed by applying a vacuum. The time required depends on the viscosity of the composite. MMA-containing composites were not treated with vacuum. Instead, an aging process was used and the composites were air-free spontaneously after a few days. At such a silica content, at least a day is necessary to remove the air bubbles fully from R805 composites due to its high viscosity. Composites containing FS-C3-M show the lowest viscosity and FS-C8-M-2 is an ideal choice for composite polymer electrolytes since it offers a moderate viscosity which allows for the bubbles to be removed readily and for the gel to be physically stable.

Figure 30 shows IR spectra of a composite polymer electrolyte before and after cross-linking. The absorption at 1640 cm<sup>-1</sup> due to the methacrylate double bond (which overlaps with water deformation mode) disappeared, and the carbonyl peak at 1705 cm<sup>-1</sup> shifted to 1724 cm<sup>-1</sup> as a result of loss of the double bond conjugation. The UV-initiated polymerization kinetics were monitored using IR spectroscopy. The spectrum at time zero was taken as the reference so that all of the spectra shown in Figure 31 are difference spectra. As can be seen, the double bond and carbonyl peaks are consumed with irradiation time. The relative intensity (peak height) of these peaks at different times represents the conversion of monomer to polymer and were recorded in Table 8 and used to make Figure 32. It is easy to see that polymerization was complete in less than 20 min.

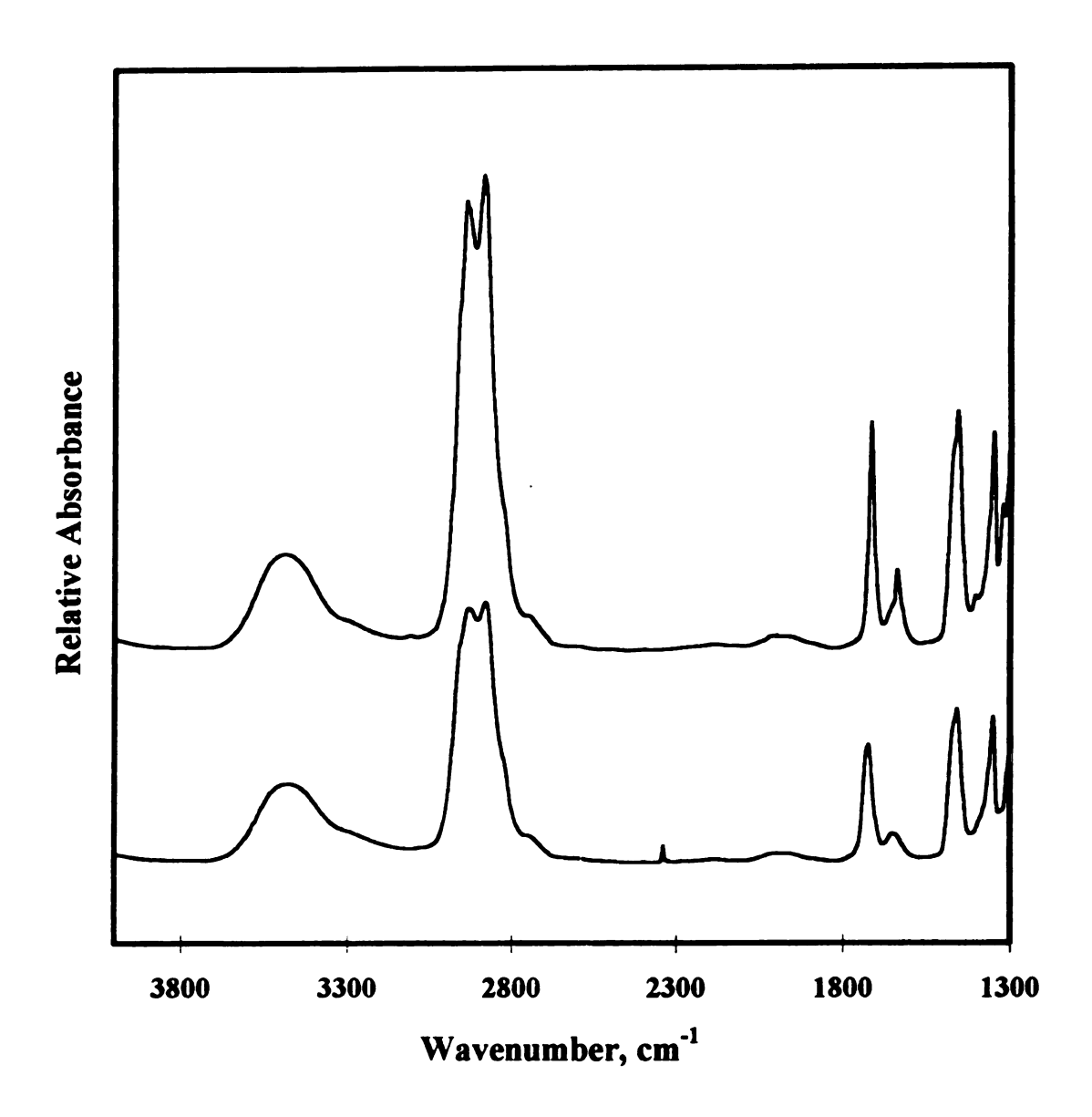


Figure 31. IR spectra of composites before (top) and after (bottom) cross-linking.

Table 7 IR data for UV initiated polymerization.

Intensity	Intensity	Time	Conversion, %	Conversion, %
C=O	C=C	minutes	C=O	C=C
8.0	2.5	1.0	12.3	21.2
12.5	3.5	2.0	19.2	29.7
15.8	4.0	3.0	24.3	33.9
20.0	4.6	4.0	30.8	39.0
29.3	6.0	6.0	45.1	50.8
42.5	7.5	8.0	65.4	63.6
55.0	9.0	10.0	84.6	76.3
60.0	9.7	12.0	92.3	82.2
63.0	10.2	14.0	96.9	86.4
65.0	11.2	18.0	100.0	94.9
63.0	11.8	26.0	96.9	100.0

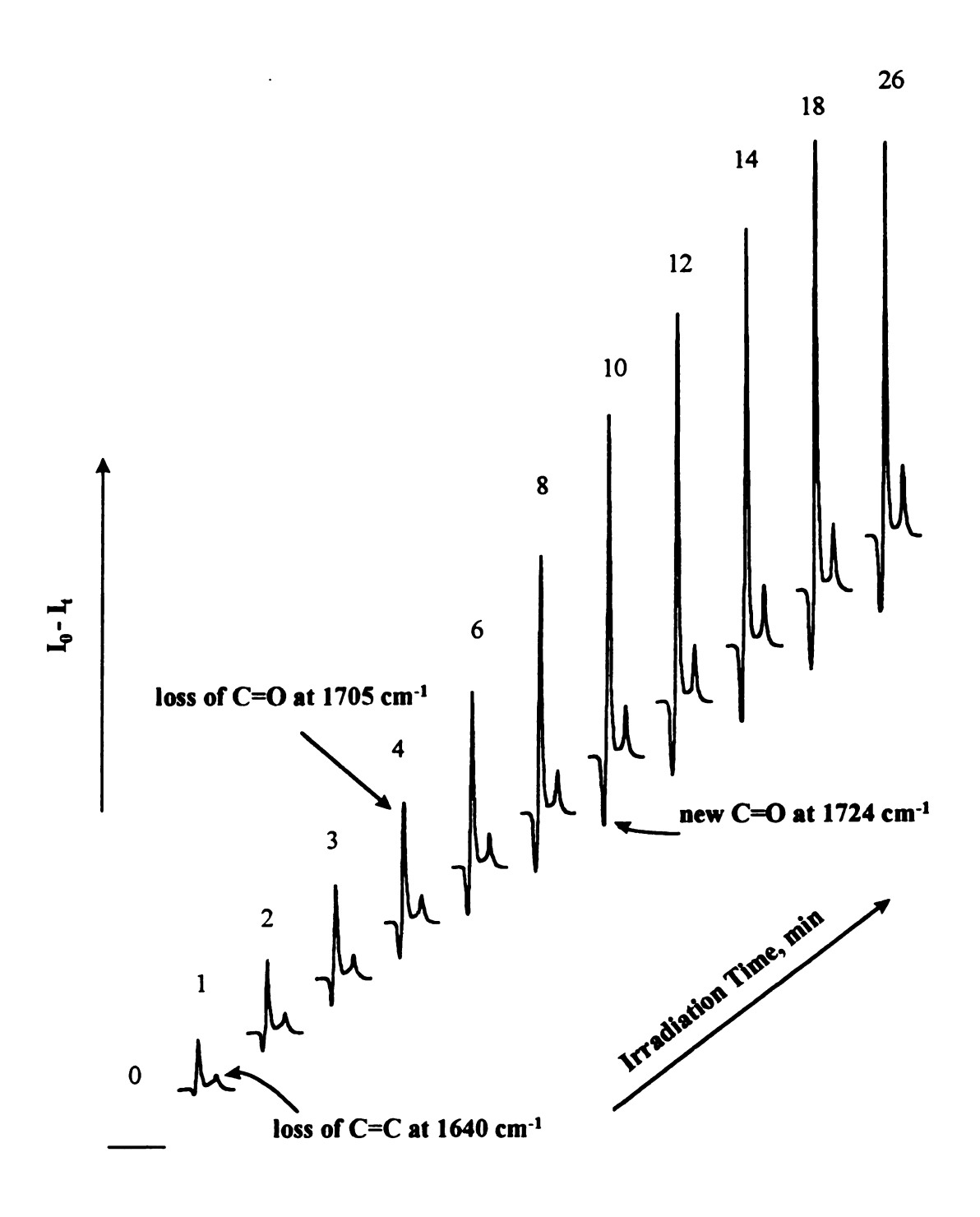


Figure 32. IR-generated cross-linking kinetics. Spectra are a series, and correspond to the original spectrum-the spectrum taken at time t.

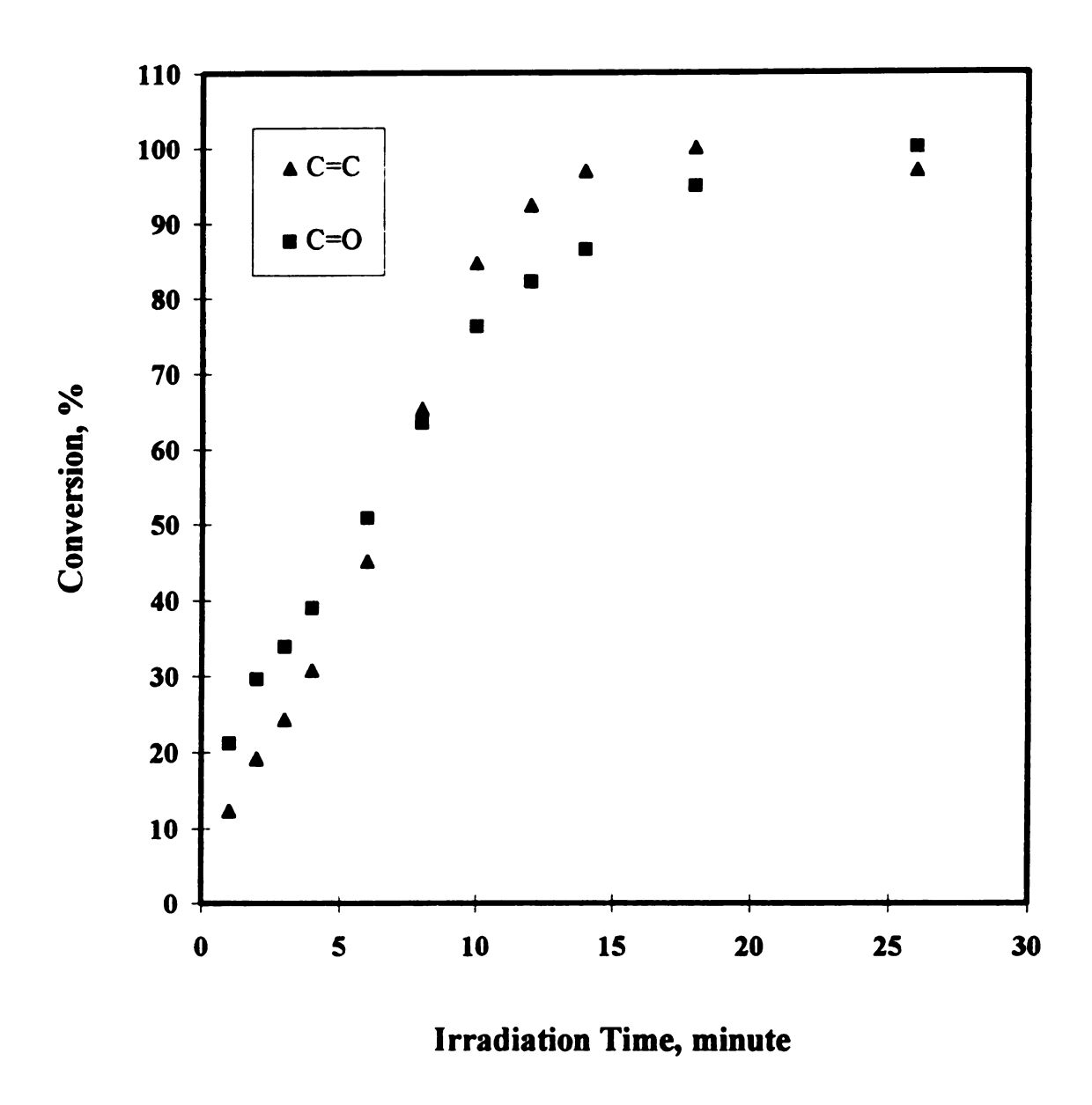


Figure 33. Conversion of polymerization vs irradiation time.

The conversion curve obtained from the carbonyl peak deviates slightly from that achieved from the double bond peak, probably due to the overlapped absorption of carbonyl group before and after cross-linking.

In order to study the effects of silica and subsequent cross-linking on the glass transition temperature of polyether matrix, a series of DSC experiments were carried out.

Our DSC measurements of PEGDME/LiClO<sub>4</sub> mixtures without added silica are shown in Figure 33 and thermal transition data are listed in Table 9. These data are second scans, taken after flash quenching samples from 100 °C. At high O/Li ratios (low LiClO<sub>4</sub>)

Table 8. Thermal properties of PEGDME-LiClO<sub>4</sub> system

O/Li	8	12	15	18	22	26	29	35	39	60	139
$T_{g}(\mathcal{C})$	-50	-58	-67	-69	-73	-74	-55	-58	-59	-61	-66
$T_c(\mathcal{C})$	•	-14	-40	-53	-61	-64	•	•	•	-	-
$T_m(\mathcal{C})$	•	6	6	9	9	11	13	14	13	13	14

content), DSC traces show a single broad melting peak that corresponds to the melting of a pure PEGDME phase. Addition of LiCLO<sub>4</sub> causes both the melting point and the enthalpy for the transition to decrease, and at an O/Li ratio of 8, the transition is no longer detectable. A low temperature exothermic peak visible at intermediate salt concentrations corresponds to crystallization of a portion of the sample, presumably a pure PEGDME phase. A glass transition is also seen for these samples that, as expected, shifts to higher temperatures with increasing salt content. No crystallization was observed by DSC for samples with low salt contents, since for these materials, the PEGDME relaxation times are short and the PEGDME chains crystallize while being quenched from 100 °C.

DSC scans of composites with silica (Figure 34) are remarkable in that the thermal transitions (see also Table 9 and 10) for composites with and without silica appear at the same temperatures. These results show that the mobility of the PEGDME, as measured by Tg, is unaffected by the added silica. This is strong experimental verification of the notion that the properties of the PEGDME phase are strongly decoupled from the added silica, and that the improved mechanical properties provided by the fumed silica matrix are gained without significant losses in conductivity.

DSC traces for cross-linked composites containing LiClO<sub>4</sub> are shown in Figure 35.

Qualitatively, they resemble those taken for composites before cross-linking. Some slight shifts in position and intensity are seen for the melting and crystallization transitions, but

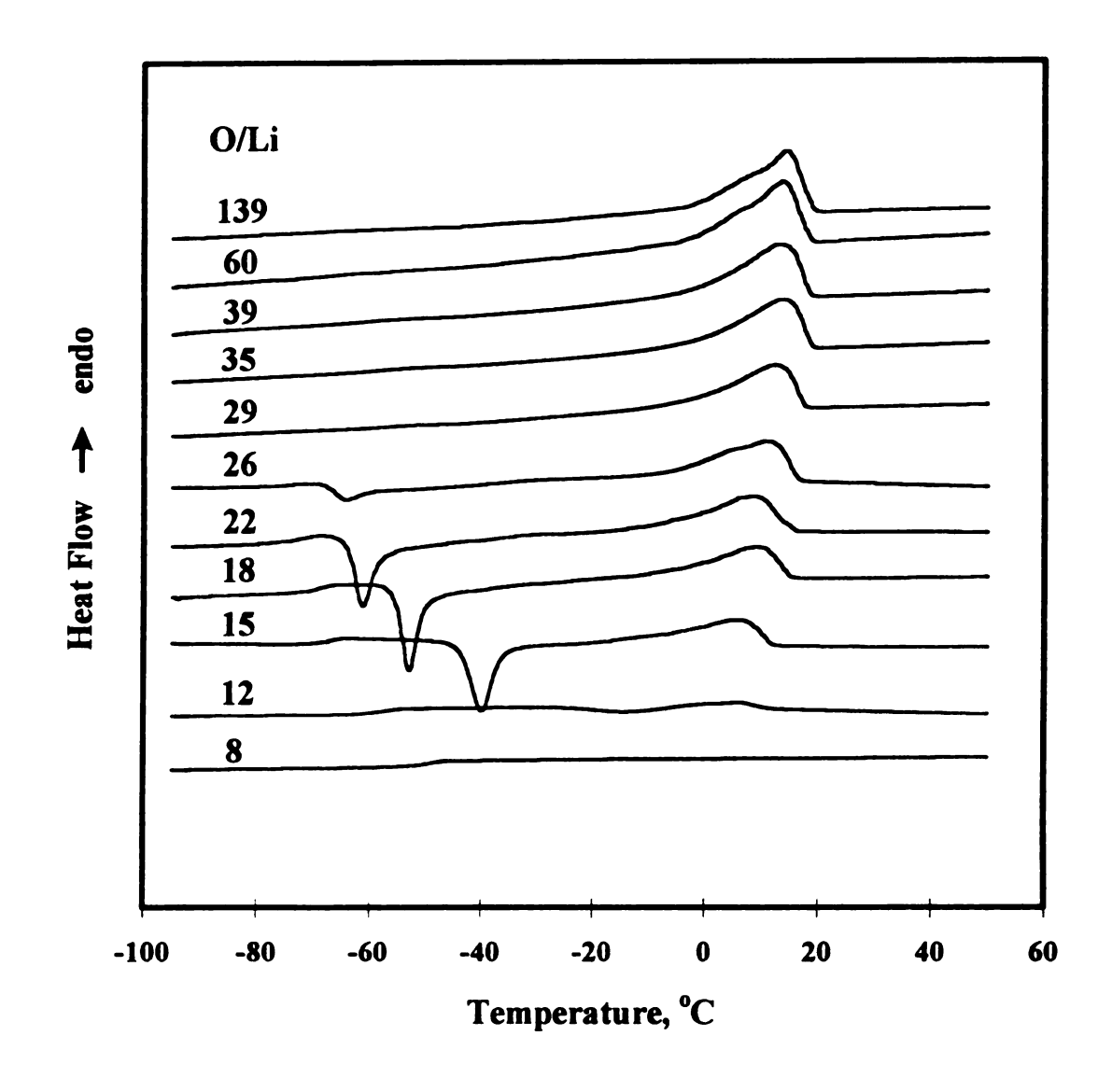


Figure 34. DSC second heating scans for PEGDM-500/LiClO<sub>4</sub> electrolytes.

Conditions: run under He at a heating rate of 10 °C/min.

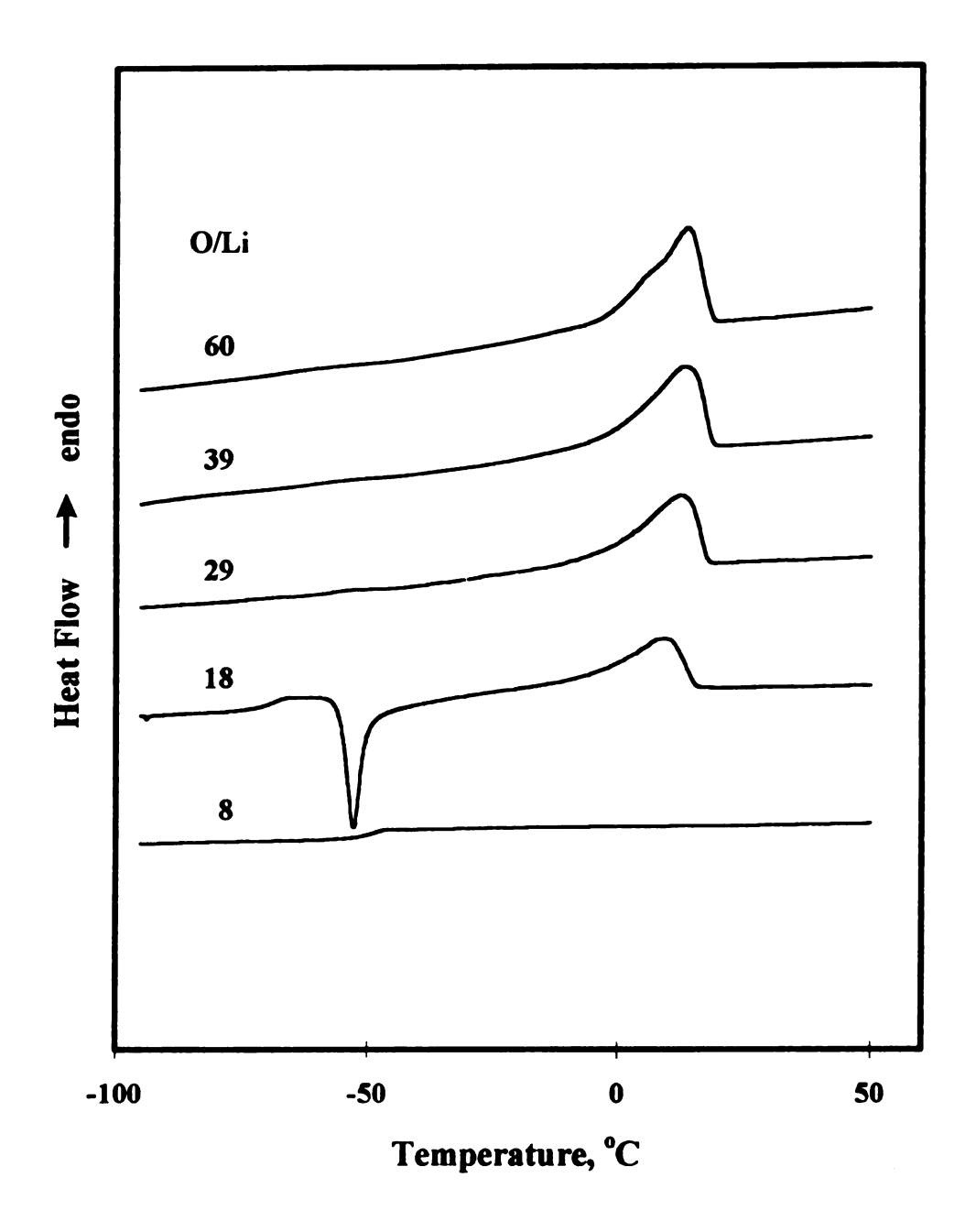


Figure 35. DSC second heating scans for PEGDM-500/fumed silica/LiClO<sub>4</sub> electrolytes. Conditions: run under He at a heating rate of 10 °C/min.

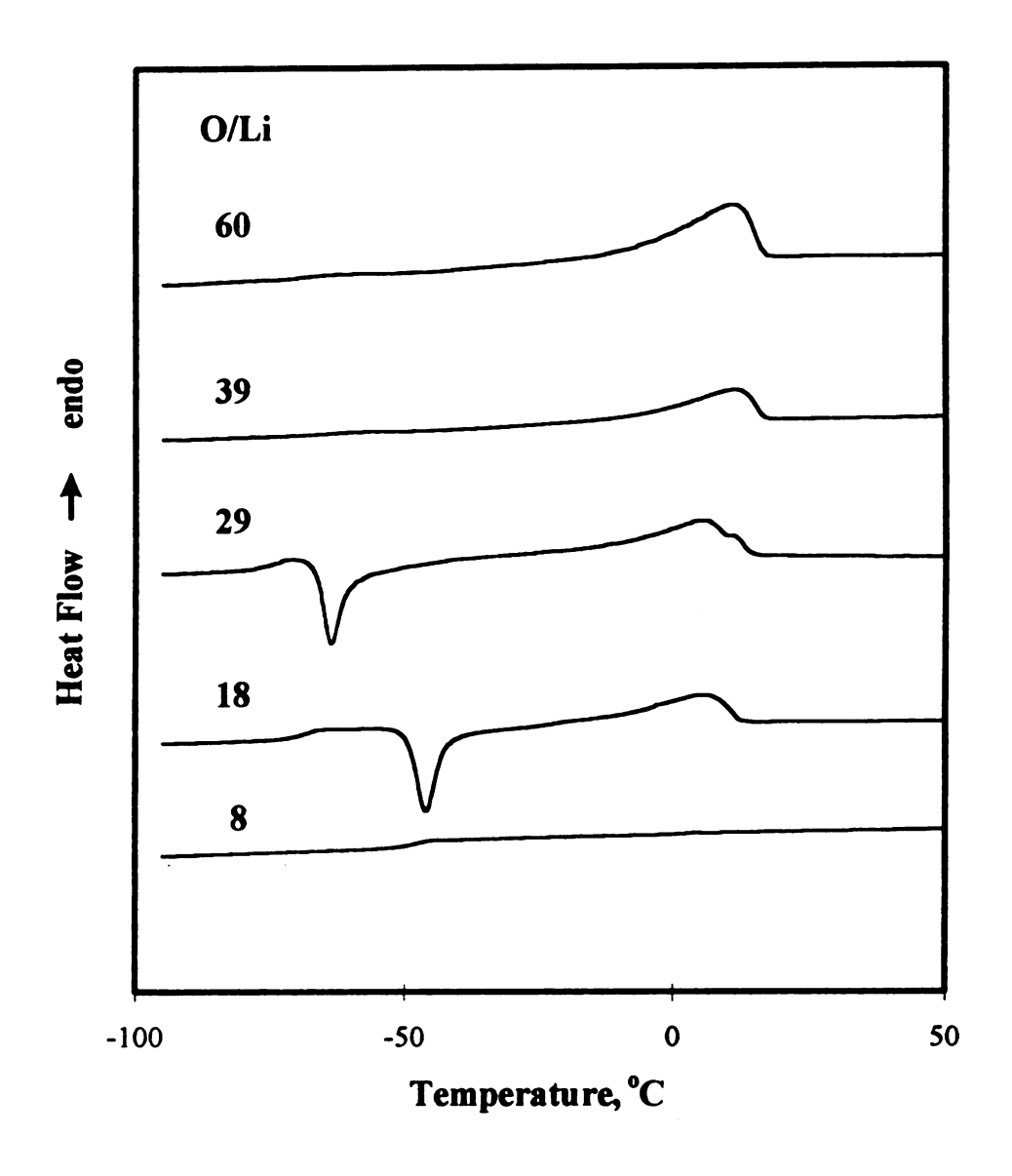


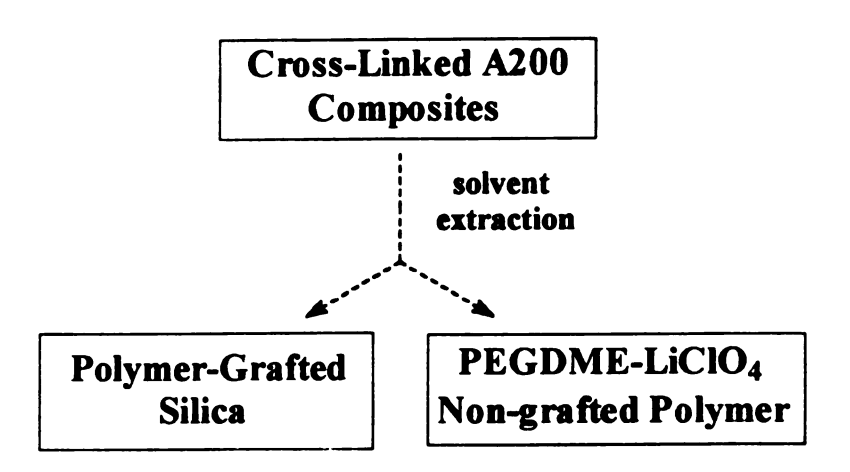
Figure 36. DSC second heating scans for cross-linked PEGDM-500/fumed silica/LiClO<sub>4</sub> electrolytes. Conditions: run under He at a heating rate of 10 °C/min.

Table 9. Thermal transition data of composites before and after cross-linking.

O/Li	8	18	29	39	60
Before $T_g(\mathcal{C})$	-51	-75	-61	-65	-66
$T_c(\mathcal{C})$	-	-60	-	-	-
T <sub>m</sub> (°C)	-	6.0	9.0	11	11
After $T_g(\mathcal{C})$	-48	-69	-75	-62	-66
$T_c(\mathcal{C})$	-	-46	-64	-	-
$T_m(\mathcal{C})$	-	5.6	5.4	11	11

the values of the glass transitions are unchanged. Some hints of the chemistry that takes place during the cross-linking reaction can be inferred by monitoring changes in the IR spectrum of composites, and the TGA data for cross-linked electrolytes. An electrolyte was prepared from PEGDM-500, cross-linkable fumed silica LiClO<sub>4</sub> and butyl methacrylate. As shown in Figure 36, the C=O and C=C vibrational bands characteristic of methacrylates are found in the spectrum of this uncross-linked silica (middle scan), and after irradiation, these bands shift to positions expected for a polymerized methacrylate. The bottom scan in Figure 36 corresponds to the residue of a cross-linked sample that was extracted exhaustively with acetone, a good solvent for poly(butyl methacrylate), and then dried (Scheme 24). Prominent C=O and C-H stretching bands of the polymethacrylate dominate the spectrum. TGA scans of the same silica/polymer residue (Figure 37, bottom scan) show a 52% weight loss. The predicted weight loss, assuming all of the butyl methacrylate co-polymerized with the methacrylates bound to the fumed silica, was 56%.

Scheme 25. Solvent extraction experiments to analyzed surface-grafted polymer.



Thus, we conclude that nearly all of the added monomer was chemically bound to the functionalized silica during cross-linking.

TEM imaging techniques were used to investigate changes in the structure and morphology of the silicas and their composites. Figures 39, 40, and 41 are TEM images of A200, cross-linkable A200, and the extraction residue of cross-linked composite. For comparison purposes, images taken at two different magnifications are shown in each case. As can be seen, the network structure of these three samples become more even and denser in going from most polar (A200) to least polar (residue). The same phenomenon was also observed by others. 42

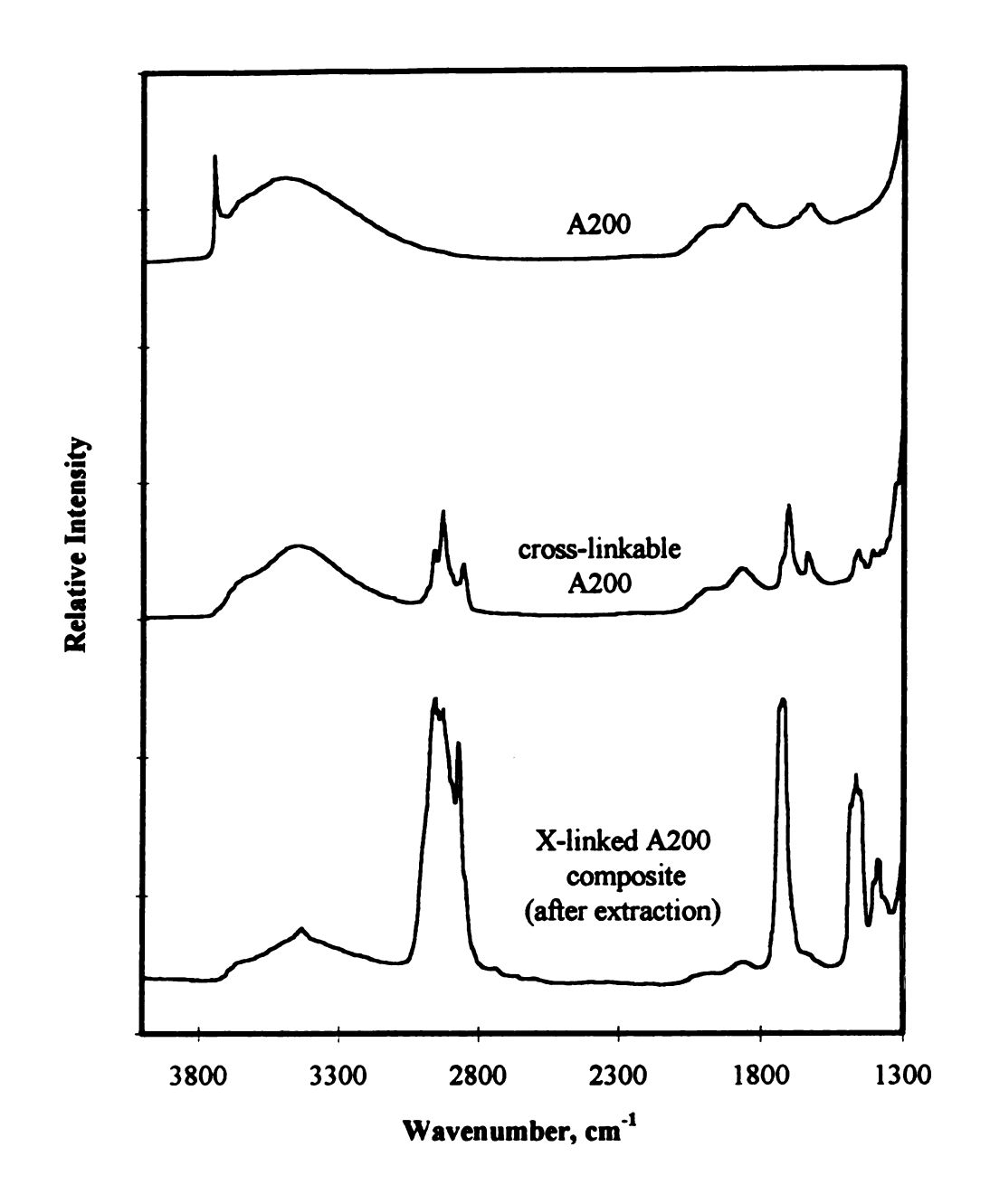


Figure 37. IR spectra of surface modified silicas. *Top scan:* Aerosil A-200 fumed silica; *middle scan:* A-200 modified with surface-bound methacrylates; *bottom scan:* cross-linked composite electrolyte after exhaustive extraction with acetone.

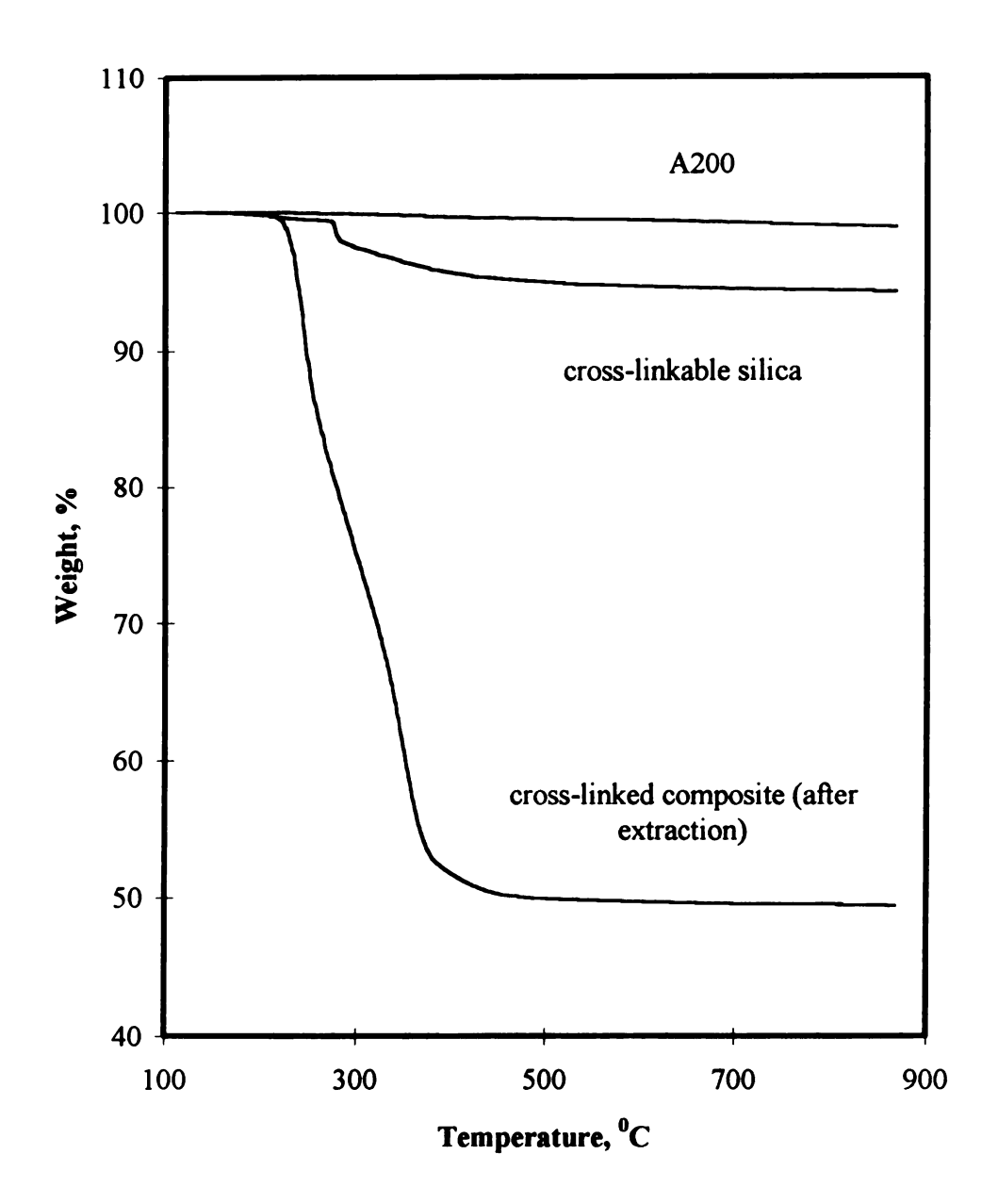


Figure 38. TGA scans of surface-modified fumed silicas. *Top scan:* Aerosil A-200 fumed silica; *middle scan:* A-200 modified with surface-bound methacrylates; *bottom scan:* cross-linked composite electrolyte after exhaustive extraction with acetone.

Conditions: run in air at a heating rate of 10 °C/min.

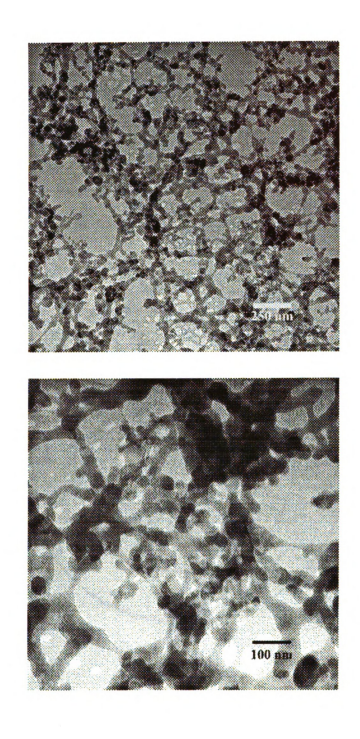


Figure 39. TEM micrographs of A200.

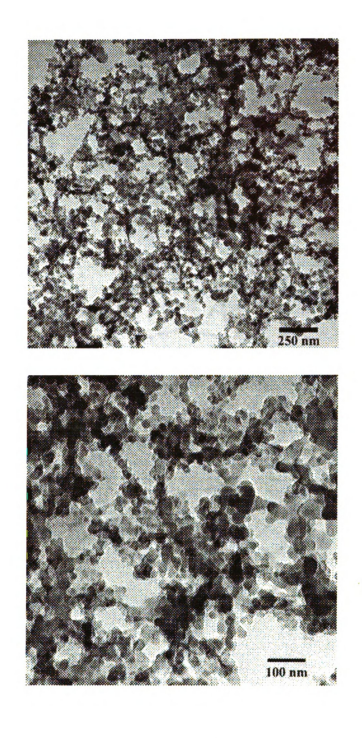


Figure 40. TEM micrographs of cross-linkable silica.

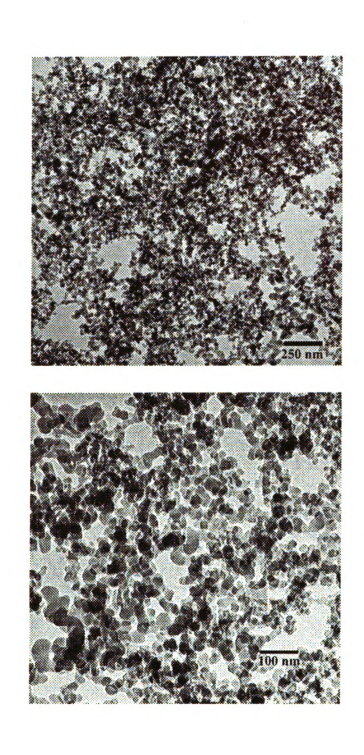


Figure 41.TEM micrograph of extraction residue of cross-linked composite.

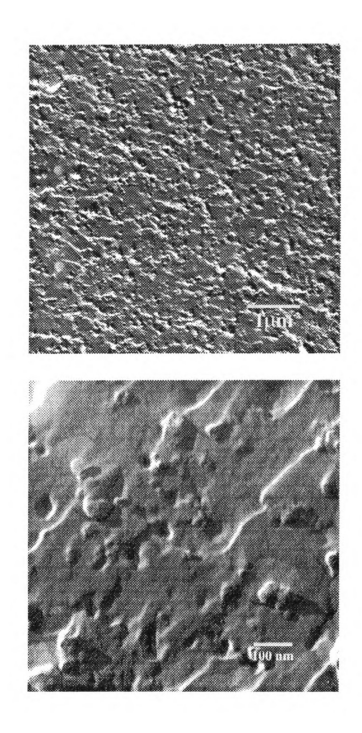


Figure 42. Freeze-Fracture TEM images of composites before cross-linking.

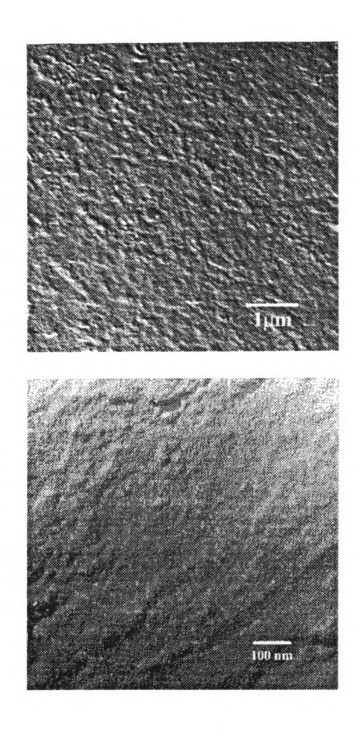


Figure 43. Freeze-Fracture TEM images of composites after cross-linking.

In order to study the morphology of composites in situ, replicas of electrolytes were made using Freeze-Fracture techniques. Typically, The sample was placed on a copper cap and fractured to generate a fresh surface which was replicated. The silica network structure is clearly seen before cross-linking (Figure 42), but more featureless after cross-linking (Figure 43). Two possible explanations might be possible. First, before cross-linking, adhesion between the silica and PEGDME-500 is poor, and fracture preferentially occurs at the silica-PEGDME-500 interface. Polymerizing the added methacrylate binds the silica particles together, strengthens the silica-PEGDM-500 interface, and leads to fracture within the PEGDME-500 phase. Second, before crosslinking, silica network is only temporary and is easily broken down. Upon cross-linking, all the particles are bound together and the network resists to the fracture. Thus, uncrosslinked composites looks particulate, while the cross-linked samples appear smooth. The featureless morphology of polymer latex films has recently been correlated with the physical properties of the two polymer phases. 85 Additional experiments are needed to corroborate this model.

Conductivity measurements show that the cross-linking reaction has little effect on the ionic conductivity of the composites. As shown in Table 10 and Figure 44, the room temperature data for a sample before and after cross-linking are nearly identical,  $2-4 \times 10^{-4}$  S/cm. These results are consistent with the thermal analysis data that show little change in the  $T_8$  of composites after cross-linking. The conductivity depends on the lithium salt content and reaches a maximum at O/Li ratios of 20-40. The conductivity data were also

analyzed using an Arhennius plot (Figure 45) and from these plots, an interesting trend emerges. At high O/Li ratios, the slopes of the plots (activation energies) are similar, but as the O/Li ratio further decreases, the apparent activation energies steadily increase. In addition, the data taken at a given salt content are not linear, and are suggestive of a phase transition near 55 °C. The nonlinearity is most pronounced for materials with high salt contents, which would be consistent with a crystalline-amorphous phase transition. However, to date we have been unable to verify such a transition by DSC or optical microscopy.

Table 10. Conductivity data (×10<sup>4</sup>) for Figure 43.

O/Li	368 K	348 K	328 K	318 K	298 K	298 K
8	12.6	6.62	3.62	2.16	0.62	1.14
18	13.2	11.4	7.29	5.08	2.25	2.93
29	13.5	11.9	8.13	6.32	4.15	2.63
39	8.13	6.94	5.08	4.15	2.13	2.17
60	5.04	4.12	3.16	2.53	1.44	0.9

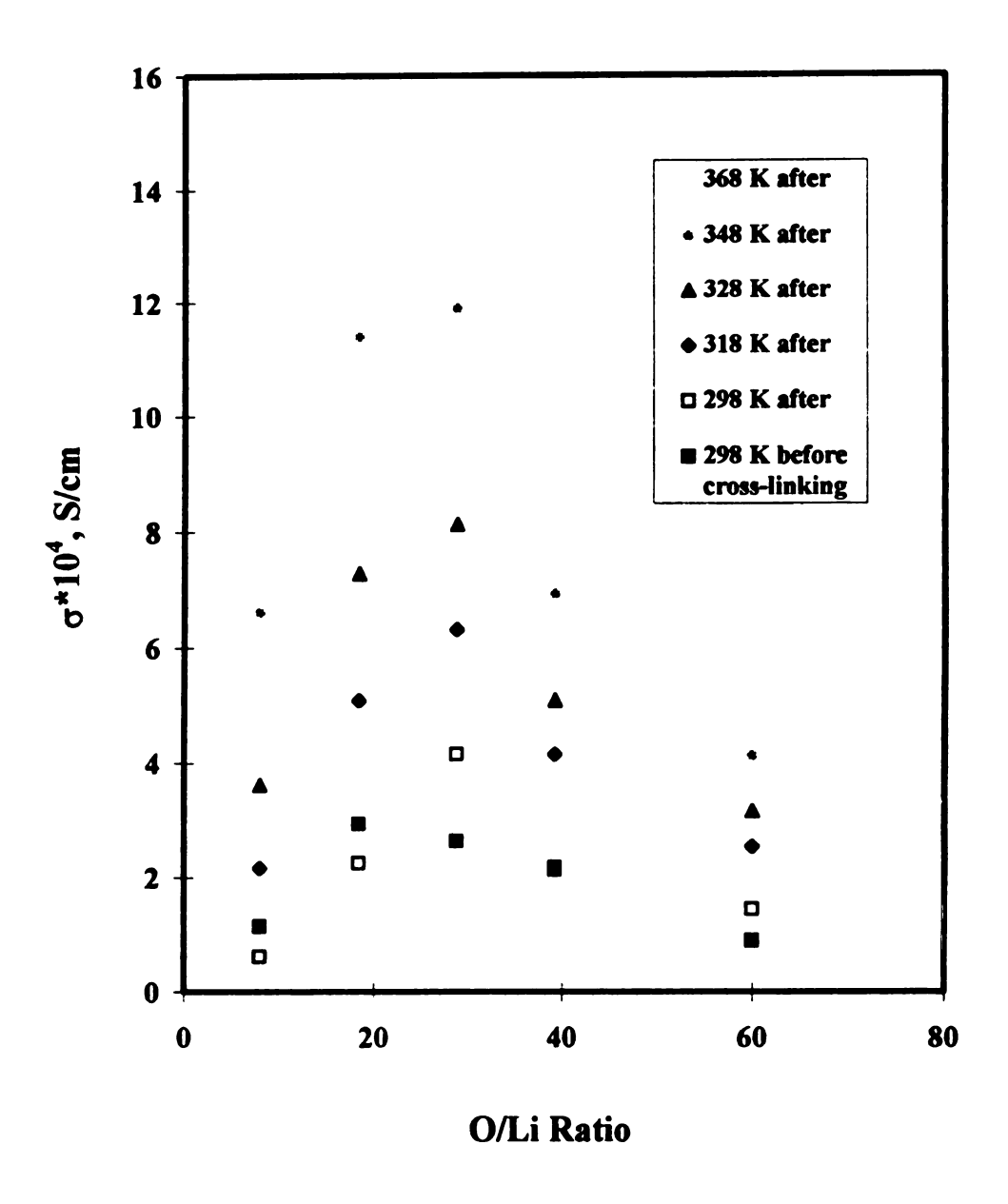


Figure 44. Conductivity of composite electrolytes at selected temperatures before and after cross-linking.

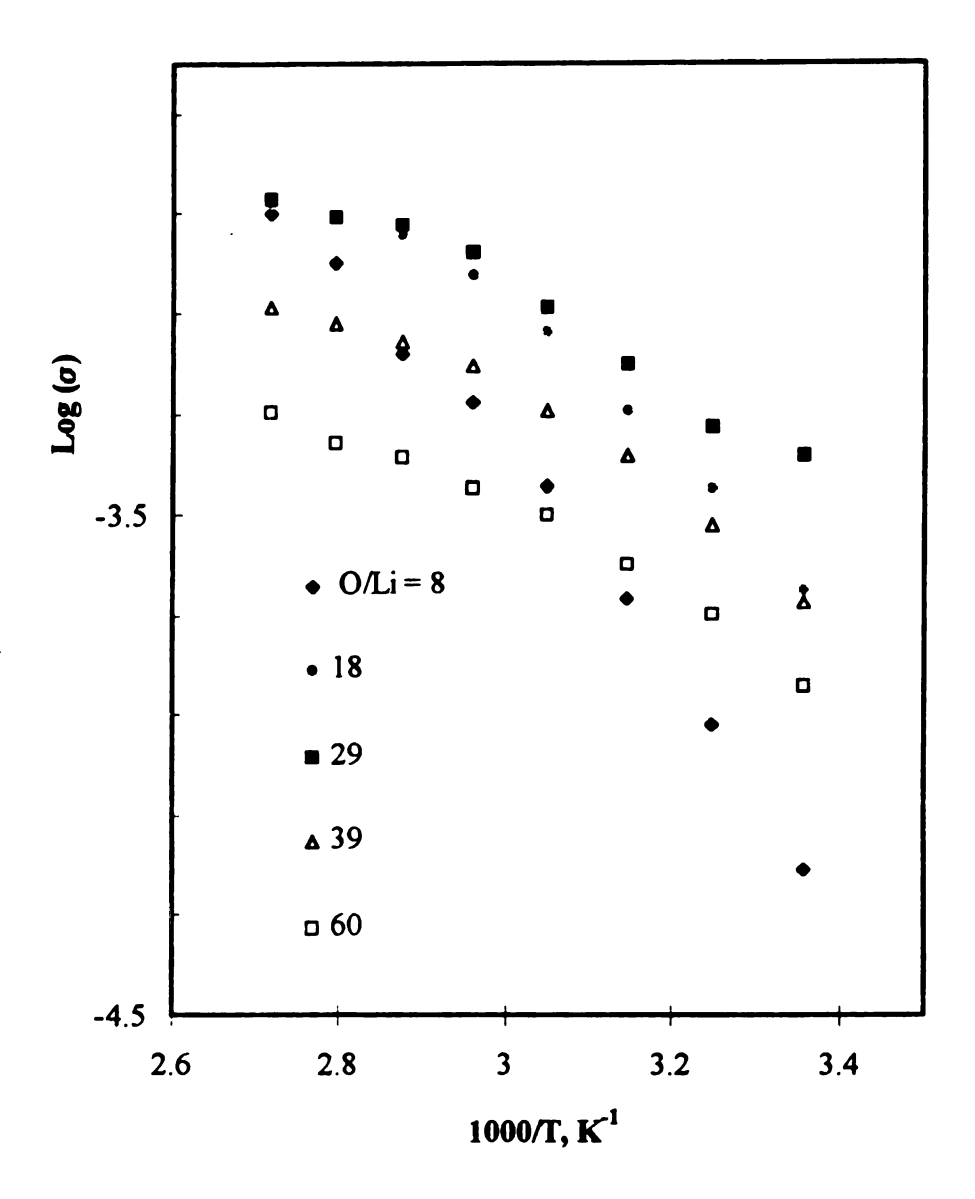


Figure 45. Arrhenius plots of the conductivity of cross-linked composite electrolytes.

# **DISCUSSION**

# I. Current System

# 1. Composite Reinforcing mechanism: phase separation

We have shown that highly processable furned silica-based electrolytes, consisting of PEGDME, LiClO<sub>4</sub>, butyl methacrylate, and furned silica with hydrophobic and cross-linkable groups, can be converted via photopolymerization into mechanically robust electrolytes with no apparent loss in conductivity. These results are in stark contrast to the data typically obtained with cross-linked polymer electrolytes. Usually cross-linking or the formation of interpenetrating network structures are accompanied by a large drop in conductivity, often by an order of magnitude. <sup>26,86,87</sup> The principal difference between the furned silica system and traditional polymer electrolytes is that the mechanical properties of the composite and the ion conducting characteristics are decoupled, and thus these two important characteristics can be optimized independently.

A simple model to understand these results can be based on phase separation processes. For example, the addition of fumed silica to polyethers-LiClO<sub>4</sub> mixtures yields a two-phase system, the silica network structure that provides mechanical reinforcement of the composite and the polyether-LiClO<sub>4</sub> phase that results in high conductivity. Single phase (or at least highly dispersed) polyether/silica mixtures can be prepared by appropriate surface modifications. For example, as discussed in the Results section, using standard chemical techniques, we attached short polyether chains to A200. As long as its

content is low enough (<10% by weight), the modified silica completely dispersed in PEGDME-500 to give a clear viscous liquid. Similarly, there are many reports of the preparation of silicas by hydrolysis of tetraethoxysilane followed by surface modification to match the chemical characteristics of a particular matrix. These also form homogeneous solutions. 64,65 Mechanical properties appreciably better than the matrix itself requires a silica network structure, which in turn requires a fumed silica that does not disperse, but instead aggregates. This structure must then be preserved in the cross-linked electrolyte.

Cross-linked composites based on polymerizable fumed silica alone were mechanically weak and fractured easily, a sign of minimal chemical connectivity between adjacent silica particles. For strong composites, added monomer is needed to knit the silica particles into a mechanically stable framework. Given that the starting point for our model is a two-phase system of silica dispersed in a polyether, the most important question is the fate of the monomer added to the composite before photopolymerization. We know from test polymerizations of butyl methacrylates in PEGDM-500 that monomer/polyether solutions are initially homogeneous, but phase separate when lithium salt is present. When fumed silica is added to the above mixture, phase separation is not visible on a macroscopic level. Upon cross-linking, the slurry becomes cloudy, an obvious indication of phase separation, suggesting that phase separation might have occurred even before cross-linking on a microscopic scale. Moreover, polymerizations using octyl methacrylate yield the most turbid products while the more polar methyl methacrylate and poly(ethylene glycol) ethyl methacrylate appears to be the most clear. These results are in line with the

relative differences in solubility parameters for the methacrylate polymers relative to PEGDME-500. Since none of these polymers are completely soluble in PEGDME-500, these results are not surprising, but they do point to a phase separation model. At least three limiting cases can be considered. (1) The monomer phase separates from the PEGDME-500 phase to form monomer droplets which develop into distinct polymer phases upon cross-linking (Figure 46, A). if this model were true, the glass transition temperature of polyethers would remain the same, but the guest polymer phase would be extractable. (2) The monomer mixes with polyethers and develops into a homogeneous phase on macroscopic level after polymerization (Figure 46, B). In this case, not only would the guest polymer be extractable, but the glass transition of polyethers would be affected. (3) The monomer separates from polyethers to form a thin layer surrounding the silica network where copolymerization between monomer and surface functional groups takes place (Figure 30). The first two scenarios are ruled out by extraction and DSC experiments carried out on cross-linked composites. Fully cross-linked samples were extracted to remove the free polymer and the PEO-LiClO<sub>4</sub> and the insoluble residue was analyzed. If pure homopolymer formed a distinct polymer phase, then it should be easily removed, and the weight loss in the TGA experiment should be comparable to that seen for the surface-modified silica alone (i.e., 6%). The results, however, point to nearly all (> 90 %) of the monomer being chemically connected to the silica. The scenario (2) is further ruled out by the DSC data which show that the glass transition temperature for polyethers in the composite was unchanged before and after cross-linking. Thus, some version of scenario (3) must be at play. This model (Figure 30) can be rationalized by the

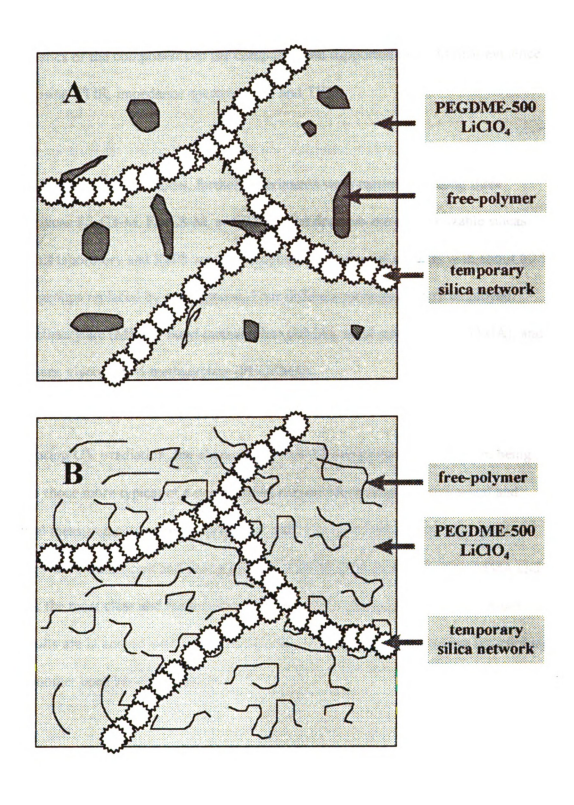


Figure 46. Scenario 1 (top) and 2 (bottom) as defined in the text.

characteristics of the components of the composite and supported by additional evidence obtained using FTIR, impedance spectroscopy, and TEM.

In order to test the model, further experiments were carried out using three different silicas FS-C3-M, FS-C8-M, and R805. The first two are polymerizable silicas made in this laboratory and R805 was a hydrophobic commercial product with about 50 % of silanol groups replaced by octyl groups. Four different monomers were employed: methyl methacrylate (MMA), butyl methacrylate (BMA), octyl methacrylate (OMA), and poly(ethylene glycol) ethyl methacrylate (PEGEMA).

During UV irradiation, the characteristics of the composites evolved from being gel-like to those more typical of a cured silicon rubber. More detailed mechanical and rheological measurements are in progress and will be reported elsewhere. The cured composites were translucent and scattered light, with those cross-linked using MMA and PEGEMA the most clear and those prepared using octyl methacrylate the most cloudy. These results are in accord with increasing degrees of phase separation during crosslinking as the monomer used becomes less polar.

Conductivities of this series of composite polymer electrolytes were measured and the results are listed in Table 12. Solubility parameters for each polymethacrylate was calculated based on its structure and group molar attraction constants according to equation 25:88

$$\delta = \rho \sum G / M \tag{25}$$

where  $\rho$  represents the density and M is the mer molecular weight of the polymer. Group molar attraction constants have been calculated and are readily available in many textbooks. The solubility parameter for PEO was calculated to be 9.9. and the solubility parameter difference between PEO and the guest polymer should determine the miscibility of the two polymers. A large difference would mean a large driving force for phase separation and since only the PEO phase is responsible for ionic conductivity, a strong phase segregation would correspond to a high conductivity.

The conductivity data listed in Table 11 do not differ appreciably, but Figure 47 shows that the the conductivity increases with the difference in solubility parameters of the two polymers. In addition to using solubility parameters, we also tried to correlate the conductivity with the carbon to oxygen ratio in an individual polymer since it is a rough

Table 11. Conductivity data for Figures 47 and 48.

PMA	C/O	$\delta_{PMA}$	$\delta_{PEO}$ - $\delta_{PMA}$	O	*10 <sup>4</sup> S/cm	
Type	Ratio	Data	Data	FS-C3-M	FS-C8-M	R805
PEGEMA	2.4	9.8	0.1	1.94	2.00	2.15
PMMA	2.5	9.1	0.8	2.15	2.07	2.13
PBMA	4	8.8	1.1	2.32	2.23	2.28
POMA	6	8.4	1.5	2.9	2.76	2.64

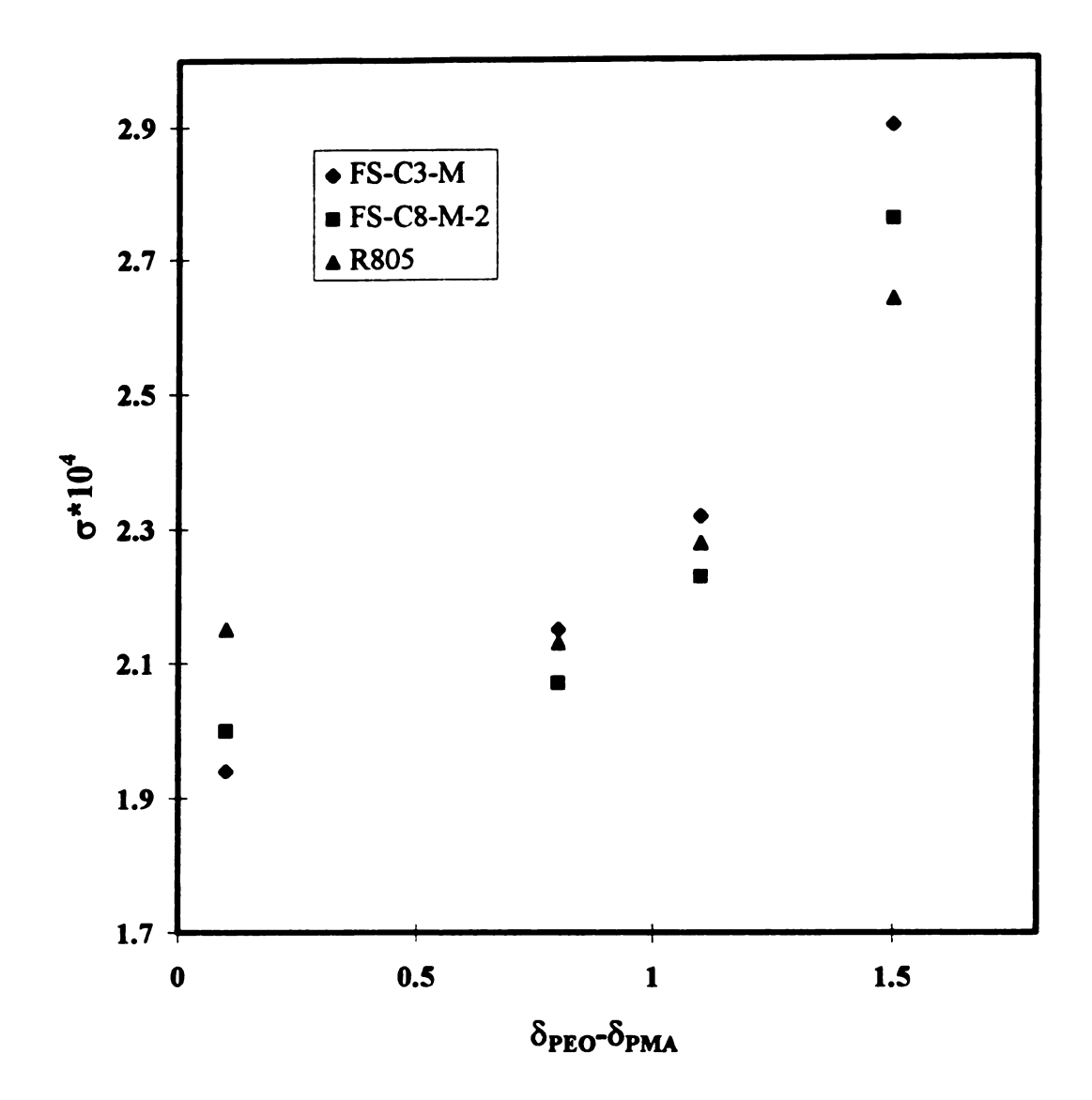


Figure 47. Conductivity vs. solubility parameters difference between PEO and PMA.

but independent estimate for the polarity of that polymer. The plot of C/O ratio vs conductivity is shown in Figure 48. Again, composites prepared using polymers that have a high C/O ratio (less polarity) show high conductivity, in good agreement with solubility parameter results.

As before, a combination of solvent extraction and TGA analysis was used to determine the amount of grafted polymer on the silica surface. Attempts to extract R805containing composites after cross-linking were not successful since the fine silica particles dispersed in the liquid phase and did not settle out - a good indication of no chemical bonding between silica surfaces and the polymer. However, when cross-linkable silicas (FS-C3-M and FS-C8-M-2) were used. large solid particles settled out as soon as the stirring was terminated. TGA measurements were used as before to analyze grafting efficiency. Two extremes could be considered. If none of the monomer copolymerized with the silica surface, the predicted TGA weight loss after extraction would be the same as the starting silica, i.e., ca. 6 - 9% (Figure 49); if, however, all of the monomer molecules cross-linked with silica, the predicted weight loss would be 56 - 59 %. In the case of composites made with FS-C8-M and when BMA is used, the actual weight loss is ca. 50% - nearly 90% of the predicted value. When a polar monomer, poly(ethylene glycol ethyl methacrylate (PEGEMA), was used, the corresponding weight loss dropped to 40% - 70% of the predicted value. Thus, ca. 30% of the PEGEMA monomer formed homopolymer in the PEGDME phase which could account for the drop in conductivity. Interestingly, the composite made from FS-C3-M showed the same characteristics as composites from FS-C8-M. This is not surprising considering the fact that they both share

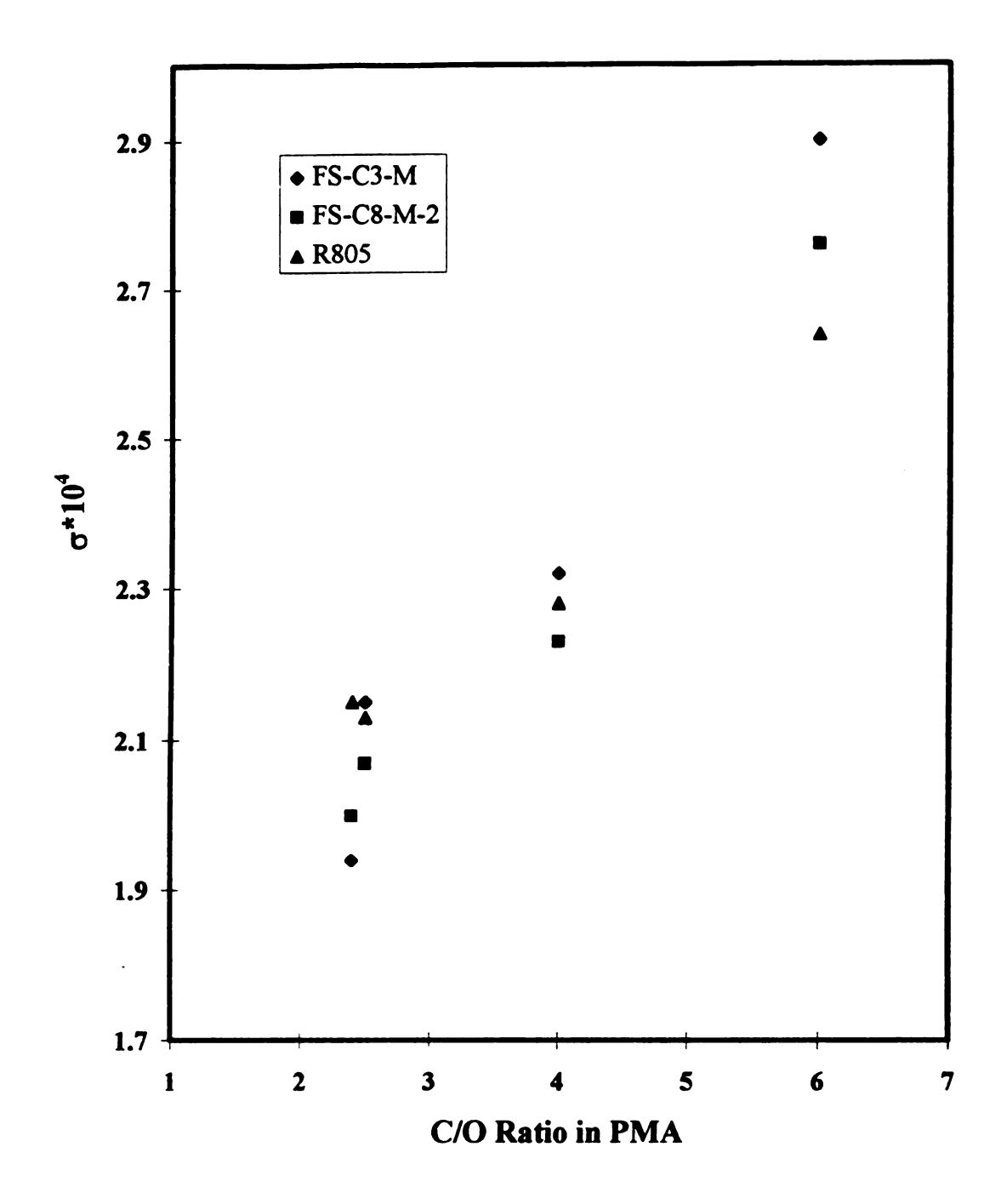


Figure 48. Conductivity vs. carbon to oxygen ratio in PMA.

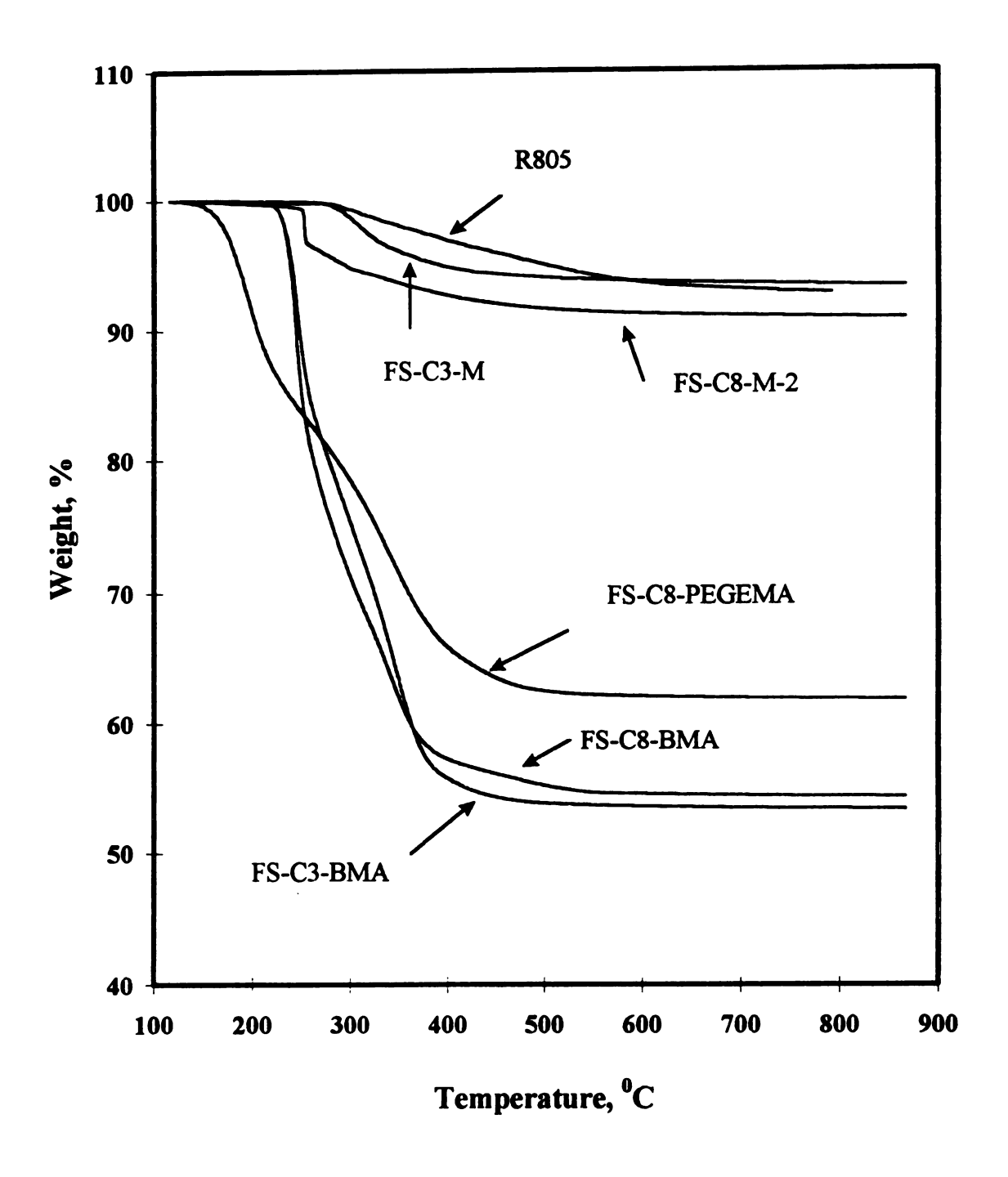


Figure 49. TGA weight losses for samples as labeled.

the same polymerizable group as the guest monomer, and although the  $C_8$  chain is more hydrophobic than the  $C_3$  chain, as discussed in the previous section, the difference was overcome quickly upon copolymerization with their nearest layer of monomer molecules. When the cross-linking is complete, the two composites are all rubbery materials.

### 2. Cross-Linking and Emulsion Polymerization: A Comparison

Our cross-linking system is related to an emulsion polymerization regime. To understand this point better, a little background material regarding emulsion polymerization formulations will be helpful. A typical formulation for a traditional emulsion polymerization contains monomer, a dispersing medium - usually water, an emulsifier or surfactant, and a water-soluble initiator. Emulsifier are typically amphiphilic molecules and their physical state depends on concentration. The critical micelle concentration (CMC) is the concentration beyond which emulsifier molecules aggregate to form micelles. Monomer is dispersed in the water phase to form monomer droplets whose sizes are much larger and whose total surface areas are much smaller than the micelles. Since the initiator is water-soluble, the initiating radicals are generated in water phase and diffuse into micelles where the monomer and the initiating radicals meet and polymerization takes place.

In recent years, novel composite polymeric materials have been prepared using emulsion polymerization techniques in the presence of various inorganic particles such as calcium carbonate, barium sulfate, 89-93 silica, titanium dioxide, quartz, 94,95 limestone, 96 calcium sulfite, 97 silica gel, activated alumina, white carbon, zeolite, et al. 98 In systems where the filler material does not carry polymerizable functional groups, the filler particles are encapsulated in situ by the growing polymer chains during emulsion polymerization. The amount of encapsulated polymer and the extractable portion of polymer depend on the surface property and the composition of the filler used, the kind and amount of the

surfactant, and the monomer type. A series of experiments<sup>89-97,99</sup> showed that surface modification of inorganic particles with anionic surfactants or titanates led to polymerization localized at the surface of the particle. Presumably, polymerization takes place in the hydrophobic chemical environment defined by the adsorbed surfactant. Some homopolymer also forms in the aqueous phase (the expected emulsion polymerization product), but by keeping the surfactant level below the critical micelle concentration, the amount of monomer dispersed in the aqueous phase and the amount of free polymer was minimized. In most cases, however, the adhesion between filler and polymer is poor due to the lack of chemical bonding. After exhaustive extraction with solvent, only a small portion the encapsulated polymer can be retained on the particle surface.

Attempts have been made to increase the interaction between polymer matrices particle surfaces to improve the physical properties of structural composite. For instance, Hasegawa and coworkers <sup>96</sup> reported a soapless emulsion polymerization system incorporating newly ground limestone particles. The strength of adhesion between the encapsulated polymer and solid surface was improved - a consequence attributed to the existence of active centers such as defects and disturbances in the crystal lattice. In addition, a report closely related to the chemistry of our work describes the emulsion polymerization of ethyl acrylate in the presence of fumed silica functionalized with acrylate groups. <sup>67</sup> The results reported are in accord with the added monomer separating from the continuous (aqueous) phase, and copolymerizing with surface-bound acrylates. <sup>100</sup> Composites prepared from these latexes show improved mechanical properties.

Their method of making composite polymeric material and properties of the resulted products are closely related to ours. The major difference is that they were aiming at grafting polymer on separate silica particle, while we wanted to bind silica particles together to create a permanent three-dimensional network. Table 13 lists the two formulations. The polymerizable silica they used was made by modification with either TPM or hydroxyethyl methacrylate, in other words, the hydrocarbon spacer between silica surface and methacryloyl group is either a C<sub>2</sub> or C<sub>3</sub>. As we discussed in our previous section, a surface like this is characteristic of ester functional group which lacks the hydrophobicity needed to attract the monomer molecules. A surfactant had to be used to increase the driving force of the monomer moving from water phase to silica surface. In our system, low molecular weight PEO containing dissolved lithium salt serves as dispersant. In addition, a surfactant was not necessary since the monomer we chose, BMA, is much more hydrophobic than the one they used (hydroxyethyl methacrylate) and will be driven to the silica surface even more as the polymerization proceeds. As far as the polymerization site is concerned, we do not expect it to occur in the PEO phase due to the phase separation between BMA and PEO, and also due to the poor solubility of our initiator (AIBN) in PEO.

Additional evidence for strong segregation of the polymer and PEGDM-500 phases in our system comes from comparisons of the mechanical and electrical properties of cross-linked electrolytes with those prepared without added monomer. As noted in the

Table 12. Formulations of our and Bourgeat-Lami's systems.

	Bourgeat-Lami's	ours
silica	cross-linkable <sup>a</sup>	cross-linkable <sup>b</sup>
dispersant	water	LiClO <sub>4</sub> in PEO
emulsifier	SDS°	none
monomer	ethyl acrylate	butyl methacrylate
initiator	potassium peroxodisulfate	AIBN

<sup>&</sup>lt;sup>a</sup> Modified with TPM or ethyl methacrylate.

Results section, data sensitive to the segmental mobility of the PEGDM-500 phase such as conductivity and T<sub>8</sub> values, show little or no change with cross-linking.

Bulk mechanical measurements coupled with impedance spectrocopy best illustrate the independence of mechanical properties and conductivity. As shown in Figure 50, the composite is a physical gel prior to cross-linking as evidenced by the elastic modulus (G') being larger than the viscous modulus (G''). Following cross-linking, the elastic modulus increases by almost two orders of magnitude to a value comparable to that of rubbery solids. At the same time, the conductivity showed only slight declines. Note that the

<sup>&</sup>lt;sup>b</sup> Modified with methacrylate having C<sub>8</sub> hydrocarbon spacer or by mixed silylation.

<sup>&</sup>lt;sup>c</sup> Sodium dodecyl sulfate.

conductivity for this sample (Figure 51) is high because of switching from LiClO4 to lithiul imide as the salt.

To summarize, we have achieved our goal to synthesize composite polymer electrolytes with good mechanical stability and high conductivity and the ability to tune these two factors independently.

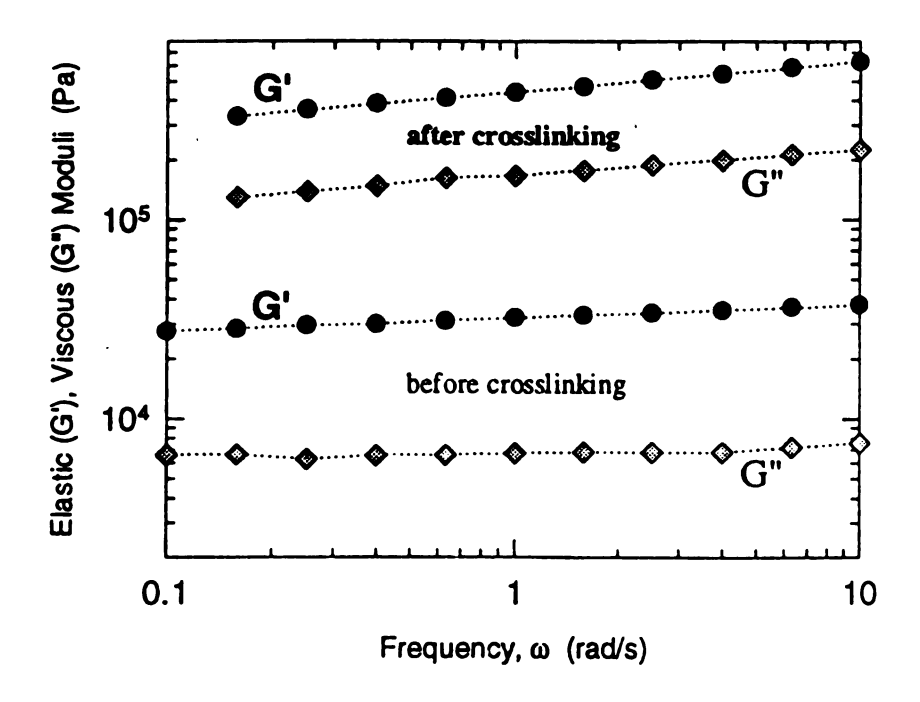


Figure 50. Dynamic moduli (G' and G'') before and after cross-linking for composites containing 10% cross-linkable silica and 10% butyl methacrylate in a PEGDME-LiClO<sub>4</sub> matrix.

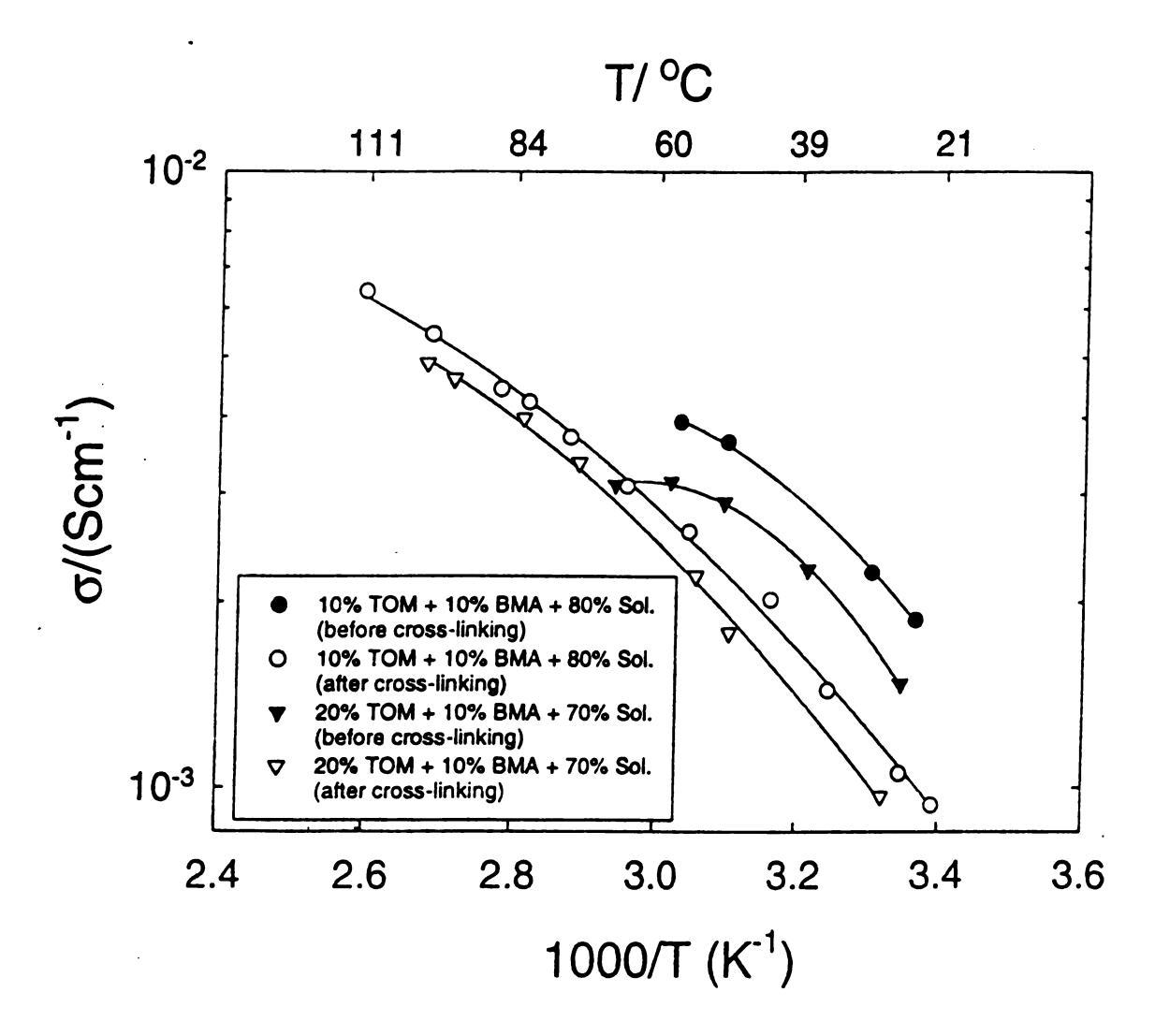


Figure 51. Conductivity of cross-linkable composite polymer electrolytes before and after cross-linking. Solution (Sol.) in legend is Li imide + PEGDME. Proportions are given in weight percentage.

### II. Future Work and Suggestions

#### 1. Optimization of Current System

We have successfully achieved our goal, i.e., a composite polymer electrolyte system with high conductivity and good mechanical stability and processability. Further efforts could be devoted to optimizing the system. For example, the mechanical stability could be enhanced by increasing the amount of cross-linkable fumed silica up to 20% by weight. Further increases would result in decrease in conductivity due to the formation of an insulating silica region. As far as the monomer content is concerned, it is likely that smaller amounts (5-10% by weight) would be enough to bring the same mechanical stability to the system.

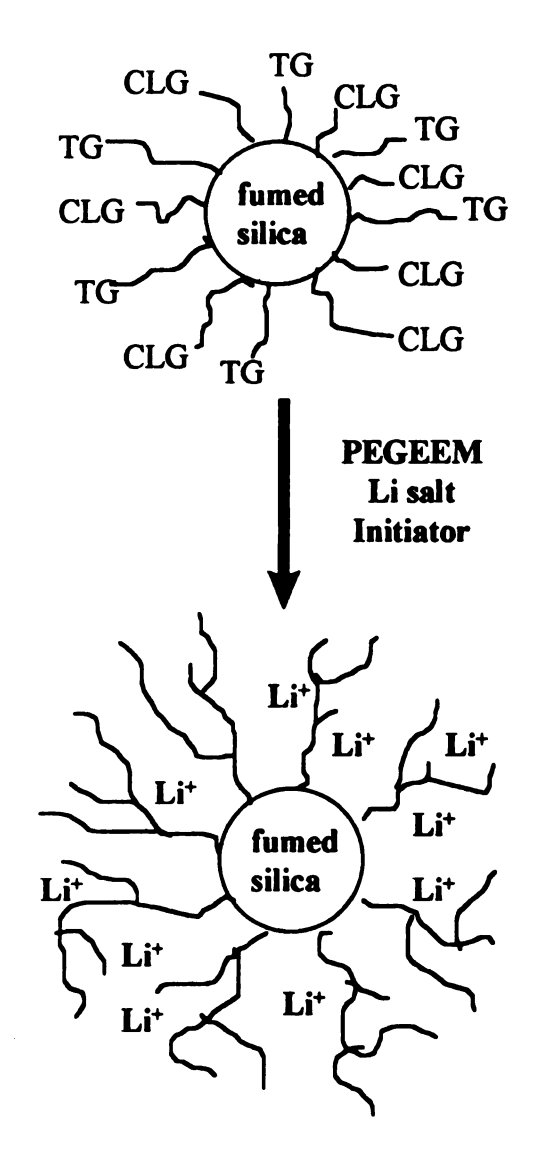
#### 2. Core-active Initiators

In the Introduction, we introduced the use of coreactive initiators to make covalently bound polymer (Scheme 7). 70 This method is well-suited for our system and provides us with an alternative way of making our target products. Since the initiating radicals are generated *in situ*, it is possible to limit the polymerization to silica surface. In order for the silica particle to form a network structure and for the non-polar monomer to localize around this network, it is necessary to attach organic groups carrying both hydrophobic and light- or heat-sensitive groups to the silica surface. This can be done by modifying Koehler and Ohngemach's initiator, 70 i.e., by replacing their spacer with a suitable hydrocarbon spacer. The composite polymer electrolytes thus formed would

expected to show similar behavior to our reported products in terms of conductivity and mechanical stability, yet provide us with an alternative to achieve our goals.

### 3. Two-Component Core-Shell Composites

We discussed in the Results section that when fumed silica is modified with PEO oligomers, it becomes more compatible with the PEGDME matrix. The extreme case would be when the surface coverage of PEO chain on silica surface is high enough, the PEO-grafted fumed silica itself will be a good ionic conductor upon adding lithium salts. By controlling the molecular weight and chain length, the PEO could be kept amorphous and therefore the conductivity of the composite should be high. The main advantage of this composite would be that the core-shell structure provides both good conductivity and mechanical stability. The preparation of this composite should be fairly easy. For example, Figure 52 shows a schematic route to such a product. Cross-linkable fumed silica can be made by silylation reactions using either a single silane incorporating both a cross-linkable group and a hydrophilic spacer, or a mixture of a coupling agent (e.g., TPM) and a second silane containing hydrophilic group. By changing the length of the spacer or the ratio of the two silane molecules, the desired silica surface can be realized. By dispersing this silica in a mixture containing lithium salt, a polar initiator, and a monomer carrying ethylene oxide units (e.g., PEGEMA), followed by polymerization, a composite polymer electrolyte will be generated. This system would resemble a hyperbranched PEO system but without problems such as poor conductivity and creep.



PEGEEM = poly(ethlene glycol) ethyl ether methacrylate CLG = cross-linkable group TG = tunable group, used to adjust polarity

Figure 52.A proposed route to a core-shell composite polymer electrolyte.

### 4. Highly Dispersible & Cross-Linkable Silicas for Emulsion Polymerization

We showed above that emulsion polymerization has been used to prepare polymer encapsulated inorganic particles. The ideal case is that, instead of a network structure, one would like to disperse the inorganic particles completely in the dispersant, usually water. This has proved to be difficult to achieve so far, since particles such as silicas<sup>66,68</sup> and quartz powders<sup>95</sup> show a strong tendency to form large aggregates in aqueous media. Through our research, we have gained knowledge about interactions between particles and particle-solvent molecules. For instance, if a polar solvent is chosen, a network will form with the addition of a hydrophobic filler material, while a good dispersion can be achieved when a hydrophilic filler, e.g., a PEO or polyoxymethylene modified silica, is used. Two examples of hydrophilic and cross-linable fumed silicas are shown in Figure 53. We believe that by using such filler materials, an improved dispersion of particles in aqueous media could be achieved, the therefore "ideal" silica-polymer encapsulated composites could be realized. This methodology applies not only to silica system, but also to any other inorganic system where MOH (M = Al, Ti, B, etc.) groups are present on its surface.

$$SiO_2$$
  $O$   $O$   $O$ 

Figure 53. Schematic of hydrophilic fumed silicas: (a) silica modified with a single silane;

(b) silica modified with a mixture of two silanes

### III. Summary

We have prepared various surface-modified fumed silicas and explored their behavior in polyether solutions. Results show that PEO modified hydrophilic silicas tend to disperse well in PEO derivatives due to the compatibility between surface groups and the dispersant. When a three-dimensional network is desired, the use of such fillers is not favorable since a large amount of filler material is needed. However, fumed silicas bearing both hydrophilic and cross-linkable groups would likely be suitable as seeds for emulsion polymerizations to make polymer encapsulated inorganic materials owing to their good dispersibility. Hydrophobic silicas, on the other hand, tend to form aggregates and network structures at a small loadings and are useful materials for controlling the mechanical properties of the inorganic-organic composite materials.

Modified fumed silicas featuring both hydrophobic and cross-linkable characteristics are the center of this research. These materials were prepared using either a single silylation or a mixed silylation process. When a polyether-Li salt solution was gelled using the above silica, the hydrophobic portion of the silica, through van der Waals attractions, formed a temporary open structured three-dimensional network, giving the composite good mechanical stability and processability. The polyether-Li salt phase was responsible for the good ionic conductivity (10<sup>-4</sup> S/cm) via the large open spaces provided by the network. Therefore, the mechanical properties and conductivity of the composite came from two different phases, the silica and polyether-Li salt phases, respectively. These two properties were decoupled and could be tuned independently.

The possibility of tuning the mechanical properties was provided by the crosslinkable groups on the silica surface. We were able to lock the temporary threedimensional network in place by adding a non-polar monomer, BMA, and an oil-soluble initiator, AIBN, to silica/polyether-Li salt composites. The monomer and the initiator, due to their non-polar characteristics, phase separated from the polyether-Li salt phase and formed a thin monomer layer near the hydrophobic silica surface. Upon photo-initiation, the added BMA monomer and the cross-linkable group on the silica surface copolymerized to lock the network structure in place, converting a temporary network into a permanent network, and a physical gel into a solid rubbery material. Our extraction experiments combined with TGA analyses show that nearly all of the polymer had been grafted onto fumed silica surface. The conductivity was not affected by the above crosslinking process, suggesting that the electrochemical and mechanical properties had been decoupled. In addition to the mechanical properties, we were also able to tune the conductivity independently. By replacing lithium perchlorate with lithium imide, we were able to realize a conductivity as high as 10<sup>-3</sup> S/cm, a value which is competitive with gel electrolytes.

# **EXPERIMENTAL**

### I. Materials

Unless otherwise specified, ACS reagent grade starting materials and solvents were used as received from commercial suppliers without further purification. Aerosil 200 (A200) was a gift from Degussa A.G., Frankfurt, Germany. This silica has a surface silanol content of 1 mmol/g, and was pre-treated in two different ways. The term "evacuated A200" is used for samples dried under vacuum at room temperature for 5 min; and the term "hydrated A200" is used for samples stored over a half-saturated NH<sub>4</sub>NO<sub>3</sub> solution in a desiccator for at least one week.

# II. Analytical Methods

<sup>1</sup>H and <sup>13</sup>C nuclear resonance analyses were carried out at room temperature in deuterated chloroform (CDCl<sub>3</sub>) on a Varian Gemini-300 spectrometer with the solvent proton and carbon signals being used as chemical shift standards.

<sup>13</sup>C and <sup>29</sup>Si solid state NMR spectra were obtained at 79.5 and 100.6 MHz, respectively, on a Varian 400 spectrometer under the conditions of <sup>1</sup>H and <sup>29</sup>Si crosspolarization, magic angle spinning. Samples (ca 100 mg) were packed in 7.0 mm zirconia rotors. Chemical shifts are reported in ppm and are referenced to talcum for <sup>29</sup>Si and adamantane for <sup>13</sup>C. A spinning frequency of 4 kHz was used.

A Nicolet IR/42 spectrometer purged with dry nitrogen was used to obtain infrared spectra. Samples used were 1 cm<sup>2</sup> pressed pellets prepared from *ca*. 10 mg of the various pure silicas. All spectra reported were acquired by signal averaging 32 scans at a resolution of 4 cm<sup>-1</sup>.

Differential scanning calorimetry (DSC) were performed under a helium atmosphere at a heating rate of 10 °C/min on a Perkin Elmer DSC 7. Thermogravimetric analyses (TGA) were performed in air atmosphere at a heating rate of 10 °C/min on a Perkin Elmer TGA 7 instrument. For DSC measurements, the temperature was calibrated

with an indium standard and samples were initially heated to 100 °C to erase the sample's thermal history, and then were quenched to -100 °C prior to starting the run. Samples for TGA measurements were first dried in vacuum at 120 °C overnight. Dried samples (~5-10 mg) were held at 115 °C in the TGA until a stable weight reading was obtained, and then the run was started.

Images of pristine and modified silicas were obtained as follows. One drop of a silica dispersion in acetone was placed on a carbon-coated grid. The solvent was allowed to evaporate for a few minutes and the grid was observed in the microscope. Images of composite polymer electrolytes were based on replicas prepared using freeze-fracture techniquess. The sample was placed on a copper cap and fractured to generate a fresh surface which was then replicated. The sample was fractured at -90 °C at 10 6 torr and replicated using unidirectional shadowing with platinum and carbon at an angle of 45°. The replicas and the grids were observed in a JEOL 100 CX II transmission electron microscope.

Silanol group analyses were performed by LiAlH<sub>4</sub> titration using literature procedures as guides. <sup>46</sup>, <sup>101</sup> All samples were dried at 150 °C under vacuum to 10<sup>-3</sup> mm Hg before being tested. About 1 g of sample and an excess amount (20 mL, 0.4 wt%) of lithium aluminum hydride in diglyme were used for each run. The volume of hydrogen gas released from the reaction was measured and the silanol groups were calculated according to the ideal gas equation.

The electrical properties of the samples were measured by ac impedance spectroscopy over the frequency range 6 Hz - 11 MHz using an HP 4192A LF Impedance Analyzer. An applied voltage of 0.1 V was used to collect the data. Cross-linked samples were prepared by sandwiching uncross-linked electrolyte between a glass slide and a stainless steel disk, with the desired thickness maintained using a Teflon spacer. The composites were polymerized as described previously, and after polymerization, the glass slide was peeled off gently and replaced with another stainless steel disc. The electrolyte thickness was obtained by subtracting the thickness of the steel discs from the total thickness measured using a micrometer. Conductivity measurements were taken from high to low temperatures, with the samples held at each temperature for at least 15 minutes under a nitrogen gas purge before being measured.

# III. Hydrophobic silicas

FS-TEMS-1. The experimental procedure employed in this example is typical of those used to make FS-TEMS-1, FS-TEMS-2, FS-TEMS-3, FS-TEMS-0, FS-TEMS-2H, and FS-TEMS-13H. To 2 g of evacuated A200 were added 40 mL of toluene containing 2 μL (0.02 mmol) of diethylamine (DEA) and a mixture of 10 mL of toluene and 1.4 g (8.0 mmol) of methytriethoxysilane. The slurry was shaken until homogeneous after each addition. The reaction was allowed to proceed in a stoppered Schlenk flask for 2 h. The slurry was filtered, washed with 100 mL of dry toluene and evacuated at room temperature and then at 150 °C until a 10<sup>-3</sup> mm Hg vacuum was reached.

Table 13. Reaction conditions for FS-TEMS series.

Sample Name	DEA (mmol)	Time (h)
FS-TEMS-1	0.02	2
FS-TEMS-2	0.50	2
FS-TEMS-3	2.0	2
FS-TEMS-0	0	2
FS-TEMS-2H	1.0	2
FS-TEMS-13H	1.0	13

FS-TMCS-1. The experimental procedure employed in this example is typical of those used to make FS-TMCS-2, TMCE-3, and TMES-1.To 2 g of evacuated A200 were added 40 mL of toluene containing 0.2 mL (2.0 mmol) of diethylamine and a mixture of 10 mL of toluene and 54 mg (0.50 mmol) of trimethychlorosilane (TMCS). The slurry was shaken to homogeneous each time of addition. The reaction was allowed to proceed in a stoppered Schlenk flask for 2 h. The slurry was filtered, washed with 100 mL of dry toluene and evacuated at room temperature and then at 150 °C until 10<sup>-3</sup> mm Hg vacuum was reached.

Table 14. TMS modified silicas.

Sample Name	Silane (mmol)
FS-TMCS-1	TMCS (0.5)
FS-TMCS-2	TMCS (1.4)
FS-TMCS-3	TMCS (2.0)
FS-TMES-1	TMES (2.0)

FS-C2. The experimental procedure employed in this example is typical of those used to make FS-C8 and FS-C18. Using a transfer needle, 300 mL of toluene containing 1.7 mL (16 mmol) of diethylamine was added to 16 g of evacuated A200 followed by a mixture of 2.1 mL (16 mmol) of ethyltrichlorosilane (ETCS) in 10 mL of toluene. The slurry was shaken until homogeneous after each addition. The reaction was allowed to proceed in a stoppered Schlenk flask for 2 h. The slurry was separated by centrifugation

and washed sequentially with two portions of toluene, ethanol/water (50:50), ethanol, and diethyl ether. The diethyl ether was evaporated and the solid was transferred into a Schlenk flask and dried under vacuum at 150 °C for at least 2 h.

Table 15. Reaction conditions for FS-Cn series.

Sample Name	A200 (g)	DEA (mmol)	Silane (mmol)
FS-C2	12	16	ETCS (16)
FS-C8	12	13	OTCS (13)
FS-C18	16	15	ODTCS (15)

OTCS = octyltrichlorosilane.

ODTCS = octadecyltrichlorosilane.

FS-DM-C8-1. The experimental procedure employed in this example is typical of those used to make FS-DM-C8-2 and FS-DM-C8-3. Toluene (300 mL) containing 25 μL (0.25 mmol) of diethylamine followed by a mixture of 0.10 mL (0.41 mmol) of chlorodimethyloctylsilane in 10 mL of toluene was added through a transfer needle to 12 g of evacuated A200. The slurry was shaken to homogeneous each time of addition. The reaction was allowed to proceed in a stoppered Schlenk flask for 2 h. The slurry was separated by centrifugation and washed sequentially with two portions of toluene, ethanol/water (50:50), ethanol, and diethyl ether. The diethyl ether was evaporated and the solid was transferred into a Schlenk flask and vacuum dried at 150 °C for at least 2 h.

Table 16. Reaction conditions for FS-DM-C8-n series.

Sample Name	A200 (g)	DEA (mmol)	CDMOS (mmol)
FS-DM-C8-1	12	0.25	0.41
FS-DM-C8-2	14	2.9	3.3
FS-DM-C8-3	12	12	12

FS-DM-H. To 60 g of the evacuated A200 were added 600 mL of toluene containing 7.5 mL (71 mmol) of diethylamine. After the silica was well dispersed through shaking, a mixture of 10 mL of toluene and 8.2 mL (72 mmol) of chlorodimethylsilane was added. The slurry was shaken again to assure a good dispersion of added silane. The reaction was allowed to proceed overnight in a stoppered Schlenk flask. The slurry was separated by filtration and washed sequentially with two portions of toluene, ethanol/water (50:50), ethanol, and diethyl ether. The diethyl ether was evaporated and the solid was transferred into a Schlenk flask and vacuum dried at 150 °C for at least 2 h.

FS-H. Evacuated A200 (25g) was replaced in a 1 L RBF equipped with a condenser, an addition funnel with equalizing tube, an oil bath, and a magnetic stirrer. Dioxane (600 mL) containing 35 mL of 2.3 M HCl was then added. The mixture was heated to 75 °C, and a solution of 5.8 mL triethoxysilane in 100 mL dioxane was added dropwise over a period of 1 h. After gently refluxing for two h, the product was centrifuged and washed consecutively with 20:80 water/THF, THF, and diethyl ether

(twice with each solvent). The final product was dried at 60 °C and then at 150 °C under vacuum.

FS-OEt-H. To 2 g of the evacuated A200 were added 40 mL of toluene containing 0.10 mL (1.0 mmol) of diethylamine and a mixture of 10 mL of toluene and 0.8 mL (4.1 mmol) of triethoxysilane. The slurry was shaken until homogeneous after each addition. The reaction was allowed to proceed for 4 h in a stoppered Schlenk flask. The slurry was separated by filtration and washed 3 times with toluene and diethyl ether. The diethyl ether was evaporated and the solid was transferred into a Schlenk flask and vacuum dried at 150 °C for at least 2 h.

FS-OH-H. FS-OEt-H (0.50 g) was added to a mixture containing 20 mL of dioxane, 1.0 mL of 2 N HCl, and 1.0 mL distilled water. The slurry was stirred and brought to reflux for 1 h. The solid product was collected through centrifugation and washed consecutively with water/THF (20:80), THF, and diethyl ether (twice with each solvent). The diethyl ether was evaporated and the solid was transferred into a Schlenk flask and vacuum dried at 150 °C for at least 2 h.

FS-TMS-H. FS-OH-H (0.20 g) was dispersed in 20 mL of toluene containing 0.05 mL (0.50 mmol) diethylamine. Chlorotrimethylsilane (0.10 mL, 0.78 mmol) was added, and the reaction proceeded for 2 h. The solid product was collected through centrifugation and washed consecutively with water/THF (20:80), THF, and diethyl ether

(twice with each solvent). The diethyl ether was evaporated and the solid was transferred into a Schlenk flask and vacuum dried at 150 °C for at least 2 h.

#### IV. PEO-Modified Silicas

Ethylene Glycol Allyl Methyl Ether (EGAME) (7). The experimental procedure described in this example was used to make diethylene glycol allyl methyl ether (8), triethylene glycol allyl methyl ether (9), and poly(ethylene glycol) allyl methyl ether (10, 11, 12). In a 500 mL round bottom flask was loaded 25 g NaH (1.1 mol, 60% dispersion in mineral oil), 50 g (0.42 mol) ethylene glycol monomethyl ether (1) diluted with 250 mL dry THF was added to the flask through a dropping funnel under nitrogen. After refluxing for 1 h, 56 g allyl bromide was added dropwise and refluxing continued for 3 hours. After cooling in ice water for 0.5 h, the mixture was quenched with ethanol and then water and was refluxed for 0.5 h. The liquid portion was separated through decantation and concentrated. The residue was extracted with methylene chloride and ice water 3 times. The organic layer was dried over anhydrous magnesium sulfate. After removing the solvent, the mixture was distilled. 41 g (69%) product was collected; bp 61 °C/70 mm Hg (lit 102 56 °C/60 mm Hg). H NMR: 8 3.37 (3H, s), 3.50-3.60 (4H, m), 4.05 (2H, d), 5.14-5.28 (2H, m), 5.85-5.98 (1H, m).

Di(ethylene Glycol) Allyl Methyl Ether (DEGAME) (8). DEGAME was prepared as above using 50 g (0.42 mol) of diethylene glycol monomethyl ether (2), 25 g (1.1 mol) of NaH (60% dispersion in mineral oil), and 40 mL (0.46 mol) of allyl bromide. Yield: 85 %; bp 111 °C/60 mm Hg (lit<sup>102</sup> 86 °C/15 mm Hg). <sup>1</sup>H NMR: δ 3.37 (3H, s), 3.5-3.7 (12H, m), 4.0-4.4 (2H, dt), 5.15-5.30 (2H, m), 5.84-5.98 (1H, tt).

Tri(ethylene Glycol) Allyl Methyl Ether (TEGAME) (9). DEGAME was prepared using 52 g (0.30 mol) of triethylene glycol monomethyl ether (3), 16 g (0.63 mol) of NaH (95%), and 30 mL (0.34 mol) allyl bromide. Yield: 83 %; bp 119 °C/19 mm Hg. <sup>1</sup>H NMR: δ 3.37 (3H, s), 3.5-3.7 (12H, m), 4.0-4.4 (2H, dt), 5.15-5.30 (2H, m), 5.84-5.98 (1H, tt).

Poly(ethylene glycol-350) Allyl Methyl Ether (PEGAME-350) (10). PEGAME-350 was prepared as above using 274 g (0.78 mol) of poly(ethylene glycol-350) monomethyl ether (4), 47 g (2.0 mol) of NaH (95%), and 88 mL (1.0 mol) of allyl bromide, except that, instead of distillation, the product were extracted with methylene chloride, washed with NaHCO<sub>3</sub> solution and water, and dried over anhydrous MgSO<sub>4</sub>.

After removing the solvent, the products were evacuated at 120 °C for 1 h.

Poly(ethylene glycol-550) Allyl Methyl Ether (PEGAME-550) (11).

PEGAME-550 was prepared as for 10 using 274 g (0.50 mol) of poly(ethylene glycol-550) monomethyl ether (5), 50 g (1.3 mol) of NaH (60% dispersion in mineral oil), and 61 mL (0.65 mol) of allyl bromide.

Poly(ethylene glycol-750) Allyl Methyl Ether (PEGAME-750) (12). PEGAME-750 was prepared as for 10 using 200 g (0.27 mol) of poly(ethylene glycol-750) monomethyl ether (6), 17 g (0.67 mol) of NaH (95%), and 35 mL (0.40 mol) of allyl bromide.

Chlorodimethyl(4,7-dioxaoctyl)silane (13). The experimental procedure employed in this example was also used for preparing chlorodimethyl(4,7,10-trioxaundecyl)silane (14) and chlorodimethyl(4,7,10,13-tetraoxatetradecyl)silane (15). A 13-mm Pyrex tube was charged with 5.0 g (43 mmol) of EGAME (7), 6.1 g (65 mmol) of chlorodimethylsilane, and 5 μL of Speier's catalyst (0.12 M H<sub>2</sub>PtCl<sub>6</sub> 6H<sub>2</sub>O in isopropyl alcohol). The tube was sealed and heated for 0.5 hour at 100 °C. The product was collected by vacuum distillation. Yield: 6.9 g (76%); bp 92 °C/10 mm Hg (lit<sup>103</sup> 110 °C/15 mm Hg). ¹H NMR: δ 0.4 (6H, s), 0.79-0.84 (2H, t), 1.64-1.74 (2H, m), 3.47 (3H, s), 3.44 (2H, t), 3.50-3.58 (4H, m).

Chlorodimethyl(4,7,10-trioxaundecyl)silane (14). Silane 14 was prepared as above using 10 g (62 mmol) of diethylene glycol ally methyl ether (8) and 10 mL (92 mmol) of chlorodimethylsilane. Yield: 9.0 g (56%); bp 135 °C/40 mm Hg.  $^1$ H NMR: (CDCl<sub>3</sub>).  $\delta$  0.4 (6H, s),  $\delta$  0.79-0.84 (2H, t),  $\delta$  1.64-1.74 (2H, m),  $\delta$  3.47 (3H, s),  $\delta$  3.44 (2H, t),  $\delta$  3.50-3.68 (8H, m).

Chlorodimethyl(4,7,10,13-tetraoxatetradecyl)silane (15). Silane 15 was prepared as above using 5.8 g (28 mmol) of triethylene glycol ally methyl ether (9) and 5.0 mL (43 mmol) of chlorodimethylsilane. Yield: 5.5 g (66%); bp 77 °C/0.4 mm Hg. <sup>1</sup>H NMR: δ 0.4 (6H, s), 0.79-0.84 (2H, t), 1.64-1.74 (2H, m), 3.47 (3H, s), 3.44 (2H, t), 3.50-3.68 (12H, m).

Poly(ethylene glycol-350) methyl 3-(chlorodimethylsily)propyl ether (PEGMPE-350) (16). Silane 16 was prepared as above using 7.7 g (16 mmol) of PEGAME-350 (10), 5 μL of Speier's catalyst, and 3.0 mL (26 mmol) of chlorodimethylsilane. The product was difficult to distill; vacuum and heat were therefore applied to remove volatile impurities.

Poly(ethylene glycol-550) methyl 3-(chlorodimethylsily)propyl ethers (17). Silane 17 was prepared as above using 9.2 g (13 mmol) of PEGAME-550 (11), 5  $\mu$ L of Speier's catalyst, and 3.0 mL (27 mmol) of chlorodimethylsilane. The workup procedure was the same used for (16).

Poly(ethylene glycol-750) methyl 3-(chlorodimethylsily)propyl ethers (18). Silane 18 was prepared as above using 11 g (12 mmol) of PEGAME-750 (12), 5  $\mu$ L of Speier's catalyst, and 3.0 mL (26 mmol) of chlorodimethylsilane. The workup procedure was the same used for (16).

FS-DM-EO<sub>1</sub>. The experimental procedure employed in this example was used to make FS-DM-EO<sub>2</sub> through FS-DM-EO<sub>5</sub>. To 15 g of evacuated A200 in a 500 mL Schlenk flask was added through a transfer needle 300 mL of toluene containing 1.7 mL (16 mmol) of diethylamine followed by a mixture of 3.5 g (17 mmol) of chlorodimethyl(4,7-dioxaoctyl)silane (13) in 50 mL of toluene. The slurry was shaken until homogeneous after each addition. The reaction was allowed to proceed in a stoppered Schlenk flask overnight. The slurry was separated by filtration and washed

sequentially with two portions of toluene, ethanol/water (50:50), ethanol, and diethyl ether. The diethyl ether was evaporated and the solid was dried at 150 °C in a vacuum oven for at least 2 hours.

Table 17. Preparation of PEO attached silicas: Method 1.

Sample Name	A200	Silane (mmol)	DEA (mmol)
FS-DM-EO <sub>1</sub>	15	13 (17)	16
FS-DM-EO <sub>2</sub>	15	14 (12)	16
FS-DM-EO <sub>3</sub>	15	<b>15</b> (17)	16
FS-DM-EO <sub>8</sub>	12	16 (20)	12
FS-DM-EO <sub>12</sub>	14	17 (14)	14
FS-DM-EO <sub>17</sub>	12	18 (14)	12

FS-EO<sub>1</sub>. The experimental procedure employed in this example was used to make FS-EO<sub>3</sub>, FS-EO<sub>8</sub>, FS-EO<sub>12</sub>, FS-DM-S-EO<sub>1</sub>, and FS-DM-S-EO<sub>8</sub>. To a solution containing 2.3 g (20 mmol) of EGAME (7), 0.10 mL Speier's catalyst, and 50 mL dry toluene was added 4.5 g of FS-H. The mixture was stirred and refluxed for 24 hours. The solid sample was collected through centrifugation and washed with toluene and methylene chloride three times each and dried at 120 °C under vacuum overnight.

Table 18. Preparation of PEO attached silicas: Method 2.

Sample Name	Silica (g)	Organic Substrate (g)
FS-EO <sub>1</sub>	FS-H (4.5)	7 (2.3)
FS-EO <sub>3</sub>	FS-H (3.0)	8 (2.5)
FS-EO <sub>8</sub>	FS-H (4.5)	10 (7.0)
FS-EO <sub>12</sub>	FS-H (3.0)	11 (7.0)
FS-DM-S-EO <sub>1</sub>	FS-DM-H (5.0)	7 (2.2)
FS-DM-S-EO <sub>8</sub>	FS-DM-H (5.0)	10 (7.0)

## V. Polymerizable Silicas

5-(Tetrahydropyran-2-yloxy)pent-1-ene (20). To a magnetically stirred solution of 2.7 mL (0.025 mol) of 4-penten-1-ol and 0.35 g of p-toluenesulfonic acid monohydrate (18 mmol) in 35 mL anhydrous dioxane at room temperature was added 7.3 mL (0.08 mol) of dihydro-4H-pyran (19) dropwise over a period of 3 min. After an additional 5 min, half saturated methonolic ammonia was added until the products were slightly basic.

Removal of the solvent gave an oil which was dissolved in 60 mL chloroform and the solution was washed with 20 mL of 15% NaHCO<sub>3</sub> The chloroform layer was dried over anhydrous MgSO<sub>4</sub> and then concentrated. Distillation gave 2.2 g (51%) of 20; bp 93

°C/33 mm Hg (lit 104 98-100 °C/10 mm Hg). H NMR: δ 0.65 (2H, t), 1.23 (9H, t), 1.35-1.85 (8H, m), 3.34-3.55 (2H, m), 3.72 (2H, t), 3.78-3.86 (6H, q), 4.80 (1H, t).

2-(8-Chlorooctyloxy)tetrahydropyran (25). <sup>105</sup> To a magnetically stirred solution of 8-chlorooctanol (25 g, 0.15 mol) and reagent grade p-toluenesulfonic acid monohydrate (1.9 g, 9.8 mmol) in anhydrous 1,4-dioxane (280 mL) at room temperature was added drop-wise 3,4-dihydro-2H-pyran (45 mL, 0.52 mol) over a period of 15 min. After stirring an additional 10 min, half-saturated methonolic ammonia was added until the mixture was slightly basic. Removal of solvent gave a viscous solution which was washed with 15% aqueous sodium bicarbonate extracted and extracted into chloroform. The organic layer was dried over MgSO<sub>4</sub> for 2 h, filtered and the solvent removed to yield 2-(8-chlorooctyloxy)tetrahydropyran. This material was used without further purification.

2-(7-Octenyloxy)tetrahydropyran (23). <sup>106</sup> To a 1 L round bottomed flask were added 600 mL DMSO and 34 g (0.29 mol) KOt-Bu. The mixture was stirred until homogeneous. The crude 2-(8-chlorooctyloxy)tetrahydropyran from the previous preparation was added through a dropping funnel over a period of 30 min. After stirring for 2 h, the mixture was extracted with pentane and half-saturated NaHCO<sub>3</sub>. The organic layer was washed with distilled water and dried over MgSO<sub>4</sub>. Concentration and distillation gave the desired product as a clear oil; yield: 27.4 g (88%); b.p.: 94-96 °C/0.4 mm (lit. <sup>107</sup> 130 °C/12 mm). <sup>1</sup>H NMR: δ 5.87-5.74 (1H, ddt), 5.02-4.90 (2H, m), 4.57 (1H, t), 3.90-3.34 (2H, m), 2.07-2.01 (2H, m), 1.87-1.33 (16H, m).

FS-C8-P. To a solution containing 4.0 mL (19 mmol) of 2-(7-octenyloxy)tetrahydropyran (23), 0.23 mL Speier's catalyst, and 50 mL dry toluene was added 10 g of FS-DM-H. The mixture was stirred and refluxed for 24 h. The solid sample was collected through centrifugation and washed with three portions of toluene and methylene chloride, and dried at 120 °C under vacuum overnight. FS-C5-P was prepared in the same way.

FS-C8-OH. To 120 mL of acidified ethanol [prepared from 500 mL ethanol and 5 mL 0.10 M HCl] was added 7.0 g of FS-C8-P. The slurry was heated on an oil bath under reflux for 4 hours. The product was centrifuged, washed 3 times with ethanol and diethyl ether, and dried at 120 °C under vacuum for at least 2 h. The same procedure was used to prepare FS-C5-OH.

FS-C8-M-1. FS-C8-OH (1.0 g) was dispersed in 14 mL of toluene containing 2 mL of pyridine. Methacryloyl chloride (1.0 mL, 9.2 mmol) in 4 mL of toluene was added dropwise during a period of 15 min while the slurry was cooled in an ice water bath. The mixture was then heated to and kept at 60 °C for 2 h. The solid portion was separated through centrifugation and washed with water/ethanol (50:50), ethanol, and finally diethyl ether. The sample was dried at room temperature and at 120 °C in vacuum for at least 2 h. The same procedure was employed to prepare FS-C5-M-1.

7-Octen-1-ol (21).Using a literature procedure as a guide, <sup>105</sup> 7.2 g (34 mmol) of 8-tetrahydropyranyl-1-octene was added to 200 mL of acidified ethanol, and the mixture was heated with an oil bath to the reflux temperature for 30 min. The ethanol was removed and the product was diluted with CH<sub>2</sub>Cl<sub>2</sub> and dried over MgSO<sub>4</sub>. After concentration and distillation, 4.0 g (90% yield) of the deprotected product was obtained; bp 40 °C/0.2 mm (lit<sup>108</sup> 64-66 °C/7 mm). <sup>1</sup>H NMR: δ 5.88-5.74 (ddt, 1H), 5.03-4.91 (m, 2H), 3.62 (t, 2H), 2.08-2.01 (dt, 2H), 1.61-1.52 (m, 2H), 1.44-1.28 (m, 6H). <sup>13</sup>C NMR: δ 139.1, 114.2, 63.0, 33.7, 32.7, 28.9, 28.8, 25.6.

Acrylic acid pent-4-enyl ester (27a). To a slurry of 7.7 g (0.088 mol) of 4-penten-1-ol and 24 g of dry 3A molecular sieves in 70 mL CCl<sub>4</sub> was added dropwise 9.7 g (0.11 mol) of acryloyl chloride in 10 mL CCl<sub>4</sub>. The mixture was heated at the reflux temperature for 4 h. The mixture was filtered and product was distilled to afford 7.4 g

(60%) of 27a; bp 71 °C/20 mm Hg. <sup>1</sup>H NMR: δ 1.72-1.84 (2H, m), 2.11-2.20 (2H, m), 4.15-4.21 (2H, m), 4.98-5.08 (2H, m), 5.76-5.89 (3H, t), 6.38-6.44 (1H, dd).

Methacrylic acid pent-4-enyl ester (27b). Ester 27b was prepared from the same procedure as in (27a) using 8.5 g (0.073 mol) of 4-penten-1-ol and 12 g (0.10 mol) of methacryloyl chloride. The product was purified using a column chromatography (SiO<sub>2</sub>/hexane). Yield: 10.4 g (92%). <sup>1</sup>H NMR: δ 6.08 (1H, s), 5.86-5.73 (1H, ddt), 5.53 (1H, s), 5.06-4.95 (2H, m), 4.14 (2H, t), 2.17-2.10 (2H, dt), 1.92 (3H, s), 1.80-1.71 (2H, m). IR (cm<sup>-1</sup>): 3079, 1642 [ν(-CH=CH<sub>2</sub>), ν(-CH<sub>3</sub>C=CH<sub>2</sub>)], 1713 [ν(OCO)].

7-Octenyl methacrylate (28). To a 100 mL round bottomed flask were added 30 mL CCl<sub>4</sub>, 4.0 g (31 mmol) of 7-octen-1-ol, and 8 g of crushed 3A molecular sieves. The mixture was heated to reflux and 4.4 g (47 mmol) methacryloyl chloride in 10 mL CCl<sub>4</sub> was added over a period of 15 min under dry N<sub>2</sub>. Heating was continued overnight. The molecular sieves were removed by filtration, and after removing the solvent, the product was purified using column chromatography (SiO<sub>2</sub>/hexane); yield: 5.8 g (95%). <sup>1</sup>H NMR: δ 6.09 (1H, s), 5.88-5.74 (1H, ddt), 5.54 (1H, s), 5.03-4.91 (2H, m), 4.13 (2H, t), 2.08-2.01 (2H, dt), 1.94 (3H, s), 1.71-1.60 (2H, m), 1.44-1.30 (6H, m). <sup>13</sup>C NMR: δ 167.5, 138.9, 136.5, 125.1, 114.3, 64.7, 33.6, 28.7, 28.7, 28.5, 25.8, 18.3. IR (cm<sup>-1</sup>) 3079, 1642 [v(-CH<sub>2</sub>CH<sub>2</sub>CH<sub>2</sub>)], 1713 [v(OCO)]. MS m/z M<sup>+</sup> 196.

8-(Trichlorosilyl)octyl methacrylate (31). In a dry box, a 13-mm Pyrex tube was charged, with 5.8 g (30 mmol) of 7-octenyl methacrylate, 0.1 mL Speier's catalyst<sup>61</sup> (0.12 M H<sub>2</sub>PtCl<sub>6</sub> in isopropanol), and 4.8 g (35 mmol) HSiCl<sub>3</sub>. The tube was sealed and heated at 60°C overnight. The product was evacuated under vacuum at room temperature and stored under vacuum until use. <sup>1</sup>H NMR: δ 6.09 (1H, s), 5.54 (1H, s), 4.13 (2H, t), 1.94 (3H, s), 1.69-1.53 (4H, m), 1.44-1.30 (10H, m). <sup>13</sup>C NMR: δ 167.5, 136.5, 125.2, 64.7, 31.7, 29.0, 28.9, 28.5, 25.9, 24.3, 22.2, 18.3. IR (cm<sup>-1</sup>): 1640 [v(-CH<sub>3</sub>C=CH<sub>2</sub>)], 1712 [v(OCO)], 590, 567 [v(Si-Cl)]. MS m/z M<sup>+</sup> 331. 5-(Triethoxysilyl)pentyl methacrylate (29) and 8-(triethoxysilyl)octyl methacrylate (30) were prepared similarly using triethoxysilane.

FS-C8-M-2. To 30 g of hydrated A200 in a 1L round bottomed flask were added 600 mL of toluene containing 3.0 mL (1.5 mmol) of diethylamine. The flask was attached to a mechanical shaker, and a mixture of 9.8 g (29 mmol) 8-(trichlorosilyl)octyl methacrylate (31) in 30 mL of toluene were added. The reaction was allowed to proceed at room temperature overnight. The product was separated by filtration, and washed with three portions of both toluene and diethyl ether. The residual diethyl ether was evaporated and the solid was transferred into a Schlenk flask and dried under vacuum at 120 °C overnight.

FS-C3-M. FS-C3-M was prepared by the same procedure as FS-C8-M-2 except 15 g of A200, 1.5 mL (15 mmol) of diethylamine, and 3.1 g (12 mmol) of TPM were used.

FS-OTMS. FS-OTMS was prepared by the same procedure as FS-C3-M except 2.9 g (12 mmol) of OTMS was used.

FS-TOM-1. To 15 g of hydrated A200 in a 500 mL round bottomed flask was added 450 mL of toluene containing 1.5 mL (15 mmol) of diethylamine. The flask was attached to a mechanical shaker, and a mixture of 2.7 g (11 mmol) octyltrimethoxysilane (OTMS) and 0.28 g (1.1 mmol) trimethoxysilylpropyl methacrylate (TPM) in 30 mL of toluene were added. The reaction was allowed to proceed at room temperature overnight. The product was separated by filtration, and washed with three portions of both toluene and diethyl ether. The residual diethyl ether was evaporated and the solid was transferred into a Schlenk flask and dried under vacuum at 120 °C overnight.

Table 19. Products of mixed silylation reactions.

Sample Name	A200 (g)	TPM (g)	OTMS (g)	
FS-TOM-1	15	0.28	2.7	
FS-TOM-2	15	0.61	2.3	
FS-TOM-3	30	1.5	4.4	
FS-TOM-4	9.0	0.46	0.98	
FS-TOM-5	15	1.5	1.5	

## IV. Preparation of composites

Compatible composites. All compatible electrolytes were prepared using the same procedure. A generic preparation is described below. To a blender cup were added 12 g of 1 M LiClO<sub>4</sub> in PEGDME-500, small portions of PEO modified fumed silica. The mixture was blended in a Waring blender for 2-5 minutes with each addition. The addition of silica was terminated when the gel stops flowing upon tilting. After evacuation to remove air bubbles at 50 °C in vacuum, the sample was stored in a desicator until use. A small portion of the electrolyte was sandwiched between two blocking stain-less steel electrodes separated by a thin Teflon ring.

Cross-linkable composites. All cross-linkable electrolytes were prepared using the same procedure. A generic preparation is described below. To a blender cup were added 1.5 g of butyl methacrylate, 15 mg of AIBN initiator, 1.5 g of methacrylate-modified fumed silica, and 12 g of a PEGDME-500/LiClO<sub>4</sub> solution with the desired O/Li ratio. The mixture was mixed in a Waring blender for 2-5 minutes and then was transferred to a vial. After evacuation to remove air bubbles, the sample was stored in a desicator until use. Polymerization of the composite electrolyte was initiated with a 450W medium pressure UV lamp. Samples were placed ≈ 3 cm from the lamp, and were exposed until rubbery. Cross-linking was performed under nitrogen and in air; curing under nitrogen allowed shorter reaction times.

## **BIBLIOGRAPHY**

- 1. Herr, R. Electrochimica Acta 1990, 35, 1257.
- 2. Dev. A. N. Thin Solid Films 1977, 43, 131.
- 3. Peled, E.; Yamin, H. Israel J. Chem. 1979, 18, 131.
- 4. Armand, M. B.; Chabagno, J. M.; Duclot, M. Second International Meeting on Solid Electrolytes St. Andrews, Scotland, 1978.
- 5. MacCallum, J. R.; Vincent, C. A. *Polymer Electrolyte Reviews-1*; Elsevier Applied Science: New York, 1987; Vol. 1.
- 6. MacCallum, J. R.; Vincent, C. A. *Polymer Electrolyte Reviews-2*; Elsevier Applied Science: New York, 1989; Vol. 2.
- 7. Gray, F. M. Solid Polymer Electrolytes: Fundamentals and Applications; VCH
  Publishers, Inc.: New York, 1991.
- 8. Berthier, C.; Gorecki, W.; Minier, M.; Armand, M. B. Solis State Ionics 1983, 11, 91.
- Cameron, G. C.; Ingram, M. D. "Polymer Electrolyte Reviews-2"; MacCallum, J.
   R. and Vincent, C. A. ed.; Elsevier Applied Science: New York, 1989; Vol. 2, pp
- 10. Nicholas, C. V.; Wilson, D. J.; Booth, C. *Polymer J.* **1988**, *20*, 289.
- 11. Blonsky, P. M.; Shriver, D. F.; Austin, P.; Allcock, H. R. J. Am. Chem. Soc. 1984, 106, 6854.

- 12. Fish, D.; Khan, I. M.; Wu, E.; Smid, J. Brit. Polymer J. 1988, 20, 281.
- 13. Allcock, H. R.; Kuharcik, S. E.; Reed, C. S.; Napierela, M. E. Macromolecules 1996, 29, 3384.
- 14. Allcock, H. R.; Napierala, M. E.; Cameron, C. G.; O'Connor, S. J. M. Macromolecules 1996, 29, 1951.
- Borghini, M. C.; Matragostino, M.; Passerini, S.; Scrosati, B. J. Electrochem. Soc.
   1995, 142, 2118.
- 16. Xia, D. W.; Soltz, D. Solid State Ionics 1984, 14, 221.
- 17. Cowie, J. M. G.; Martin, A. C. S. *Polymer* 1987, 28, 627.
- 18. Yamaguchi, Y.; Aoki, S.; Watanabe, M.; Sanui, K.; Ogata, N. Solid State Ionics
  1990, 40/41, 628.
- 19. Hawker, C. J.; Chu, F.; Pomery, P. J.; Hill, D. J. T. *Macromolecules* **1996**, *29*, 3831.
- 20. Qiao, J. Ph.D. Dissertation; Michigan State University: E. Lansing, 1996.
- 21. Mixed polymer systems Gray, F. M. "Polymer Electrolyte Reviews-1"; MacCalum, J. R. and Vincent, C. A. ed.; Elsevier Applied Science: New York, 1987; Vol. 1, pp 139.
- 22. Choe, H. S.; Carroll, B. G.; Pasquariello, D. M.; Abraham, K. M. Chem. Mater. 1997, 9, 369.
- 23. Wieczorek, W.; Stevens, J. R. J. Phys. Chem. B 1997, 101, 1529.

		,	
		*	
·			

- Wang, Z.; Huang, B.; Wang, S.; Xue, R.; Huang, X.; Chen, L. J. Electrochem.
   Soc. 1997, 144, 778.
- Chiang, C. K.; Bauer, B. J.; Briber, R. M.; Davies, A. T. Polymer Commun. 1987,
   28, 105.
- 26. Hudson, M. J.; Sequeira, C. A. C. J. Electrochem. Soc. 1995, 142, 4013.
- 27. LeNest, J. F.; Cheradame, H.; Ghandhini, A.; Cohen-Addad, J. P. Polym. Commun. 1987, 28, 302.
- 28. Ichino, T.; Matsumato, M.; Rutt, J. S.; Nishi, S. J. Polym. Sci., Part A: Polym. Chem. 1993, 31, 1701.
- Tsuchida, E.; Ohno, H.; Tsunemi, K.; Kobiyashi, N. Solis State Ionics 1983, 11, 227.
- Gray, F. M.; MacCallum, J. R.; Vincent, C. A. Solid State Ionics 1986, 18/19,
   252.
- 31. Such, K.; Florjanczyk, Z.; Wieczorek, W.; Przyluski, J. "Proceedings of the Second International Symposium on Polymer Electrolytes"; Scrosati, B. ed.; Elsevier: London, 1990, pp 119.
- 32. Florjanezyk, Z.; Such, K.; Wieczorek, W.; Przyluski, J. 7th International

  Symposium on Solid State Ionics Hakone, 1989.
- 33. Weston, J. E.; Steele, B. C. H. Solid State Ionics 1982, 7, 75.
- 34. Plocharski, J.; Wieczorek, W. Solid Sate Ionics 1988, 28-30, 979.

- Wieczorek, W.; Such, K.; Wycislik, H.; Plocharski, J. Solid State Ionics 1989, 36, 255.
- 36. Capuano, F.; Croce, F.; Scrosati, B. J. Electrochem. Soc. 1991, 138, 1918.
- 37. Gang, W.; Ross, J.; Brinkmann, D.; Capuano, F.; Croce, F.; Scrosati, B. Solid State Ionics 1992, 53-56, 1102.
- Appetecchi, G. B.; Dautzenberg, G.; Scrosati, B. J. Electrochem. Soc. 1996, 143,6.
- 39. Fritz, H. P.; Stein, K.; Herr, R. J. Power Sources 1992, 37, 315.
- 40. Khan, S. A.; Baker, G. L.; Colson, S. Chem. Mater. 1994, 6, 2359.
- 41. Fan, J.; Fedkiw, S. J. Electrochem. Soc. 1997, 144, 399.
- 42. Michael, G.; Ferch, H. "Technical Bulletin Pigments," Degussa AG, 1993.
- 43. Jezorek, J. R.; Freiser, H. Anal. Chem. 1979, 51, 366-373.
- 44. Tundo, P. J. Chem. Soc., Chem. Commun. 1977, 641-642.
- Weetall, H. H. Immobilized Enzymes, Antigens, and Antibodies, and Peptides
  New York, 1975.
- 46. Mathias, J.; Wannemacher, G. J. Colloid Interface Sci. 1988, 125, 61.
- 47. Morrow, B. A.; McFarlan, A. J. *Langmuir* **1991**, *7*, 1695.
- 48. Tripp, C. P.; Hair, M. L. Langmuir 1992, 8, 1961.
- 49. Tripp, C. P.; Hair, M. L. Langmuir 1992, 8, 1120.

- 50. Liu, C. C.; Maciel, G. E. J. Am. Chem. Soc. 1996, 118, 5103.
- 51. Odlyha, M.; Scott, R. P. W.; Simpson, C. F. J. Thermal Anal. 1993, 40, 1197.
- 52. Blitz, J. P.; Murthy, R. S. S.; Leyden, D. E. J. Am. Chem. Soc. 1987, 109, 7141.
- 53. Blitz, J. P.; Murthy, R. S. S.; Leyden, D. E. J. Colloid Interface Sci. 1988, 121,63.
- 54. Blitz, J. P.; Murthy, R. S. S.; Leyden, D. E. J. Colloid Interface Sci. 1988, 126,387.
- 55. Tripp, C. P.; Hair, M. L. Langmuir 1991, 7, 923.
- 56. Tripp, C. P., Hair, M. L. J. Phys. Chem. B 1993, 97, 5693.
- 57. Tripp, C. P.; Hair, M. L. Langmuir 1995, 11, 149.
- 58. Sandoval, J. E.; Pesek, J. J. Anal. Chem. 1989, 61, 2067.
- 59. Sandoval, J. E.; Pesek, J. J. Anal. Chem. 1991, 63, 2634.
- 60. Chu, C.-H.; Jonsson, E.; Auvinen, M.; Pesek, J. J.; Sandoval, J. E. Anal. Chem. 1993, 65, 808.
- 61. Speier, J. L., Webster, J. M., Barnes, G. H. J. Am. Chem. Soc. 1957, 79, 974.
- 62. Ferch, H. "Technical Bulletin Pigments," Degussa AG, 1993.
- 63. Plueddemann, E. P. Silane Coupling Agents; Plenum Press: New York, 1982.
- 64. Sunkara, H. B.; Jethmalani, J. M.; Ford, W. T. Chem. Mater. 1994, 6, 362.
- 65. Joseph, R.; Zhang, S.; Ford, W. T. Macromolecules 1996, 29, 1305.

- 66. Bourgeat-Lami, E.; Espiard, P.; Guyot, A. Polymer 1995, 36, 4385.
- 67. Bourgeat-Lami, E.; Espiard, P.; Guyot, A.; Gauthier, C.; David, L.; Vigier, G. Die

  Angewandte Makromolekulare Chemie 1996, 242, 105.
- 68. Espiard, P.; Guyot, A. Polymer 1995, 36, 4391.
- 69. Espiard, P.; Guyot, A.; Perez, J.; Vigier, G.; David, L. Polymer 1995, 36, 4397.
- 70. Coreactive Photoinitiators for Surface Polymerization Koehler, M.; Ohngemach, J. "Radiation Curing of Polymeric Materials"; Hoyle, C. E. and Kinstle, J. F. ed.; Americam Chemical Society: Washington, DC, 1989; Vol. 417, pp 106.
- 71. Photocurable Coatings Hoyle, C. E. "Core-active Photoinitiators for Surface Polymerization"; Hoyle, C. E. and Kinstle, J. F. ed.; American Chemical Society: Washington, DC, 1989; Vol. 417, pp 1.
- 72. Sen Gupta, P. K.; Bevington, J. C. Polymer 1973, 14, 527.
- 73. Borer, A.; Kirchmayer, K.; Rist, G. Helv. Chim. Acta 1978, 61, 305.
- 74. Sandner, M. R.; Osborn, C. L. Tetrahedron Lett. 1974, 415.
- 75. Delzenne, G. A.; Laridon, U.; Peeters, H. Eur. Polym. J. 1970, 6, 933.
- 76. Suppan, P.; Porter, G. Trans. Faraday Soc. 1965, 61, 1664.
- 77. Ledwith, A.; Ndaalio, G.; Taylor, A. R. Macromolecules 1975, 8, 1.
- 78. Berner, G.; Kirchmayer, R.; Rist, R. J. Oil Chem. Assoc. 1978, 61, 105.
- 79. Hamity, M.; Scaiano, J. C. J. Photochem. 1975, 4, 229.

- Sadhir, R. K.; Smith, J. D. B.; Castle, P. M. J. Polymer. Sci. A: Polym. Chem.
   1983, 21, 1315.
- 81. Odian, G. *Priciples of Polymerization*; 3rd ed.; John Wiley and Sons, Inc.: New York, 1991.
- 82. Bartholomew, R. F.; Dividson, R. S. J. Chem. Soc., Chem. Commun. 1971, 2347.
- 83. Decker, C. Makromol. Chem. 1979, 180, 2027.
- 84. Organosilanes Armitage, D. A. "Comprehensive OrganometallicChemistry: The Synthesis, Reaction and Structures of Organometallic Compounds"; Wilkinson, G., Stone, G. A. and Abel, E. W. ed.; Pergamon Press: New York, 1982; Vol. 2, pp 1.
- 85. Permeation and Morphology in Polymer Latex Films Containing Leachable
  Additives Steward, P. A.; Hearn, J.; Wilkinson, M. C.; Wilson, A. J.; Roulstone, B.
  J. "Film Formation in Waterborne Coatings"; Provder, T., Winnik, M. A. and
  Urban, M. W. ed.; American Chemical Society: Washington, DC, 1996; Vol. 648,
  pp 359.
- 86. Nazri, G. A.; Meibuhr, S. G. J. Electrochem. Soc. 1989, 136, 2450.
- Wieczorek, W.; Such, K.; Chung, S. H.; Stevens, J. R. J. Phys. Chem. Chem.
   1994, 98, 9047-55.
- 88. Sperling, L. H. *Introduction to Physical Polymer Science*; 2nd ed.; John Wiley & Sons, Inc.: New York, 1992.
- 89. Hasegawa, M.; Arai, K.; Saito, S. J. Polym. Sci., Polym. Chem. Edn. 1982, 20, 1021.

- 90. Hasegawa, M.; Arai, K.; Saito, S. J. Polym. Sci., Polym. Chem. Ed. 1987, 25, 3117.
- 91. Hasegawa, M.; Arai, K.; Saito, S. J. Chem. Eng. Japan 1988, 21, 30.
- Janssen, A. W. G.; Van Herk, A. M.; German, A. L. ACS Polym. Prepr 1993, 34,
   532.
- 93. Konno, M.; Arai, K.; Saito, S. J. Polym. Sci., Polym. Chem. Ed. 1987, 25, 223.
- 94. Hergeth, W.; Starre, P.; Schmutzler, K.; Wartewig, S. Polymer 1988, 29, 1323.
- 95. Hergeth, W.; Steinau, U.; Bittrich, H.; Simon, G.; Schmutzler, K. Polymer 1989, 30, 254.
- 96. Hasegawa, M.; Arai, K.; Saito, S. J. Appl. Polym. Sci. 1987, 33, 411.
- 97. Arai, M.; Arai, K.; Saito, S. J. Polymer Sci., Polymer Chem. Ed. 1982, 1021.
- 98. Fukano, K., Kageyama, E. J. Polym. Sci., Polym. Chem. Ed. 1975, 13, 1309.
- 99. Hasegawa, M.; Arai, K.; Saito, S. J. Polym. Sci., Polym. Chem. Ed. 1987, 25, 3231.
- Wu, P.-W.; Holm, S. R.; Duong, A. T.; Dunn, B.; Kaner, R. B. Chem. Mater.
   1997, 9, 1004.
- 101. Kramer, G. W.; Levy, A. B.; Midland, M. M. "Organic Synthesis Via Borane"; Brown, H. C. ed.; John Wiley & Sons: New York, 1975, pp 243.
- 102. Mitchell, T. N.; Kerstin, H. W. J. Organomet. Chem. 1992, 436, 43.

- 103. Steward, O. W.; Lutkus, A. G.; Greenshields, J. B. J. Organomet. Chem. 1978, 144, 146.
- 104. Bestmann, H. J.; Koschotzky, K. H.; Schaetzke, W.; Sness, J.; Vostrosky, O. L. Liebigs Ann. Chem. 1981, 9, 1705.
- 105. Van, J. H.; Hershied, J. D. M. Synthesis 1973, 169.
- 106. Wood, N. F.; Chang, F. C. J. Org. Chem. 1965, 30, 2054.
- 107. Matsuda, H.; Yamamoto, A.; Iwamoto, N.; Matsuda, S. J. Org. Chem. 1978, 43, 4567.
- Tolstikov, G. A.; Odinokov, V. N.; Galeeva, R. I.; Bakeeva, R. S.; Akhunova, V. R. Chem. Nat. Compd. (Engl. Transl.) 1982, 18, 219.

